Model Optimisation and Predictive Control of a Pneumatic Driven Ankle Rehabilitation Robot

Dexter Felix Brown

University of Leeds

School of Electronic and Electrical Engineering



Submitted in accordance with the requirements for the degree of

Doctor of Philosophy

March 2026

Intellectual Property Statement

I confirm that the work submitted is my own and that appropriate credit has been given where reference has been made to the work of others.

This copy has been supplied on the understanding that it is copyright material and that no quotation from the thesis may be published without proper acknowledgement.

The right of Dexter Felix Brown to be identified as Author of this work has been asserted by Dexter Felix Brown in accordance with the Copyright, Designs and Patents Act 1988.

Acknowledgements

Firstly, I would like to sincerely thank my supervisor Professor Shane Xie for his constant support and guidance throughout my research. His expertise in the field of rehabilitation robotics and experience with postgraduate research has allowed me to take my first steps into the world of academia confidently. He has remained optimistic about my future, always pushing me for greater things and giving me every opportunity to succeed. Without his continued advice and willingness to proofread every document I sent him, this work would not have been possible.

My deepest thanks go to the University of Leeds Graduate School and Institute of Robotics, Autonomous Systems and Sensing for allowing me the opportunity to pursue my higher education and achieve my PhD degree. In particular my thanks go to the School of Electrical and Electronic Engineering Administrative Manager Clair Atkinson for helping with all my administrative needs and handling a great deal of internal bureaucracy on my behalf.

I would also like to sincerely thank the EPSRC DTP for providing me with a full scholarship throughout these years of research. The generous funding they provided has allowed me to focus on my studies without financial worry and for the first time be truly independent.

Finally, I would like to sincerely thank my family for always being there for me throughout this journey in their own ways. To my parents, thank you for raising me and caring for me even as I moved

to the other side of the country to pursue my degree at Leeds, and showing me all the unconditional love and support I needed. To my wonderful wife Asha, thank you for always being there with me no matter how stressed and unsure I might have been, and constantly reassuring me that I am capable of whatever I put my mind to. Lastly, thank you to my late father Martin, the original inspiration for my following of a doctoral degree. I hope I did you proud.

This is for, and because of, all of you.

Dexter Brown

2026

Abstract

Rehabilitation robotics is an emergent field of research aimed at assisting healthcare services and impaired patients in reducing the workload of physical therapists and making therapeutic exercises more accessible. However, with any system designed to be used in direct contact with a human and especially with those in a vulnerable or injured state, rehabilitation robots must be held to a high standard of performance and reliability. Improved patient comfort and safety can be achieved by using compliant actuators like pneumatic muscles; however, any inherently compliant structural element of a system introduces time-variance and nonlinearity to its dynamics. Intelligent controller design is essential to this end. Therefore, this thesis presents the development, application, and verification of a predictive intelligent control scheme for use with an ankle rehabilitation robot.

The Compliant Ankle Rehabilitation Robot (CARR) is used as the platform for developing intelligent control strategies during this work. Actuated by Pneumatic Artificial Muscles (PAMs), the system is inherently compliant but also time-varying and dynamically complex. Initially, a feasibility study is conducted to develop modelling and control methods for a single PAM, in which the PSO modelling method is created, approximating a PAM to a mass-spring-damper system and using particle swarm optimisation to calculate optimal parameters, effectively simplifying the system. A

piecewise method is also proposed, accounting for nonlinearity by using multiple models for different operating modes and positions. This modelling method is then used to develop an MPC strategy for the PAM, alongside other intelligent controllers, ILC and optimised PID. In comparative experiments, the developed MPC is confirmed to perform well, reducing the motion lag associated with other control methods and providing accurate and smooth motion.

The developed MPC is then implemented to the CARR. Kinematics equations are used to combine the four actuators in parallel to effectively control multiple degrees of freedom. Based on the complex arrangement of the CARR mechanisms, two controller setups are proposed: single-model in which one dynamic model is used to approximate all four actuators, and dual-model, in which the upper- and lower-pairs are modelled separately. Experiments validate the functionality of the developed controllers in comparison with PID and ILC, and results show that each MPC implantation has strengths and weaknesses in different operating scenarios.

Finally, experiments with 15 participants are performed to validate the controller's performance in a situation approximating the real function of the CARR. Measurements show good tracking accuracy for the single-model setup and good consistency between participants for the dual-model setup, while participant responses suggested several improvements to the CARR design.

The research problems addressed in this thesis are the difficulty in accurate motion tracking control of inherently compliant systems, which are necessary in rehabilitation robotics to provide improved

safety and comfort to patients, and the necessity of rehabilitation robots to be validated with participants. The contributions of the work presented here are development of a PSO-based modelling method for dynamic modelling of PAMs, MPC scheme for motion tracking of PAMs, experimental comparison data validating the developed MPC alongside other intelligent controllers, application of the developed controller to the CARR, and participant involved validation experiments of the intelligently controlled CARR. Using the developed strategies, results, and suggested further work in this thesis, a compliant ankle rehabilitation robot suitable for use in clinical environments can be realised.

CONTENTS

Introduction..... 1

1.1 Background..... 2

1.1.1 Physical Rehabilitation Requirements 2

1.1.2 Robot-Assisted Rehabilitation 3

1.1.3 Control Strategies..... 4

1.1.4 Research Challenges 6

1.2 Research Aim and Objectives 7

1.2.1 Feasibility Study for Intelligent Control of Compliant Pneumatic Actuators 7

1.2.2 Application of Intelligent Control Systems to Compliant Ankle Rehabilitation Robot 8

1.2.3 User Study of Intelligently Controlled Compliant Ankle Rehabilitation Robot 9

1.3 Research Scope 10

1.4 Contributions 11

1.4.1 PSO-based Modelling Method.....11

1.4.2 MPC Algorithm for PAM Motion Control 12

1.4.3 Experimental Comparison Data for Intelligent Control of Pneumatic Artificial Muscle.....12

1.4.4 MPC Algorithm for CARR Motion Control.....12

1.4.5 User Study for Online Validation of Model Predictive Controlled CARR 13

1.5 Thesis Outline 14

1.6 Chapter Summary 16

Effectiveness of Intelligent Control Strategies in Robot-Assisted Rehabilitation – A Systematic Review.....17

2.1 Introduction 18

2.2 Method 19

2.2.1 Search Strategy 19
2.2.2 Inclusion/Exclusion Criteria 20
2.2.3 Stages of Review 21
2.2.4 Search Results 22
2.3 Review Results and Analysis 23
2.3.1 Control Optimisation 25
2.3.2 Fuzzy Logic Control 26
2.3.3 Adaptive Controllers 28
2.3.4 Learning Control 30
2.3.5 Other Controllers 33
2.3.6 Controller Comparisons 34
2.4 Discussion 34
2.4.1 Summary of Results 34
2.4.2 Safety and Ethical Considerations 36
2.4.3 Meta-Analysis and Evaluation 37
2.4.4 Gaps and Opportunities 40
2.5 Chapter Conclusion 45
A Piecewise Particle Swarm Optimisation Modelling Method for Pneumatic Artificial Muscle Actuator 47
3.1 Introduction 48
3.2 Materials and Methods 53
3.2.1 Phenomenological Model 53
3.2.2 Particle Swarm Optimisation Algorithm 55
3.2.3 Piecewise Model 56
3.2.4 Experimental Setup 59
3.3 Results 61
3.3.1 Model Generation 61
3.3.2 Model Accuracy Experiments 64
3.4 Discussion 70
3.5 Chapter Conclusion 75
Model Predictive Control with Optimal Modelling for Accurate Pneumatic Artificial Muscle Motion 77
4.1 Introduction 78
4.2 Materials and Methods 85
4.2.1 Controllers 85
4.2.2 Experimental Setup 89
4.2.3 Experiment Plan 89

4.2.4 Algorithm Parameters 91
4.3 Results 94
4.4 Discussion 102
4.5 Chapter Conclusion 106
Model Predictive Control with PSO Modelling Approach for Position Control of Compliant Ankle Rehabilitation Robot 109
5.1 Introduction 110
5.2 Robot Design 116
5.2.1 Layout and Functionality 116
5.2.2 Kinematics 119
5.3 Modelling and Control 120
5.3.1 Modelling Methodology 120
5.3.2 Control Methodology 122
5.4 Experiment Methodology 125
5.5 Results 127
5.6 Discussion 129
5.7 Chapter Conclusion 133
User Study of Intelligently Controlled Compliant Ankle Rehabilitation Robot 136
6.1 Introduction 137
6.2 System Setup 141
6.2.1 Ankle Rehabilitation Robot Setup 141
6.2.2 Model Predictive Controller Setup 142
6.3 Experiment Methodology 144
6.3.1 Participants 144
6.3.2 Experiment Protocol 144
6.4 Motion Tracking Results 148
6.4.1 Displacement Measures 148
6.4.2 Discussion 152
6.5 Questionnaire Results 154
6.5.1 Participant Responses 154
6.5.2 Discussion 157
6.6 Chapter Conclusion 159
Conclusion and Future Work 163
7.1 Outcomes and Contributions 164
7.1.1 PSO-based Modelling Method 165
7.1.2 MPC Algorithm for PAM Motion Control 167

7.1.3 Experimental Comparison Data for Intelligent Control of Pneumatic Artificial Muscle 168
7.1.4 MPC Algorithms for CARR Motion Control 169
7.1.5 User Study for Online Validation of Model Predictive-Controlled CARR 171
7.2 Future Work 172
7.2.1 PSO-based modelling method improvements 172
7.2.2 MPC motion tracking accuracy 173
7.2.3 Further experiments for MPC implementations 173
7.2.4 CARR mechanical design 174
7.3 Summary 175
Bibliography 177
Ethical Approval for Research Projects involving Human Participants 201
List of Materials 202

LIST OF FIGURES

Figure 1. 1: Examples of rehabilitation robots. (a) Rex bionics exoskeleton [5]; (b) ARBOT [6]; (c) ARMin rehabilitation robot [7]; (d) Rehab-Exos [8]; (e) Lokomat [9] 3

Figure 2.1: A generalised diagram for control of a rehabilitation robot. This controller diagram is applicable to the majority of rehabilitation robots. 24

Figure 2.2: A generalised adaptive controller diagram. The Adaption Algorithm block includes the adaptive law for the system and represents the use of intelligence in adaptive controllers. The adaptive law is typically unique to the controller/study it is presented with. 28

Figure 2.3: A generalised Iterative Learning Controller diagram. 30

Figure 3.1: Phenomenological model of the PAM showing displacement $\boldsymbol{x}$; contractile force element $\boldsymbol{Fc}$; external load element $\boldsymbol{Fl}$; and PAM parameters $\boldsymbol{M}$, $\boldsymbol{C}$, and $\boldsymbol{K}$. 54

Figure 3.2: A diagram of the experimental setup, circuitry, and computer communications. 60

Figure 3.3: The experimental setup, showing the FESTO DMSP-20-400N PAM (1), FUTEK LCM300 load cell (2), FESTO MLO-POT-300-TLF displacement encoder (3), and external load attachment (4). 61

Figure 3.4: Measurement values for the full stroke sin wave experiment. (a) shows the displacement readings, (b) shows the error values. 66

Figure 3.5: Measurement values for the lower stroke sin wave experiment. (a) shows the displacement readings, (b) shows the error values. 66

Figure 3.6: Measurement values for the upper stroke sin wave experiment. (a) shows the displacement readings, (b) shows the error values. 67

Figure 3.7: Measurement values for the triangle wave experiment. (a) shows the displacement readings, (b) shows the error values.....67
Figure 3.8: Measurement values for the square wave experiment. (a) shows the displacement readings, (b) shows the error values.....67
Figure 3.9: Measurement values for the rapid sin wave experiment. (a) shows the displacement readings, (b) shows the error values. 68
Figure 3.10: Measurement values for the weighted sin wave experiment. (a) shows the displacement readings, (b) shows the error values. 68
Figure 4.1: MPC Structure. The system model is generated according to the methods described in chapter 3. 86
Figure 4.2: Steady-state relationships between voltage input to the pressure regulator, internal air pressure in the PAM, and actuator displacement. 91
Figure 4.3: Measurement values for the 0cm-10cm sin wave experiment. (a) shows the displacement readings, (b) shows the error values. 94
Figure 4.4: Measurement values for the 0cm-5cm sin wave experiment. (a) shows the displacement readings, (b) shows the error values. 94
Figure 4.5: Measurement values for the 5cm-10cm sin wave experiment. (a) shows the displacement readings, (b) shows the error values. 95
Figure 4.6: Measurement values for the rapid motion sin wave experiment. (a) shows the displacement readings, (b) shows the error values. 95
Figure 4.7: Measurement values for the triangle wave experiment. (a) shows the displacement readings, (b) shows the error values.....95
Figure 4.8: Measurement values for the square wave experiment. (a) shows the displacement readings, (b) shows the error values.....96
Figure 4.9: Measurement values for the 5kg weighted 0cm-10cm sin wave experiment. (a) shows the displacement readings, (b) shows the error values.....96
Figure 4.10: Measurement values for the 10kg weighted 0cm-10cm sin wave experiment. (a) shows the displacement readings, (b) shows the error values.....96
Figure 4.11: Measurement values for the 5kg weighted square wave experiment. (a) shows the displacement readings, (b) shows the error values.....97

Figure 4.12: Measurement values for the 10kg weighted square wave experiment. (a) shows the displacement readings, (b) shows the error values. 97
Figure 4.13: Measurement values for the 10kg weighted rapid sin wave experiment. (a) shows the displacement readings, (b) shows the error values. 97
Figure 4.14: Measurement values for the 10kg weighted 0cm-5cm sin wave experiment. (a) shows the displacement readings, (b) shows the error values. 98
Figure 4.15: Measurement values for the 10kg weighted 5cm-10cm sin wave experiment. (a) shows the displacement readings, (b) shows the error values. 98
Figure 4.16: Measurement values for the 0cm-4cm changing to 0cm-8cm sin wave experiment. (a) shows the displacement readings, (b) shows the error values. 98
Figure 4.17: Measurement values for the 0cm-10cm changing to 2.5cm-7.5cm sin experiment. (a) shows the displacement readings, (b) shows the error values. 99
Figure 4.18: Measurement values for the 0cm-5cm changing to 5cm-10cm sin experiment. (a) shows the displacement readings, (b) shows the error values. 99
Figure 4.19: Measurement values for the slow changing to rapid sin experiment. (a) shows the displacement readings, (b) shows the error values. 99
Figure 4.20: Measurement values for the rapid changing to slow sin experiment. (a) shows the displacement readings, (b) shows the error values. 100
Figure 4.21: Measurement values for the 5kg weight added experiment. (a) shows the displacement readings, (b) shows the error values. 100
Figure 4.22: Measurement values for the 10kg weight added experiment. (a) shows the displacement readings, (b) shows the error values. 100
Figure 4.23: Measurement values for the 5kg weight removed experiment. (a) shows the displacement readings, (b) shows the error values. 101
Figure 4.24: Measurement values for the 10kg weight removed experiment. (a) shows the displacement readings, (b) shows the error values. 101

Figure 4.25: Measurement values for the 10kg weight added experiment. (a) shows the displacement readings, (b) shows the error values. 101
Figure 4.26: Measurement values for the 10kg weight removed sin wave experiment. (a) shows the displacement readings, (b) shows the error values. 102
Figure 4.27: Measurement values for the 5kg weight added and removed sin wave experiment. (a) shows the displacement readings, (b) shows the error values. 102
Figure 5.1(a) and 5.1(b): Images of the CARR. Figure 5.1(a) shows the PAMs and connection points. Figure 5.1(b) shows the bar linkage mechanism for the footplate and the rotary encoders used to measure angular displacement. 117
Figure 5.2(a), 5.2(b), and 5.2(c): Coordinate system of the CARR. Figure 5.2(a) shows the upper fixed platform coordinates, figure 5.2(b) shows the moving platform coordinates, and figure 5.2(c) shows the combined coordinate systems along with the measured values $\boldsymbol{H}$, $\boldsymbol{h}$, and the muscle length $\boldsymbol{Li}$ 118
Figure 5.3(a) and 5.3(b): Control structure for the CARR, including setpoint calculation, and structure of the MPC loop including application of the PSO dynamic model. 124
Figure 5.4: Measured angle values for the X and Y axis of the CARR during the X axis experiment. 127
Figure 5.5: Measured angle values for the X and Y axis of the CARR during the Y axis experiment. 127
Figure 5.6: Measured angle values for the X and Y axis of the CARR during the X and Y axis experiment. 128
Figure 5.7: Measured angle values for the X and Y axis of the CARR during the rapid X axis experiment. 128
Figure 5.8: Measured angle values for the X and Y axis of the CARR during the rapid Y axis experiment. 128
Figure 6.1: Setup of the CARR for experiments with participants. (a) and (b) show the setup without a participant, (c) shows the setup with a participant in the chair with their foot in the footplate and calf strapped to the calf rest. 141

Figure 6.2: The user interface for the MPC systems in NI LabVIEW. (a) shows the interface for the single-model setup, and (b) shows the interface for the dual-model setup. 143
Figure 6.3: Motion undertaken by the footplate during plantar/dorsiflexion motion. (a) shows the footplate at the equilibrium position and the directions of motion are indicated, (b) shows the footplate at its most downward extended position, and (c) shows the footplate at its most upwards extended position. 147
Figure 6.4: Motion undertaken by the footplate during ab/adduction motion. (a) shows the footplate at the equilibrium position and the directions of motion are indicated, (b) shows the footplate at its rightmost extended position, and (c) shows the footplate at its leftmost extended position. 147
Figure 6.5: Associated line colours for each participant in the displacement measurement graphs 148
Figure 6.6: Displacement measurement during the plantar/dorsiflexion motion under single-model MPC. (a) shows the motion of the X axis, (b) shows the motion of the Y axis, and (c) shows the error in the X axis motion. Technical problems with the encoders caused participants 5, 7, 8 and 11's X-axis measurements and participant 8's Y-axis measurement to be omitted. 149
Figure 6.7: Displacement measurement during the ab/adduction motion under single-model MPC. (a) shows the motion of the X axis, (b) shows the motion of the Y axis, and (c) shows the error in the Y axis motion. Technical problems with the encoders caused participants 7, and 13's X-axis measurements to be omitted. 150
Figure 6.8: Displacement measurement during the plantar/dorsiflexion motion under dual-model MPC. (a) shows the motion of the X axis, (b) shows the motion of the Y axis, and (c) shows the error in the X axis motion. Technical problems with the encoders caused participants 2, 4, and 7's X-axis measurements and participant 1's Y-axis measurement to be omitted. 151
Figure 6.9: Displacement measurement during the ab/adduction motion under dual-model MPC. (a) shows the motion of the X axis, (b) shows

the motion of the Y axis, and (c) shows the error in the Y axis motion. 152
Figure 6.10: Questionnaire used to gather participant responses during experiments. 155
Figure 6.11: Participant responses on questionnaire questions concerning the CARR while stationary. 156
Figure 6.12: Participant responses to questionnaire questions concerning the CARR motion under singe-model MPC. 156
Figure 6.13: Participant responses to questionnaire questions concerning the CARR motion under dual-model MPC. 157

List of Tables

Table 2.1: Articles Comparing Control Systems....42
Table 2.2: Algorithm Advantages and Disadvantages....43
Table 2.3: Experimental Results with Impaired Participants....44
Table 3.1: Model parameters....64
Table 3.2: Waveforms used in the model accuracy experiments....65
Table 3.3: Experiment error values....69
Table 3.4: FESTO PAM modelling method comparisons....73
Table 4.1: Experiment Outline....90
Table 4.2: PID control parameters and MPC model parameters....92
Table 5.1: Coordinates of PAM Connection Points....120
Table 5.2: Coordinates of PAM Connection Points....122
Table 5.3: Setpoint waveform Parameters....126
Table 5.4: Result Metrics....129
Table 6.1: Motion Parameters....145
Table 7.1: Outcomes and Contributions Summary....165

Abbreviations

CARR	Compliant Ankle Rehabilitation Robot
PAM	Pneumatic Artificial Muscle
DoFs	Degrees of Freedom
sEMG	Surface Electromyography
BCI	Brain-Computer Interface
PID	Proportional Integral Derivative
PD	Proportional Derivative
SMC	Sliding Mode Control
ILC	Iterative Learning Control
MPC	Model Predictive Control
RMSE	Root Mean Squared Error
PSO	Particle Swarm Optimisation
PSO-PID	Particle Swarm Optimised-PID
SEA	Series Elastic Actuator
MIMO	Multiple Input Multiple Output

CHAPTER 1

INTRODUCTION

With the ongoing development of medical robotics introducing more advanced systems to healthcare across the world, there is a requirement to ensure these robots are safe and fit for purpose. This applies not only to mechanical design, but also software and usability for both healthcare professionals and patients alike. With the push for more accessible and even home use assistive robotics in research and industry these factors are becoming increasingly imperative. However, despite all the research into mechanical and controller design, there are few studies present in the current literature focused on comparison between the many novel control systems being developed. To that end, the objective of this thesis is to develop several intelligence-based control systems for use in rehabilitation robotics, and through a series of experimental comparisons present the relative benefits and shortcomings of each.

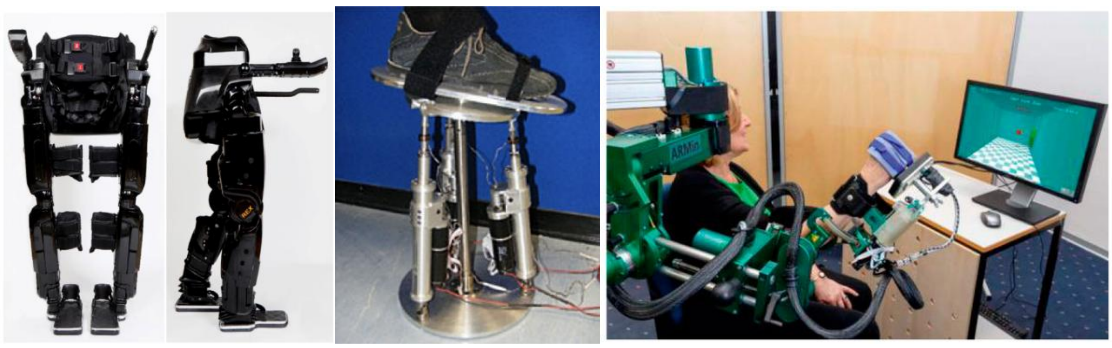
1.1 Background

1.1.1 Physical Rehabilitation Requirements

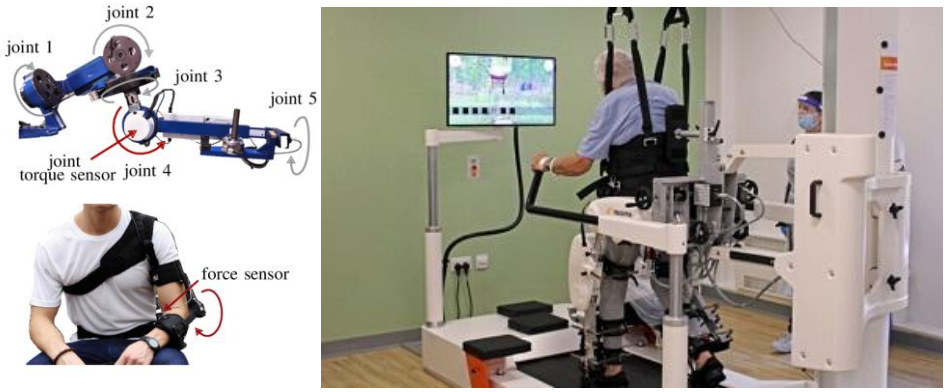
Stroke, other neurological diseases, and debilitating injuries can cause major, often lifelong, problems for their sufferers in the form of decreased mobility. Between the years 1990 and 2019 there were more than 12.2 million new stroke cases each year, and by 2019 over 101 million people live post-stroke according to the 2022 global stroke factsheet [1]. Studies have shown that physical impairment is a frequent effect of acute stroke, reporting that up to 80% of acute stroke victims experience some form of limb impairment [2]. With 20–25% of stroke survivors never being able to walk without assistance, and 65% unable to use their affected hands normally [3], this issue is widespread and affects a great number of people every year. The most prevalent and effective method to treat stroke-related motor disability is physical therapy led by a physiotherapist, but the ever-increasing number of patients puts more and more pressure on healthcare services. According to the National Institute of Health, standard inpatient treatment for stroke victims involves 3 hours of intensive treatment 5-6 days a week for up to 3 weeks, while outpatient treatment requires frequent hospital presence for several hours up to 3 days a week [4]. While stroke victims comprise the majority of patients requiring this kind of treatment, there are many other diseases and injuries which require similarly intensive rehabilitation, including but not limited to drop foot, osteoarthritis, muscular dystrophy, various sporting injuries like sprains or fractures, and recovery from other medical procedures like joint replacements.

1.1.2 Robot-Assisted Rehabilitation

In attempts to mitigate the pressure on healthcare systems caused by the requirements of physical rehabilitation, rehabilitation robotics is an open research field focused on developing mechatronics systems to aid in the process by allowing therapists to provide hands-free therapeutic exercises to patients. Over the years many different approaches to this problem have been made, with systems ranging in application from each of the commonly affected individual joints to whole limbs and even the full body, with several examples of different types and applications shown in Figure 1.1.



(a) (b) (c)



(d) (e)

Figure 1.1: Examples of rehabilitation robots. (a) Rex bionics exoskeleton [5]; (b) ARBOT [6]; (c) ARMin rehabilitation robot [7]; (d) Rehab-Exos [8]; (e) Lokomat [9]

While these systems all vary greatly in usage there are two main categories: platform-based and exoskeletons. Platform-based rehabilitation systems use a fixed base and are unmoving during use, with patients fixed in position while performing exercises. These systems are especially helpful for early stages of rehabilitation and for patients with extreme disabilities that prevent them from moving on their own. The fixed base helps with stability, and they are generally safer to use than otherwise mobile systems. Exercises that assist with muscle elasticity and build strength in specific muscles are easiest to implement on platform-based robots. Figure 1.1(b) and 1.1(c) show examples of platform-based rehabilitation systems. Exoskeleton systems are better suited to later stages of rehabilitation and less severe disability as the allowed motion during exercise helps train for day-to-day activities and allows for some freedom of motion not afforded by platform-based systems, with some examples shown in Figures 1.1(a), 1.1(d), and 1.1(e).

1.1.3 Control Strategies

While the mechanical design and intended application of a rehabilitation robot is the deciding factor for the majority of its functionality, software control governs the actual input-output capabilities of the system. As the specific motions undergone by therapeutic rehabilitation exercises are crucial to effective treatment, the specific output motions and forces exerted by a robot on a patient are paramount to its success and safety. A great many different control methodologies and architectures have been developed over the years, and despite the very specific application that rehabilitation robotics requires of these systems, many varied controllers have been identified as fit for this purpose.

Rehabilitation robots generally function under one of two operating schemes: passive and active control. Passive control sets a predefined trajectory for motion and follows it, guiding a user's joints through the motion with no input from them. This sort of exercise relies primarily on trajectory tracking control, as the exact displacements and angles are the measure of success, and is mostly used in early stages of rehabilitation to develop muscular plasticity. Active control relies heavily on the human-robot interaction by applying force either assisting or resisting the applied motion by the user, depending on whether the exercise is intended to assist with some motion and help with muscle memory or to train muscular strength by providing resistance. Active control makes use of sensor feedback and force output control and is mostly used in later stages of rehabilitation when the patient is capable of some motion under their own strength. Some rehabilitation robots are designed with one of these two operating procedures in mind, while some are developed to be able to deliver both. Control systems, however, must be developed with one in mind, for either trajectory tracking or force output control. As such, some rehabilitation robots have multiple different control schemes designed for different applications.

With the increasing interest in developing safe and effective robotics systems for use in rehabilitation, the importance of effective control systems in their functionality, and the large number of different control schemes being used in this field of research, comparison and validation of these controllers in relation to one another is a point of research interest.

1.1.4 Research Challenges

While the field of rehabilitation robotics is in development as an emergent field of medical robotics, there exist some key challenges in developing systems that meet the requirements for use in clinical environments. Robots designed to perform physical therapeutic exercises to impaired patients must be able to apply sufficient force to the correct parts of the affected limb to drive or guide motion appropriately, meaning the system must be attached to the patient. This introduces direct human-machine interaction, in which the forces exerted by the device on the patient, and vice versa, must be carefully bound to ensure the exercises are both safe and comfortable. Comfort must also be considered in the physical design of the robot to ensure patients can undergo the long exercise periods without discomfort which can reduce the efficacy of the training. Many devices introduce intrinsically compliant construction in the form of soft actuators, which allow users some flexibility while connected to the robot, reducing the perceived load of the device and improving safety. Unfortunately, compliant actuators are dynamically complex and often time-variant, depending on their construction, which makes accurate motion tracking control more difficult. Therefore, more research must be conducted to ensure robot-guided exercises are both accurately controlled and comfortable for the user.

The primary result to be considered with a rehabilitation robot is the outcome of rehabilitation. Unlike other applications of robotics such as construction and automation, in which position and force accuracy are the objectives of the device, rehabilitation robotics aims to improve the rehabilitation outcome for impaired patients. Therefore, while motion and force control tracking are important to guide exercises correctly according to a therapist's input, the resulting improvement to a patient's range of motion, muscular strength or plasticity

depending on the impairment, is the primary measure of success. Therefore, a user's experience of using a rehabilitation device should be considered as important a metric as output error.

1.2 Research Aim and Objectives

The overall aim of the research presented in this thesis is to develop, implement, and experimentally verify an intelligent control system for effective and compliant control of an ankle rehabilitation robot, with the system being tested with human participants to ensure treatment would be safe and effective. The device to be used as the plant for development of this control software is the Complaint Ankle Rehabilitation Robot (CARR), which uses four Pneumatic Artificial Muscles (PAMs) arranged in parallel for actuation. A detailed description of the CARR, including dynamics and kinematics, is presented later. The resulting algorithm developed should use machine intelligence to control the CARR in such a way that the dynamic qualities and nonlinearity are sufficiently accounted for allowing for smooth, comfortable, and safe motion while an impaired patient undergoes assisted physical therapy.

The main objectives and desired contributions of the project are details in the following sections.

1.2.1 Feasibility Study for Intelligent Control of Compliant Pneumatic Actuators

First, a feasibility study will be conducted in which a PAM is considered as the plant for development of several options for intelligent motion control. Multiple options will be considered for intelligent control with the aim of accurate motion tracking of the actuator. Comparative experiments will be conducted to

determine the relative strengths, weaknesses, and requirements of each controller. The control scheme deemed most appropriate for use in a more complex system driven by PAMs will be brought forwards for further research.

The following points summarise how this objective will be completed:

- Research, develop, and implement intelligent controllers for PAM motion
- Using a single PAM setup, test each controller using the same series of experiments
- Validate the performance of each controller in comparison with each other
- Based on certain performance metrics, determine which controller(s) are most suitable for further application

The contributions of this objective are development of multiple intelligent control schemes for accurate motion tracking of a dynamically complex and nonlinear system, and results from comparative experiments of multiple intelligent control schemes with analysis of each algorithm's performance and suitability for use in compliant actuator-driven rehabilitation robots.

1.2.2 Application of Intelligent Control Systems to Compliant Ankle Rehabilitation Robot

Secondly, based on the results from the comparative study performed as part of objective 1, any developed controller(s) deemed suitable for further research will be applied to the CARR. The CARR is a platform-based ankle rehabilitation device driven by four PAMs arranged in parallel, forming antagonistic pairs that allow for actuation of three axes of motion, giving the robot three rotational DoFs. After adjusting the successful developed controller(s) for use with the CARR, which is a much more complex system than a single PAM by virtue of the increased dimensionality, they will be experimentally verified. Several experiments will be performed to confirm the good functionality of the controller(s) on the CARR, ensuring they are safe and suitable for use with human participants.

The following points summarise how this objective will be completed:

- Using inverse kinematics, apply successful controllers from the first objective to the CARR
- Create a suitable testing scheme to validate the controllers for use in robot-assisted ankle rehabilitation
- Perform comparative experiments with successful controllers and other control systems as baseline
- Determine successes and improvements to be made to the controller before moving on to further validation experiments

The contribution of this objective is development and validation of intelligent control schemes for accurate motion tracking control of a multiple DoF rehabilitation robot, with intrinsic compliance and nonlinearity introduced by pneumatic muscle actuation.

1.2.3 User Study of Intelligently Controlled Compliant Ankle Rehabilitation Robot

The final objective of this research is a user study in which the controllers validated in objective 2 are used in online experiments with human participants. With the aim of the field of rehabilitation robotics to provide improved therapeutic exercises to impaired patients, it is imperative that any developed system is validated with users. As such, experiments will be conducted with participants' ankles connected to the CARR during motion. This will allow for both motion tracking measurements with the added loading and disturbance of a user, and participant responses to their experience using the device.

The following points summarise how this objective will be completed:

- Source suitable participants for user study of the CARR
- Create testing schedule suitable for participant-aided validation experiments

- Determine performance metrics and produce participant response questionnaire
- Perform controller and robot system validation experiments with users
- Analyse CARR motion tracking accuracy results to determine effect of a participant on controller accuracy
- Analyse participant response data to determine successes and failings of controller and CARR design

The contribution of this objective is experimental results from participant involved experiments using the intelligently controlled CARR, detailing the performance of the controllers in a situation approximating a real rehabilitation scenario and the experiences of the participants in using the CARR for guided ankle motion.

1.3 Research Scope

The scope of the research performed during this project is specifically focussed on the software control system design and experimental validation of developed systems for PAM and PAM-driven systems for robot assisted ankle rehabilitation. The model of PAM used in all experiments is the FESTO DMSP-20- 400N. Coding for software design is performed using National Instruments LabVIEW. Where a control system or associated software is designed and intended for validation, physical experimentation will be performed to determine the effectiveness and accuracy, as well as suitability for application in the field of robot assisted rehabilitation.

Mechanical design of robotic systems will be mentioned where appropriate but is not the focus of the research. Therefore, while suggestions for improvements to existing robots may be made, no design methodology or novel mechanical systems will be presented.

1.4 Contributions

The research presented here constitutes five distinct contributions to the research field, which are summarised here. Technical details of these contributions are given in each chapter, and they are discussed at further length towards the end of this thesis.

1.4.1 PSO-based Modelling Method

- Developed to address concerns with certain control methodologies, and to allow for model-based control approaches
- Phenomenological model based on mass-spring-damper approximation
- PSO method used to find optimal parameters for dynamic models of the PAM system
- Piecewise method used to account for nonlinearity - hysteresis and time-variance
- Compared to other modelling methods in literature:
    - Similar performance to other mathematical and phenomenological models but accounts for overshoot and hysteresis
    - Mathematically and computationally much more efficient than other methods, especially neural network methods
- Main benefits include:
    - Rapid model generation
    - Low model complexity
    - No requirement to know system parameters

1.4.2 MPC Algorithm for PAM Motion Control

- Predictive algorithm effectively accounts for time variance
- Increased use of compliant actuators in rehabilitation robotics makes accurate position control increasingly important
- In comparison with other commonplace control methods:
    - Lower error values
    - Faster response times
    - Reduced chattering

1.4.3 Experimental Comparison Data for Intelligent Control of Pneumatic Artificial Muscle

- Real-world comparison between controllers is essential to verify improved performance
- Exhaustive experiments including:
    - Full and partial stroke length
    - Low and high motion speed bordering PAM maximum contraction speed
    - Unusual setpoint patterns
    - Changing setpoint patterns
    - External loading and disturbance
- Results proved that intelligent controllers outperform classical, and specialised predictive algorithm proved most suitable for PAM control

1.4.4 MPC Algorithm for CARR Motion Control

- Two MPC algorithms: Single-model and Dual-model

- Based on the mechanical construction of the CARR, the upper and lower pairs of PAMs may exhibit different dynamic properties
    - Single-model assumes all four PAMs behave with the same dynamic properties
    - Dual-model assumes the angle of connection and gravity will cause the pairs of PAMs to behave differently
- System has increased complexity compared to a single PAM
- Compared with PID and ILC, both MPC implementations improved overall accuracy and response time
- Each model setup showed individual strengths and weaknesses

1.4.5 User Study for Online Validation of Model Predictive Controlled CARR

- A robot designed for human interaction, and with a human measure used for success, requires participant study to validate suitability
- Two measures gathered:
    - Motion tracking data to determine the effect of a user and associated disturbances on tracking accuracy
    - Participant responses concerning the experience to determine comfort and usability of the system
- Both single- and dual-model MPC used for comparison purposes
- Motion tracking results showed external disturbances are not accounted for by MPC, and each implantation had relative strengths and weaknesses
- Main participant response concerned comfort in sitting position based on height and proximity of footplate to calf rest

1.5 Thesis Outline

This thesis presents the work carried out in order to complete the above research objectives and is organized as follows.

Chapter 1 presents a background overview of the research field of Rehabilitation Robotics, their rise in necessity and the help they can provide to healthcare services and patients suffering from decreased joint range of motion from a variety of neurological and physical impairments. Some examples of different rehabilitation robots are shown with their differences and functionality summarised. The importance of control strategy development is highlighted with some common controller types explained and their relative merits discussed. The research aims and objectives are listed and the plan for their completion is outlined.

Chapter 2 presents a systematic review of the literature concerning intelligent controller use in rehabilitation robotics published between the years of 2015-2022. The findings summarise common research trends in the field, identifying the most commonly used control schemes and their relative performance metrics as well as potential gaps and opportunities for further research. The work presented in chapter 2 is published in IEEE Transactions on Neural Systems and Rehabilitation Engineering as:

- D. Felix Brown and S. Quan Xie, "Effectiveness of Intelligent Control Strategies in Robot-Assisted Rehabilitation—A Systematic Review," in IEEE Transactions on Neural Systems and Rehabilitation Engineering, vol. 32, pp. 1828-1840, 2024, doi: 10.1109/TNSRE.2024.3396065.

Chapter 3 introduces the feasibility study for intelligent control schemes used for pneumatic artificial muscles, as part of research objective 1. A simple setup is

created using a single PAM and linear displacement encoder, and a dynamic modelling method is proposed using particle swarm optimisation algorithm to generate accurate dynamic models of the actuator. This modelling method is intended for use later on as part of intelligent control schemes requiring plant models. The work presented in chapter 3 is published in Actuators as:

- Brown, D.F.; Xie, S.Q. A Piecewise Particle Swarm Optimisation Modelling Method for Pneumatic Artificial Muscle Actuators. Actuators 2024, 13, 286. https://doi.org/10.3390/act13080286

Chapter 4 concludes the feasibility study and realises research objective 1. 4 control strategies are developed and applied using PAM setup from chapter 3. These controllers are PID, PSO-PID, ILC and MPC. Through experimental validation, the MPC method is confirmed to provide the best motion tracking results and stability and is therefore considered for further work as part of research objective 2. The work presented in chapter 4 is published in Biomimetics as:

- Brown DF, Xie SQ. Model Predictive Control with Optimal Modelling for Pneumatic Artificial Muscle in Rehabilitation Robotics: Confirmation of Validity Though Preliminary Testing. Biomimetics (Basel). 2025 Mar 28;10(4):208. doi: 10.3390/biomimetics10040208.

Chapter 5 addresses research objective 2 using the Compliant Ankle Rehabilitation Robot (CARR). The mechanical layout and kinematics of the robot are presented. The PSO modelling method developed in chapter 3 is used in conjunction with the MPC developed in chapter 4 to apply intelligent motion tracking to the CARR. The controller is experimentally compared with PID and ILC. The work presented in chapter 5 is published in Biomimetics as:

- Brown DF, Xie SQ, Tu Y. Model Predictive Control with a PSO Modelling Approach for Position Control of a Compliant Ankle Rehabilitation Robot. Biomimetics. 2026; 11(5):349. doi: 10.3390/biomimetics11050349

Chapter 6 addresses research objective 3, with the CARR and developed MPC used in online experiments with participants. The participant's experience in using the system is recorded in a questionnaire, and the motion tracking results of the robot are measured. These results validate the functionality of the developed systems with users.

Chapter 7 concludes the work with a summary of contributions and suggested future work for further development of the developed systems.

1.6 Chapter Summary

As the field of medical robotics becomes increasingly popular in assisting healthcare services in reducing workloads and providing more accessible care, it is more important than ever that the devices designed for use with vulnerable patients and liable medical bodies are reliable, safe, and user-friendly. This chapter introduces a background to rehabilitation robotics as well as control systems used in rehabilitation robotics. The potential for improving the functionality of these robots with intelligent control is the focus of the work presented in this thesis. As such, the main objectives of this research are as follows: 1) Feasibility study for intelligent control of compliant actuators; 2) Application of intelligent control systems to compliant ankle rehabilitation robot; 3) User study of intelligently controlled ankle rehabilitation robot. Through these objectives and their associated contributions, the aim of the research to develop, implement, and experimentally verify an intelligent control system for effective and compliant control of an ankle rehabilitation robot will be achieved.

CHAPTER 2

EFFECTIVENESS OF INTELLIGENT CONTROL STRATEGIES IN ROBOT-ASSISTED REHABILITATION – A SYSTEMATIC REVIEW

This chapter aims to provide a systematic analysis of the literature focused on the use of intelligent control systems in robotics for physical rehabilitation, identifying trends in recent research and comparing the effectiveness of intelligence used in control, with the aim of determining important factors in robot-assisted rehabilitation and how intelligent controller design can improve them. Seven electronic research databases were searched for articles published in the years 2015 – 2022 with articles selected based on relevance to the subject area of intelligent control systems in rehabilitation robotics. Common usage, popular avenues of research, and performance evaluations for intelligent controllers used in rehabilitation robotics are summarised and analysed at the end of this chapter, and potential gaps and opportunities for further research are discussed.

The work presented in this chapter is published in IEEE Transactions on Neural Systems and Rehabilitation Engineering as:

- D. Felix Brown and S. Quan Xie, "Effectiveness of Intelligent Control Strategies in Robot-Assisted Rehabilitation—A Systematic Review," in IEEE Transactions on Neural Systems and Rehabilitation Engineering, vol. 32, pp. 1828-1840, 2024, doi: 10.1109/TNSRE.2024.3396065.

2.1 Introduction

There is an ever-increasing burden on therapists and healthcare systems due to the labor-intensive and long-term nature of treatment for physically impaired patients. Suffering from a range of both neurological and physical impairment such as stroke, cerebral palsy, sprains, and more, impaired patients often require a great deal of training and exercise over the course of many months to regain motion in affected areas.

To alleviate some of the workload on therapists and provide more of the needed care to patients, robotic rehabilitation is an open research field focused on developing systems to aid in the physical therapy of joints. This can be achieved by reducing the workload on therapists, providing more accurate therapeutic exercises guided by the robot, and increasing safety for both the therapist and their patient [10]. Many different systems have been developed in this field to be used for various joint exercises such as gait, ankle, and wrist rehabilitation [11, 12, 13], as well as specific research into the actuation and control of these systems [14]. The effectiveness of these systems is reliant on their ability to perform rehabilitation exercises accurately and repetitively. The safety of using these robots is also paramount as direct human-robot interaction is implicit in their design.

A number of reviews exist concerning rehabilitation robotics generally [15, 16] as well as specific applications of rehabilitation robotics [17, 18], and control techniques used in the field [19, 20]. This chapter aims to systematically search and review articles focusing on machine intelligence used in control systems for physical rehabilitation robotics. The relative effectiveness of these systems in terms of rehabilitation outcomes will be discussed and compared, important factors in improving rehabilitation outcome will be determined, and any notable research trends found will be established. In particular, the benefits and shortcomings of commonly used intelligent controllers will be discussed in the context of rehabilitation robotics.

A comprehensive search and discussion of literature focused on intelligent control of rehabilitation robotics, published in the years 2015 to 2022 to ensure up to date research, will be presented. Experimental and clinical data published as part of these articles will be examined and analyzed.

2.2 Method

2.2.1 Search Strategy

This review was limited to articles, including journal articles, conference proceedings and book chapters, published online in English. This includes articles not originally published in English which have since been translated into English. The search only includes articles published between the years 2015 – 2022. As the field of machine intelligence is rapidly increasing in popularity, the scope of this review is limited to the most recent publications and advances in the field.

Seven electronic databases were chosen for this review based on relevance to the subject area of medical engineering and volume of articles available: PubMed, ScienceDirect, Web of Science, DOAJ (Directory of Open Access Journals), Cochrane Library, Wiley Online Library, and IEEE Xplore. A free search of Google Scholar was also conducted to ensure the search was as thorough as possible and included relevant publications missed in the database search.

The search terms and search strings used for each database were tailored to the specifics of the database's search function to ensure each search was as comprehensive and relevant to the research question as possible. The general search terms used were "Robot*" AND "joint*" AND ("rehabilitat*" OR "treat*") AND "control*" AND ("system*" OR "algorithm*").

2.2.2 Inclusion/Exclusion Criteria

Robotics has been defined as "The application of electronic, computerized control systems to mechanical devices designed to perform human functions [21]", while a control system or control strategy is "a system of devices or set of devices, that manages, commands, directs or regulates the behavior of other device(s) or system(s) to achieve desired results [22]". This review will consider software control systems to be defined as "devices" in this nature, and thus any article utilizing a software control system will be included. Any robot not using a control system that is in some way automatic will be excluded. Articles that focus on bioelectric feedback such as surface electromyography will be included only if they also include comparison or reference to other control systems, as this constitutes a sensing system rather than a control system.

A rehabilitation robot will be defined as any robot designed to aid in the physical therapeutic recovery of a person suffering from neurological or physical injury.

As the aim of this review is to determine important factors in improving rehabilitation outcome, articles on purely assistive robots such as assistive exoskeletons or prosthetics will be excluded as their purpose is not rehabilitation of the targeted limb, rather assisting their motion for day-to-day tasks. As the review focusses on the rehabilitation outcome and control schemes used, there will be no intentional bias or exclusion criteria concerning which limb or joint is targeted for rehabilitation.

Articles including clinical trials of rehabilitation robots as well as simulation results will be included, so long as there is sufficient mention of the control system used.

This review focuses on intelligent control strategies used in rehabilitation robotics. Machine intelligence is notoriously difficult to define [23] with multiple conflicting definitions in literature [24], so here intelligent control systems will be defined as any which use machine learning or data-driven adaptation to adjust any control parameters, either during use or for optimisation of the control system parameters. Any article concerning the type of intelligent control system used in a rehabilitation robot will be included, with a particular focus on those which quantify the effectiveness of any control strategies mentioned. Articles not mentioning a control system, or those with no particular focus on the control system used, will be excluded, as well as articles which present traditional control strategies lacking intelligence.

2.2.3 Stages of Review

After searching each database, the articles were collated in a document for screening. Identical articles found in multiple databases were removed. The

article titles were then screened for relevance to the research question, and some were removed based on the inclusion/exclusion criteria.

The abstracts of the remaining papers were then read, and the papers further screened for relevance with more thorough exclusion criteria. The full texts of the final articles in review were then read and organized based on relevant research for discussion and data extraction. Articles found during the Google Scholar free search were included at the abstract screening stage as they were initially selected based on title relevance during the search.

2.2.4 Search Results

A total of 635 articles were found using the search method detailed in the previous section. 123 of these were found to be duplicates from different databases and were removed, resulting in 512 unique articles.

196 of these articles were removed based on their titles due to the exclusion criteria, mostly due to irrelevance in the subject area of control systems and rehabilitation robotics. 68 articles were excluded based on reading their abstracts due to lack of focus on control systems in favor of the mechanical design of the robot instead. Several literature review articles were also excluded at this stage. 248 articles met the inclusion criteria based on their abstracts, while 17 further articles were found during the Google Scholar free search which met the inclusion criteria.

After reading the full text, 48 of the remaining articles were excluded from review due to having little or no relevant discussion concerning control systems, a further 91 were excluded later due to lack of unique or relevant data and discussion points, and 56 were excluded due to exclusively using traditional controllers with no intelligence. 70 articles met the inclusion criteria for this

review, discussing intelligent control systems used in various types and models of rehabilitation robots and their relevant successes/failings.

2.3 Review Results and Analysis

Intelligent control systems have become a major focus of research for rehabilitation robotics in recent years given their ability to adapt to patient specific needs, enhancing safety and effectiveness of treatment. Most articles making use of an intelligent controller focus on it as a specific subject of research, some alongside the development of a rehabilitation robot, but others apply the controller to an existing robot.

Figure 2.1 shows a generalised control system diagram for a rehabilitation robot, including both feedforward and feedback loops, as well as the potential usage of various sensors and sources of noise and disturbances to the system. Not all features shown in the diagram will be present in all developed systems depending on the type of controller and its intended specific use case. The labeled control system section of the diagram will differ greatly from study to study. As such, Figures 2.2 and 2.3 present more specific controller cases, which are discussed in detail in later sections.

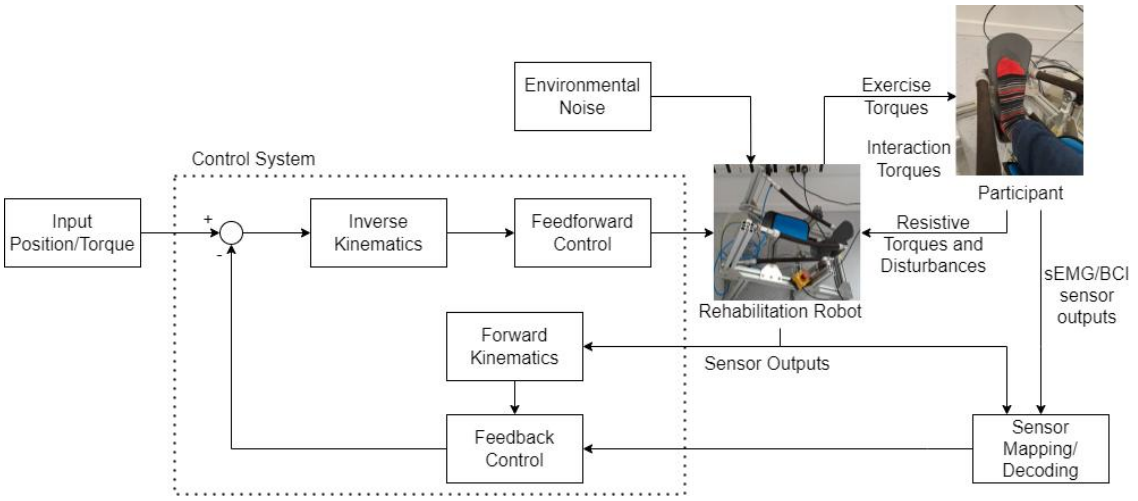


Figure 2.1: A generalised diagram for control of a rehabilitation robot. This controller diagram is applicable to the majority of rehabilitation robots.

Two main control paradigms are present in terms of rehabilitation robotics control, being passive and active control. Passive control focuses on position, with the robot guiding a patient's joint(s) through a series of predetermined motions with little or no sensing or human input to guide the training. This sort of control is suitable for patients with little motor function in the targeted joint but is inherently non-compliant and therefore the motion must be carefully regulated to ensure proper training is achieved and safety is ensured. Active control regulates the applied torques of the robotic joint to assist or resist the motion of the patient, in order to either guide motion to build muscular plasticity, or to provide resistance to improve strength. Certain control schemes are more suitable for either passive or active training, depending on their ability to react to disturbance or sensor input and whether they are specifically designed to follow trajectories or to provide torque outputs. Many articles present both passive and active training methods, often with different control schemes used for each.

2.3.1 Control Optimisation

Proportional Integral Derivative (PID) and Proportional Derivative (PD) controls are often used as the baseline controller for many robotic systems. These traditional control schemes use gain parameters for the input, its integral function, and derivative depending on the implementation to calculate control signals. Some research has gone into optimizing traditional control algorithms by applying intelligent algorithms to adjust the control gain parameters, allowing the linear controllers to perform more dynamically and more effectively reject disturbances to the system by dynamically responding to errors. Particle swarm algorithms are used to optimize PID parameters in [25, 26, 27, 28], with [27] developing a novel artificial bee colony algorithm for parameter optimisation. Particle swarm algorithms use a number of agents referred to as 'particles' in a search space of dimensions equal to the number of parameters and use an iterative process to move these particles towards an optimal solution for some objective function. The sharing of information between particles allows the 'swarm' to behave as a group, which speeds up the process. Adaptive simulated annealing method is used for parameter optimisation in [29]. Zeigler-Nichols is used in some articles for optimisation but is only mentioned briefly and is rarely a topic of focused research, however, [27] does compare two intelligent optimisation techniques with Zeigler-Nichols as a baseline. This optimisation method is specific to PID control and relies on raising the proportional gain value until the system is unstable, then calculating the integral and derivative gains based on the resulting oscillations. Results from these articles show that optimised versions of the controller consistently have better motion tracking accuracy and robustness to external disturbances and noise. The comparison results from [27] found that the developed artificial bee colony optimisation

method performed better than swarm optimisation and Ziegler Nichols in terms of error correction and settling time but had a slower response time.

Genetic Algorithms (GA) are used in several cases for optimisation of different control schemes. This optimisation method generates a population of solutions and iteratively 'evolves' them based on the objective function by sharing traits and randomly assigning new ones. GAs are used to optimize the respective control strategies in [30, 31, 32, 33, 34], while [35] uses GA to estimate friction for the robot dynamic model. GA is used to optimize joint angle and velocity parameters in a control system with a multi-layer perceptron neural network in [30]. A GA presented in [31] is used to determine and optimize impedance parameters. This controller was validated in an experiment with a patient to provide good compliance and low patient-machine interaction torques. GA is used to optimize PD control in [32], and for Sliding Mode Control (SMC) in [33, 34].

2.3.2 Fuzzy Logic Control

Despite existing for decades, fuzzy logic has become a popular logic structure for controllers in recent years with many articles utilizing it for controller development since 2015. Fuzzy logic is considered a subset of AI given its ability to make decisions by grouping continuous data into discrete subsets. This allows for many inputs/outputs to be accommodated and can assist with modelling nonlinear systems. Fuzzy logic is often applied to non-intelligent controllers such as PID as a method to improve their functionality. Fuzzy PID controllers are used in [36, 37], with [38] using fuzzy PD control. Fuzzy SMC is used for motion control in [39, 40, 41, 42, 43, 44, 45]. Fuzzy logic is used for impedance control in [40, 46, 47] and for admittance control in [41, 45]. Impedance control uses the ratio of position and force to control the force output by the system, while

admittance control uses this ratio to control the position output. Collectively these methods are sometimes referred to as compliance control. Control algorithms simply referred to as fuzzy control are used in [48, 49]. Experimental data is presented in [36] comparing a proposed fuzzy PID controller to standard PID with an unimpaired participant. The results show both controllers have overall acceptable tracking performance, but the fuzzy controller performed better. Fuzzy SMC with adaptive gain is used in [39] and is experimentally verified in both passive and active control modes. A proposed Integral sliding mode impedance control with fuzzy adjustment (IFSMIC-TDE) is experimentally compared with model-based sliding mode control in [40] with three participants. All three experiments show the superiority of the fuzzy-based controller, with smaller time delays, less chattering, and smaller impedance errors than the model-based method. Fuzzy SMC using PID-based sliding surfaces is developed in [43] and is compared with a standard PID controller in an experiment with an unimpaired participant, and the results show the proposed controller has improved tracking performance and reduced chattering. An experiment with 10 stroke patients is presented in [49] in which 5 patients use the proposed lower limb rehabilitation robot and controller for training in 20 15-minute sessions over the course of four weeks, and 5 patients designated the control group were treated with conventional post-stroke rehabilitation. Of the patients who used the robot, 3 exhibited improvements in their lower limb recovery, while none in the control group did. Experiments are presented in [42, 45, 46] to validate their respective fuzzy controllers, each finding them to have accurate motion control with minimal tracking error.

2.3.3 Adaptive Controllers

The focus of intelligent control in rehabilitation robotics is to make the robot more adaptive, allowing it to reject disturbances and adjust training or control parameters to better suit different patients or sensor inputs dynamically. Adaptability can also help provide safer and more comfortable rehabilitation by reducing the interaction torque between user and machine, also referred to as improving the transparency of the system. Figure 2.2 shows a general diagram of an adaptive control system, as an example of a specific application of the Control System section shown in Figure 2.1. The torque/position control block will differ depending on the specific use case from study to study.

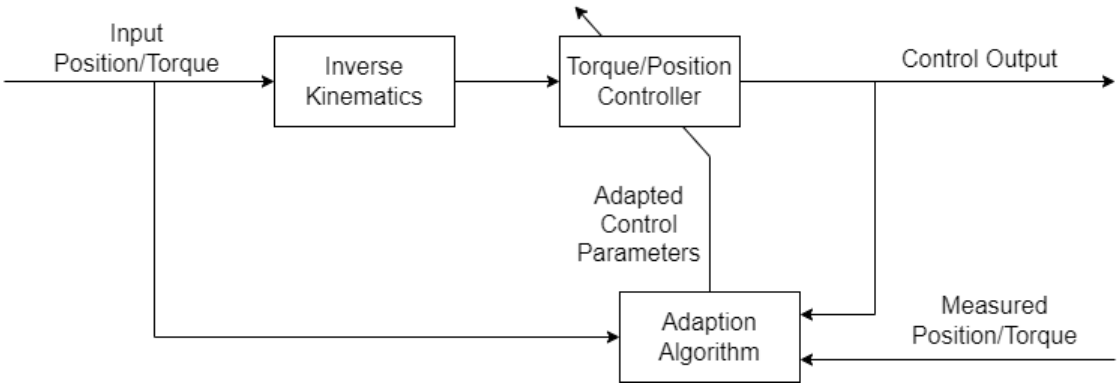


Figure 2.2: A generalised adaptive controller diagram. The Adaption Algorithm block includes the adaptive law for the system and represents the use of intelligence in adaptive controllers. The adaptive law is typically unique to the controller/study it is presented with.

While adaptability is the aim of most intelligent controllers mentioned here, several articles specifically mention the use of adaptive controllers [25, 29, 37, 38, 39, 40, 41, 42, 47, 48, 50, 51, 52, 53, 54, 55, 56, 57, 58, 59, 60, 61, 62, 63, 64, 65, 66, 67, 68, 69, 70, 71, 72, 73]. Most of these apply adaptive algorithms to other control schemes such as PID or SMC. Fuzzy logic is also often used in adaptive

controllers to help approximate system models and plants which are impossible to define with purely mathematical models. Among the articles presenting an adaptive controller, the most numerous is adaptive SMC. Adaptive PID and PD are also present, with a few using adaptive impedance and admittance control. Many of these controllers use fuzzy logic in their adaptive algorithms, while some use neural networks which will be discussed in more detail in a later section. Adaptive Iterative Learning Control is presented in [50], while [59] presents adaptive state-space control, and [66] develops a wholly novel adaptive controller based on motor primitives. The hybrid shared controller developed in [72] uses both a Mode Insertion Gradient algorithm and Optimal Controller Inner Product to adaptively adjust impedance parameters in response to user input. Another novel adaptive controller is presented in [73], with a Minimal Assist As Needed (mAAN) control scheme. This algorithm uses sensorless torque estimation to dynamically react to user inputs and adjust torque parameters accordingly. The article also presents a bound modification algorithm for adjusting allowable error, and a decayed disturbance rejection algorithm for encouraging voluntary movement during training. Generally, the purpose of adaptive algorithms in control is to dynamically adjust the control parameters during exercises based on sensor feedback or learned behaviors to provide better rehabilitation care, improve patient comfort, and optimize the output of the system. Experimental results from these articles consistently prove that adaptive control is fit for purpose. In comparative studies, it outperforms non-adaptive controllers in terms of tracking performance and stiffness control, exhibiting lower error values.

2.3.4 Learning Control

Iterative learning control (ILC) is used in a number of articles in this review. It is a tracking algorithm that relies on the system repeating a pre-set series of movements or impedances, depending on the operating mode, and iteratively adjusting parameters to better fit the required motion given the resulting sensor outputs. This allows for very accurate and repeatable motion but requires several repetitions to converge properly, meaning initially the movement is typically inaccurate. Figure 2.3 shows a general diagram for implementation of ILC in a rehabilitation robot as an example of a learning control loop. This diagram is an example of a specific application of the Control System section shown in Figure 2.1.

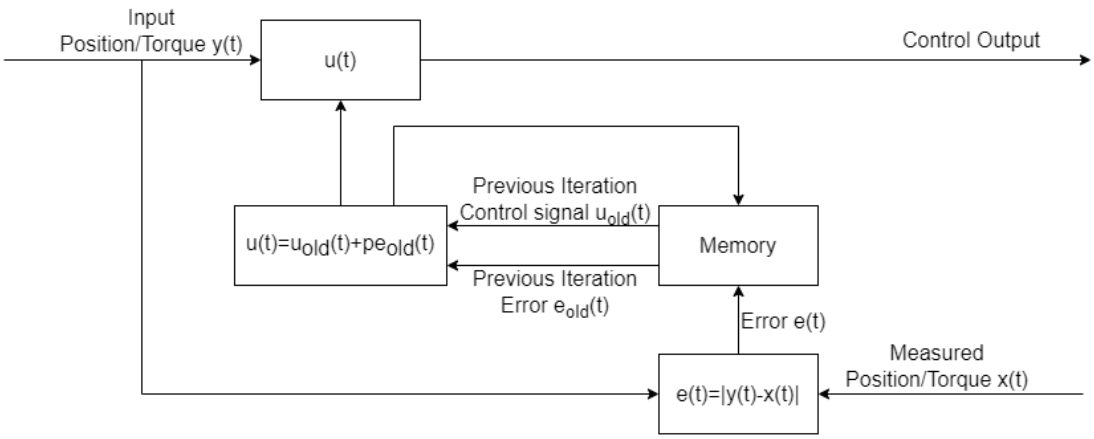


Figure 2.3: A generalised Iterative Learning Controller diagram.

ILC is used for motion control in [53, 74, 75, 76, 77, 78, 79, 80]. Experimental results are presented in [75, 77, 79] validating their respective implementation of ILC. The results in [75] show the iterative learning impedance controller is capable of consistently converging error to 0 in response to interaction torques. Experiments with 8 unimpaired subjects are presented in [77], the results of which show stable and safe interaction forces between subject and robot, as well

as adaptable parameters allowing for training exercises of different difficulties. The results presented in [79] from experiments with 3 unimpaired subjects show that the tracking error of the joint movements become smaller with increasing numbers of repetitions. Results comparing ILC with other controllers are presented in [76, 78, 80]. Active Disturbance Rejection Control (ADRC) and PID are each compared with ILC combined with ADRC in an experiment with one participant in [76]. ILC-ADRC showed faster response time and better disturbance rejection than PID, and better tracking performance than standard ILC, consistently proving it the most suitable of the tested controllers. ILC based on PID is compared with ILC based on nonlinear control in [78]. Both controllers decrease in error over more iterations, but the overall error of the PID-based controller was larger. The nonlinear method has better performance with negligible increase in required torque. Two algorithms are proposed in [80], norm-optimal ILC (NOILC) and Optimization-based proportional-type ILC (OPILC). Both controllers converged to the reference trajectory with OPILC having a more damped response.

Intelligent controllers in literature often make use of neural networks in various applications, some applied directly to the controller to learn parameter settings, some used for sensor feedback, as well as for disturbance compensation and value estimation. Many types of neural network exist but all operate on similar principles, with a network of 'neurons' which activate on a certain input threshold determined by gain parameters learned through training and pass the data on to the next layer of neurons. The different possible activation functions and limitless configurations make neural networks applicable to nearly any computational problem. Neural networks are used in software design in articles [47, 51, 52, 53, 76, 80, 81, 82, 83, 84, 85, 86, 87, 88, 89, 90]. The types of networks used in the

literature discussed here are backpropagation and convolutional neural networks, Radial Basis Function networks (RBF), as well as long-short term memory networks (LSTM). RBF networks are used mostly for compensation for disturbances and unknown values, and there are no examples in this review of RBF networks being used for motion prediction or classification. A reinforcement learning neural network is used in [51], and a central pattern generator neural network is used in [82], both used as the basis of the motion controller proposed in their respective articles. Some of these articles compare their proposed controller's network with other types, and [86] develops and tests both LSTM and convolutional neural networks for joint position prediction but does not compare the two. Results from articles with experiments or simulations consistently prove that the network used is fit for purpose, and those which compare neural networks with other algorithms and methods prove that the network performs better. Two different neural networks are compared in the same application in [83, 84, 87]. A LSTM neural network is used to create a motion perception model for control of an upper limb exoskeleton in [83], and through experiments compared to backpropagation neural network, finding that the LSTM had better performance with lower prediction error. An experiment comparing the effectiveness of several algorithms for a motion classification system is presented in [84], including perceptron and convolutional neural networks. The convolutional neural network performed the worst of the tested algorithms in terms of classification accuracy. A backpropagation neural network is used for mapping relationships between surface electromyography (sEMG) sensors and knee joint angle in [87], finding through experiments that it is superior to LSTM neural network as well as Support Vector Regression methods. The results from [83] and [87] seem to suggest that LSTM neural networks are better suited for

motion intention prediction, while backpropagation is better suited for mapping sensor outputs. Several articles [53, 84, 87, 88] compare different methods or algorithms incorporating the same type of neural network.

2.3.5 Other Controllers

A nonlinear Model Predictive Controller (MPC) is presented in [91] for more compliant human-robot interaction. MPC uses a model of the dynamic system as well as knowledge of future input values to predict future states, allowing for optimal control with future system states taken into account. The system is simulated with input torques mimicking an unimpaired and an impaired subject. In both cases the controller performs as expected, properly guiding trajectories in response to interaction torques.

K-nearest neighbors, another learning algorithm which uses proximity to make classifications and predictions, is used for motion control in [92] based on sEMG sensors by identifying motion intention. This method is experimentally validated to have a good identification accuracy rate but becomes less accurate the greater the applied load to the system. A probabilistic trajectory tracking algorithm for passive mode control and a system identification model to adapt and adjust an impedance controller in response to the user's anatomical stiffness in the active mode are both presented in [93]. Data gathered from a passive mode experiment was used to estimate anatomical stiffness for the active mode. In active mode the forces applied by the robot were considerably higher towards the extremities, and concerns for system instability in highly unstable environments were raised. It is noted that these two experiments constitute some of the only results in this review which critically evaluate their respective controllers, raising valid concerns for their functionality, rather than just concluding that they are fit for purpose.

2.3.6 Controller Comparisons

While most articles in this review use a single controller for their respective rehabilitation strategy, several experiments and simulations have been done comparing different controllers using the same platform to determine which performs best under certain conditions. Most of these comparisons are done to validate the controller developed in the article by presenting its superior qualities over more traditional controllers, most often PID, but some develop multiple controllers and compare them against each other to determine which is the most suitable for the application. All articles which compare multiple controllers using the same robotic platform either experimentally or in simulation are presented in Table 2.1. In all cases where a new controller is designed and compared with a more common classical controller such as PID, the new controller is found to be superior in performance, with the most common measure being trajectory tracking. In cases where an intelligent controller is compared to a non-intelligent controller, the intelligent controller invariably performs better. Due to the abundance of novel controllers in literature there are many comparisons missing. This makes it practically impossible to determine which controller is objectively the best for different aspects of rehabilitation such as transparency, personalization, or different control modes.

2.4 Discussion

2.4.1 Summary of Results

A summary of the algorithms used in the literature reviewed here is presented in Table 2.2, alongside observed advantages, disadvantages, and general application scope for each. Some of the most used controllers such as PID and SMC have

recently been used as the basis for intelligent controllers through adaptive algorithms to dynamically adjust control parameters, optimisation techniques, and sensor feedback systems. Passive and active control schemes are used in equal number, and most rehabilitation systems are designed to accommodate both, as they are necessary for different stages of the rehabilitation process, and this often requires multiple different control systems. Intelligent controllers have become more prevalent, making use of adaptive algorithms, neural networks, fuzzy logic, and other decision-making processes to allow rehabilitation robots to react to different patient needs and data training. This allows for improved tracking accuracy, robustness to disturbance and noise, as well as more personalized training exercises over non-intelligent systems. These improvements are presented in comparative experiments and simulations, as summarized in Table 2.1. Many articles present results comparing controllers on the same platform, with PID being the most used controller for comparison and generally considered the baseline to improve upon. In recent years compliance control and assist-as-needed control have become popular in the field of rehabilitation robots. Given the specific need for accurate force output and safe human-machine interaction, impedance and admittance control schemes prove highly effective at providing active control. Assist-as-needed control has similar usage in rehabilitation but specifically provides the minimal amount of assistance for the required task to be completed. These control methods have been shown to improve active participation in exercises, which is connected in many cases with improved rehabilitation outcomes.

2.4.2 Safety and Ethical Considerations

While the focus of many articles in this field is on the accuracy of motion and torque control, most also discuss transparency and human-robot interaction. This is essential to any robot which directly interacts with a human, and especially in rehabilitation robots as the interaction is prolonged and typically with an injured or impaired limb. The interaction force between robot and human must be kept low enough as to not injure the user but must also still be able to guide movement or provide sufficient resistance. Many experiments presented in these articles measure interaction torques to determine transparency of the system.

The compliance of the robot is another important consideration in terms of safety in rehabilitation. Solid driven actuators are inherently noncompliant, meaning motion of the user's joints are forced along the motion path of the robot. While this may assist in the efficiency of training and help promote more motion in the joint, it is unsafe in the case of rapid or unplanned movement on the user's part. This could cause injury or damage to the patient and the robot. Some systems instead opt to use compliant actuators, some of the more popular being artificial pneumatic muscles and series elastic actuators. These actuators allow for some patient-driven movement in multiple axis making them safer, but present problems in control as this inherent compliance can impact the tracking accuracy of the system. More complicated dynamic models are required to control systems based on these actuators.

Patient safety is the most discussed ethical concern in relation to robot-assisted rehabilitation, yet as an automated healthcare system more considerations are present which are less mentioned in the literature. Loss of human interaction could impact the effectiveness of rehabilitation as the improvement of these systems allows for more at-home treatment without the need for a therapist.

Accountability is another ethical consideration which is related to safety, as in the case of an injury with an automated system the person or group responsible is often nebulous. One aspect which is addressed by intelligent control is the potential loss of personalized care. In treatment with a specialist rehabilitation therapist, the condition suffered by the patient can be treated with specialized exercises, and this is lost in the case of predefined trajectories or impedance tasks. Intelligent systems can be applied to learn the needs of the patient and allow for more personalized care, and this is the topic of research in many articles focusing on machine learning control strategies. However, machine intelligence introduces another ethical dilemma. A machine learning system requires a large quantity of data to properly learn required joint torques and movements for rehabilitation exercises, and the collection of such large datasets could result in privacy issues as the incentive for data collection campaigns increases.

Risks are introduced by giving an automated system the free reign to alter larger aspects of the training, and these high-level decisions should always be made by a therapist, as errors in the machine's judgment could have serious ramifications on both the patient and the medical body responsible [94].

2.4.3 Meta-Analysis and Evaluation

After extracting data from all articles presenting experiments with human participants, it was found that the vast majority of these experiments did not include impaired subjects in their participants, with only 9 articles presenting results from experiments with impaired subjects. The results of these experiments are summarized in Table 2.3. Some of these results focus on the performance of the controller, but those which focus on the rehabilitation outcome all find that impaired subjects improve in motion range or accuracy.

Unfortunately, there were no studies in this review in which different control strategies are used for rehabilitation of impaired subjects and their effectiveness compared.

While there are other examples of experiments with participants, these are unimpaired and therefore present less useful data for this review. The effectiveness of rehabilitation is only properly measurable with a subject able to benefit from it, however the purpose of these experiments can help realise important factors in validating these systems. The most prominent of these factors is the tracking and/or torque accuracy of the control scheme used as this is the most common measure in experiments. Specifically, the most common measure in experiments is joint angle and Root-Mean-Squared Error (RMSE) in terms of deviation from the reference trajectory provided by software. Some experiments also measure the output directly from the controller or sensors to check their functionality and directly compare with the system outputs. In articles which utilize sEMG the force estimation from those sensors are typically presented as well.

As each article typically focuses on a different rehabilitation robot platform for different joints and applied with different training motion exercises, comparison between them given the data presented in experiments is made difficult. Every article presents data suggesting the controller proposed is suitable for the application, and every article comparing a developed controller experimentally to others shows that it is superior to all others used. The only consensus between articles is that those which use intelligence in the controller consistently outperform those which do not, typically in terms of motion tracking error or torque output error, and rejection of disturbances to the system. The importance of these measures in clinical practice is that lower motion tracking or torque

output error allows for more repeatable and accurate therapeutic exercises, and better disturbance rejection helps keep the patient's motion in line with the expected motion.

Participant comfort is only explicitly mentioned in [55]. It mentions comfort in terms of robot compliance and that the interaction forces of the robot must be set to ensure patients feel comfortable using it. Comfort is an important factor in rehabilitation as it can help patients actively engage in training and not distract or impair further, which is an issue that can be solved with improved compliance and better transparency, but also physically more comfortable surfaces between the robot and the patient. There is an inherent loss in patient feedback, especially patient comfort, when using robotic assisted therapy with no attending physiotherapist, and no articles reviewed here attempt to rectify this by incorporating user-input feedback systems or intelligence designed to detect patient comfort.

The most important factors in a rehabilitation system as determined by literature are: tracking performance of motion or force application; safety of human-robot interaction achieved by transparency, low interaction force, and compliance of the machine; and active and engaged participation of the subject. Patient engagement is a subject discussed in greater depth in [95]. A robust controller is essential for good tracking performance, but this can be achieved by most conventional controllers with good optimisation and parameter tuning. Compliance of the machine is a uniquely physical property that is best implemented with inherently compliant actuators. Intelligent control can allow for improved transparency, as well as more engaging and personalized training motions, and safer interaction forces.

2.4.4 Gaps and Opportunities

There exist some gaps in the literature regarding intelligent controllers used in rehabilitation robotics. The effectiveness of the training on patients who would require it in a clinical setting is not well represented, with very few articles presenting experiments with impaired participants and even fewer showing long-term effects of the training. Critical evaluation of newly developed control schemes is also lacking. Most articles presenting a novel controller conclude from their results that it is fit for purpose and meets evaluation criteria, but they rarely discuss shortcomings or potential improvements to be made. Articles [92, 93] are exceptions to this, and it is noted they do not use conventional control schemes in their development, rather developing novel algorithms. To determine which algorithms or control schemes are most appropriate for certain situations, or which is the best comparatively, articles should include any failings of the system or limitations of the results presented to allow for critical analysis of the research. More recent studies published in the past year give a good insight into the future directions of the field. The system presented in [96] uses brain-computer interface (BCI) for improved control of a lower limb rehabilitation robot, with a Convolutional Neural Network trained to classify sensor inputs and motion intention. This system is tested online with two subjects to verify its functionality. The article includes significant insight into future work, mentioning improved feedback, greater training data diversity to improve generalization, and optimisation of algorithms to improve response times. A bio-inspired control design based on the function of the cerebellum in mammals is presented in [97]. This novel neural network design is used to control an upper limb rehabilitation robot actuated by an antagonistic pair of pneumatic muscles. In simulation this control method was compared with traditional controllers and shown to

effectively compensate for uncertainties and disturbances. An adaptive sliding mode controller designed to improve safety in upper limb rehabilitation exercises is presented in [98]. The system uses interaction force estimation to adjust training dynamically. The article recommends that the system cannot quickly evaluate additional information such as stiffness and damping, and suggests future work be done to improve the system in this regard as well as using the system in robots without force sensors in order to reduce costs.

Recent work, as well as the research trends in the other literature reviewed here, suggests that intelligent control design is quickly becoming the focus in the area. Novel controllers frequently make use of computational decision-making processes like neural networks and fuzzy logic in various aspects, including intention detection, motion prediction, and sensor input mapping. There is also a focus on making rehabilitation systems more intuitive, comfortable, and safe to use, alongside the typical focus of tracking accuracy and robustness in these studies.

In order to address the gaps present, this research will validate any developed control systems in comparison with multiple other controllers of different types and result analysis will be critical, discussing both successes and failings. This will ensure that potential future work can be easily identified and improvements can be made. Any system developed enough to be suitable for human users should be validated in online experiments with participants. As the intended use case of rehabilitation robots is in a clinical setting, and a system's potential suitability cannot be measured using tracking accuracy alone, validation with participants including user responses is important to ensure a system is suitable.

Table 2.1: Articles Comparing Control Systems

Articles	Control systems compared	Relevant results/ conclusions
Q. Wu et al. 2019 [40]	Integral Fuzzy SMIC with Time-Delay Estimation (IFSMIC-TDE), Model-Based SMIC	IFSMIC-TDE has smaller error and chattering degree in multiple tests
T. Goyal et al. 2022 [48]	Fuzzy, Adaptive fuzzy	Adaptive controller has significantly smaller tracking error
Q. Wu et al. 2019 [52]	Adaptive Admittance Control with NN Disturbance Observer (AACNDO), Fuzzy cascade PID	AACNDO has smaller tracking errors and better adaptability than FCPID
Z. -Q. Ling et al. 2021 [87]	BPNN position estimation, SVR, LSTMNN	BPNN had lowest error and closest fit to motion curves. LSTMNN had partial deviation. SVR had worst performance
Xiu-Feng Zhang et al. 2018 [88]	Pattern recognition using PSO BPNN, BPNN	Network recognition rate increased across all measurements when optimised. Response time is fast
P. Zhang et al. 2020 [53]	RBFNN-based adaptive SMC, Variable SMC, PID, RBFNN, Continuous terminal SMC, Decentralized adaptive robust control	Variable SMC had severe chattering. This was reduced with RBFNN-based. RBFNN-based also had best tracking performance
W. Qian et al. 2021 [58]	Adaptive SMIC, PD impedance, SMIC	Adaptive SMIC had smallest error. Parameters converged after 20s
Wilian M. et al. 2019 [61]	Optimal impedance via model predictive control, Impedance control	Model predictive controller adaptively adjusts stiffness. Impedance has bad stability at low impedance, forces patient motion at high impedance
G. Ding et al. 2018 [68]	Adaptive proxy-based SMC, PID, Adaptive PID, Proxy-based SMC	Adaptive controllers have superior performance. APSMC maintains performance with different users where PID and PSMC do not
M. Ketelhut et al. 2020 [80]	Norm-Optimal ILC, Optimization-based Proportional-type ILC	Both controllers converge after six iterations. Norm-Optimal has low frequency oscillation after five iterations. Optimization-based has more damped response
Y. Li et al. 2020 [67]	Model Free Adaptive Control (MFAC), Improved MFAC (IMFAC)	IMFAC has better control performance, robustness, stability than MFAC
J. Liu et al. 2018 [70]	Adaptive SMC, SMC, PID	Both SMC have good tracking performance. Classical SMC shows chattering. PID has worse tracking performance than ASMC
Z. Shen 2018 [36], Q. Wu 2015 [43], L. Cheng 2018 [76], J. Li 2022 [54], Shen, Z. 2019 [71], Xiaohong Cui 2021 [77], S. Zhang 2016 [37], Y. Wang 2021 [47], X. Zhu 2015 [78], A. M. M. Ali 2021 [69]	Fuzzy PID, Fuzzy SMC with PID-based sliding surfaces, ILC with ADRC, Adaptive gain function with cascade PID, Adaptive robust position admittance, ADRC, Fuzzy adaptive impedance, Nonlinear ILC, Model Reference Adaptive control, each compared with PID	PID used as comparative baseline. All controllers have superior characteristics in respective experiments. Tracking performance, response time, interaction force, stability all worse with PID
J. Wang et al. 2019 [44]	Fuzzy compensation SMC, PD	PD showed tracking errors, movement delays, fluctuation under disturbance. FCSMC improves on these

Table 2.2: Algorithm Advantages and Disadvantages

Algorithm	Article Count	Advantages	Disadvantages	Application Scope
Proportional Integral Derivative	32	Computationally efficient, easy to implement, universally used and documented	Nonlinear and time-invariant, often inaccurate, no intelligence without additional algorithms	Applicable to any control problem but with limited effectiveness on complex systems
Sliding Mode Control	15	Nonlinear control functionality, effective at mitigating uncertainties and disturbances	Susceptible to chattering	Wide applicability to various control problems especially those with system uncertainties and bounded disturbances
Particle Swarm Optimisation	4	Applicable to any dimensional search space/optimisation function	Poor initial accuracy due to learning period, does not guarantee global optimal solutions	Optimisation method suitable for many applications including controller parameters and system modelling
Genetic Algorithm	5	Capable of optimizing very large and complex datasets, applicable to cases where traditional optimisation methods struggle	High complexity causes inefficiency for simpler optimisation problems, high computation times	Complex, nonlinear, nondifferentiable optimisation problems in many applications
Adaptive Algorithms	34	Improved response to system and sensor inputs over time	Increases computational complexity of the applied algorithm	Improvement to other algorithms to allow for improved functionality over time
Fuzzy Logic	14	Allows for heuristic decision making in data processing	Can lose some data accuracy, requires thorough testing and verification	Improved decision-making functionality in many algorithms
Iterative Learning Control	8	Model-free control of any system complexity, approaches optimal tracking control over time	Poor initial accuracy due to learning period, can result in overfitting, requires repeated input	Control of any system with repeated input function
Neural Networks	17	Deep learning allows for advanced decision making based on learned data values	Requires large amounts of training data for effective decision making	Applicable to all manner of computational decision making
Model Predictive Control	2	Optimal control for current and future timeslots	Requires a system model and future input values	Optimal control of systems with known mathematical models and input functions
Impedance Control	16	Force control helps provide safe human-robot interaction	Limited in scope to systems with required force outputs and position sensors	Applicable to systems where output force must be accurately maintained and controlled
Admittance Control	7	Position control allows for intuitive human-robot interaction	Reactive control method, cannot be used as standalone position/force controller	Applicable where interaction forces with the system should guide its motion, such as in encouraging motion in therapeutic exercises
Assist-As-Needed	1	Encourages user participation in exercises, can improve rehabilitation outcomes	Limited to use in rehabilitation robotics, requires a system model	Improved user participation in rehabilitation and assistive motion systems

Table 2.3: Experimental Results with Impaired Participants

Article	Subject Characteristics	Age	Rehab/Experiment Type	Control System	Measures	Outcomes and observations
Huang, YC et al. 2021 [49]	10 stroke patients	Not specified	Lower limb rehabilitation	Fuzzy	Brunnstrom motor recovery status	Control group did not improve, 3/5 in training group improved
Miao, M.d. et al. 2022 [81]	1 unimpaired, 1 patient (Pathology not specified)	Unimpaired 26, patient 52	Gait rehabilitation	SMC with RBF NN adaption	Motion trajectory, control torque, gain coefficients	Good coherence on straight track. Curved track had errors. Unimpaired subject affected better than patient
J. Chen et al. 2021 [31]	1 patient (Pathology not specified)	Not specified	Active training with lower limb exoskeleton	Genetic impedance and SMPIC	Joint angle, torque, GA fitness values, joint position	GA gives good interaction. Controller has good robustness and tracking
M. Zhang et al. 2017 [55]	1 ankle sprain, 1 drop foot due to stroke	Ankle sprain 29, drop foot 68	Ankle rehabilitation	PID low-level, adaptive admittance high-level	Passive ankle torque, joint position	Adaptive control has greater compliance than fixed
Asín-Prieto G et al. 2020 [57]	10 unimpaired, 1 post-stroke	Unimpaired 29.80 ± 6.32, post-stroke 37	Ankle rehabilitation with video game visual feedback and EMG	PID	Joint torque, RMSE, video game SCORE, ROM, joint velocity	Subjects satisfied. Unimpaired subjects improved, impaired subject ROM decreased initially, improved later
Maggioni S et al. 2018 [60]	5 unimpaired, 1 complete spinal cord injury	Unimpaired 27 ± 4.7, impaired 37	Gait rehabilitation	Adaptive hybrid PD and D	Normalised adaptive stiffness	Hybrid controller stiffness adapted to error over time
Rajasekaran V et al. 2018 [62]	4 incomplete spinal cord injury	21-49	Gait assistance robot with brain-machine interface	Volition adaptive impedance	Joint angle, stiffness, interaction torque	Error decreased each session. Participants showed improvement
Liu Q et al. 2017 [63]	3 unimpaired, 1 cerebral palsy	Unimpaired 27-31, impaired 42	Ankle rehabilitation	Adaptive compliance	Joint angle, torque, actuator pressure, admittance, force	Accuracy and compliance trade-off controlled by actuator pressure. Movement worse at higher stiffness
M. Zhang et al. 2019 [64]	1 ankle sprain two months prior	29	Ankle rehabilitation	Adaptive trajectory tracking	Joint position, joint force, actuator force	Good tracking performance. Small sample size means best training method cannot be proven

2.5 Chapter Conclusion

The consensus among the literature is that the adaptability and personalization offered by intelligent controllers make them superior to non-intelligent control in all control modes. They also outperform non-intelligent controllers in all comparative experiments in terms of error, rejection of disturbances to the system, and interaction torques with the user. However, it is important to note that while this seems the case in published literature, there exists a publication bias especially in emergent fields such as machine intelligence in physical applications. Any intelligent controllers which did not perform properly or were generally worse than traditional controllers would likely not be published, so this conclusion must not be taken as true globally without specific evidence.

Actual comparison between the controllers is generally limited to only what is presented in individual articles, as the results are specific to each robotic platform, movement exercises, and experiment duration. There is no universal metric for effectiveness, nor a standardized set of experiments, to quantifiably determine the effectiveness of each controller. The same can be said of other aspects of the rehabilitation robot such as actuators, sensor systems and hybrid rehabilitation systems, as while these have been extensively researched in the literature there are few experimental results demonstrating their effectiveness over more traditional methods.

While the comparative effectiveness of controllers is difficult to determine, the overall important factors in terms of rehabilitation remain similar throughout the literature. Active participation in exercise is consistently mentioned as having a great impact on the effectiveness of treatment. Transparency is often measured in experiments to ensure the robots have safe and comfortable interaction with

the human participant. Transparency can, and has been, improved by intelligent control. Active participation of the subject can be encouraged with personalized exercises and the system's ability to adapt to their specific needs. However, the most common measure of success is tracking accuracy. While accuracy of motion is important for any controller, the ability to follow reference paths with minimal error is not as important to rehabilitation outcome as the patient's experience and engagement in the training. The ability of the system to reject or compensate for disturbances is another common measurement, as it impacts the safety of the patient and generally improves training effectiveness. Other aspects such as compliance or weight of the robot itself are important as well but are more difficult to directly improve with better controllers.

To further the research and fill gaps presented in the literature, comparative experiments between commonly used controllers should be done, as well as tests over longer periods and with impaired patients, to determine their effect on the rehabilitation outcome and give conclusive results on which performs best under certain conditions. Comparing novel intelligent controllers to state-of-the-art algorithms in the field should also become more of a priority, as comparisons to traditional controllers like PID and SMC are becoming increasingly obsolete with the rapid development of more accurate and robust controllers. Feedback from participants in the experiments should also be gathered frequently, as the patient's experience is a crucial factor when undergoing physical therapy.

CHAPTER 3

A PIECEWISE PARTICLE SWARM OPTIMISATION MODELLING METHOD FOR PNEUMATIC ARTIFICIAL MUSCLE ACTUATOR

Pneumatic artificial muscles (PAMs) possess compliant properties desirable for certain applications in rehabilitation robotics design. However, this compliance along with their inherent nonlinear dynamics make them difficult to accurately model and as such accurately control under certain control architectures. As part of research objective 1, this chapter proposes an optimisation-based modelling approach based on a particle swarm optimisation (PSO) algorithm using a mass–spring–damper approximation for the PAM, as well as a piecewise modelling method that accounts for nonlinear dynamics, which will allow for the further development and testing of intelligent control algorithms for PAMs. Experimental evaluation of the developed method, comparison with other modelling techniques in literature, and successes and failings will be presented.

The work presented in this chapter is published in Actuators as:

- Brown, D.F.; Xie, S.Q. A Piecewise Particle Swarm Optimisation Modelling Method for Pneumatic Artificial Muscle Actuators. Actuators 2024, 13, 286. https://doi.org/10.3390/act13080286

3.1 Introduction

PAMs differ from more conventional actuators due to the inherently compliant behaviour and nonlinear dynamics arising from their construction of flexible materials and actuation method. These properties make them desirable for applications such as medical robotics in rehabilitation scenarios and prosthetics as they more closely mimic biological muscle than conventional actuators. This allows for a more comfortable human–robot interaction, as the compliance allows the user some give in their voluntary movement when under the external influence of a robot, as well as making the systems safer as it is less likely that unexpected forces or motion will injure the user or cause damage to the robot. They are also applicable to robotic platforms where human-like motion is desired. Various types of PAMs exist, suitable for different purposes based on differing characteristics, but all operate under the same principle. An elastic bladder is sealed and fixed at two ends, and upon pressurisation by compressed air will expand, applying force to the fixed ends of the actuator. A less elastic material surrounding the bladder, such as a harder rubber shell or braided fibre mesh, directs the force to cause the PAM to contract, expand, or bend about an axis depending on the construction [99]. The original fluidic artificial muscles used in robotics were developed by Joseph McKibben in the 1950s for orthotics [100, 101]. A more detailed review of the development of PAMs is presented in [99].

While the compliant behaviour of PAMs is desirable in many branches of industry and research, this and their nonlinear dynamics makes accurate motion control a challenge. Standard linear control systems such as PID are less effective than in more conventional applications as the friction present in the contraction/expansion of PAMs causes a hysteresis and changing behaviour with time, as well as the uncertainties caused by the fluid dynamics of pressurised air. Model-based control schemes can alleviate this problem by mapping the behaviour of the actuator to allow for more accurate control, but a similar problem arises with the complexity of these models. Many different approaches have been developed and studied in order to model PAMs that attempt to balance complexity with functionality, to find a solution that is accurate but does not take an exceedingly long time or large amount of computation to produce. The review presented in [102] describes some of the different approaches to the modelling problem of PAMs. The review suggests that geometric modelling is less suitable for these actuators as their parameters are difficult to accurately measure during use; however, their simplicity still makes the approach suitable for certain applications. The phenomenological modelling approach, which approximates the muscle as a mass–spring–damper system, is more suitable as this is a close approximation to the dynamics of PAMs based on their construction and flexible materials, and the simplicity makes them fairly easy to calculate. However, the hysteresis and nonlinearity over time is often not taken into consideration in these models. A simplified empirical model is also mentioned in which the PAM is simplified to that of a mechanical spring. Polynomial approximations of the parameters are used that allow for easy adjustment of the complexity/accuracy by increasing the degree of the model; however, again, these models suffer from not properly modelling the nonlinear behaviour of the PAMs.

Applications of these physical/mathematical models of PAMs are present throughout the literature. An early study on the phenomenological model for a McKibben muscle is presented in [103]. Experiments were performed to determine the changing parameters of the PAM with pressure, resulting in a model with 15% RMSE, with the largest error values at the peak and trough of the actuator's motion. An empirical model based on geometric constants of a McKibben muscle is presented in [104] including experimental parameter estimation. This model is used in model-based PID control of the actuator, with performance deemed satisfactory and within tolerance levels. A nonlinear numerical model for a McKibben muscle is shown in [105], showing a maximum error in experimental comparisons of 3% of the total displacement. Various models for contractile length, pulling force, and a specific application of four McKibben muscles in an arm configuration are shown in [106]. A mathematical model for an extensor PAM is presented in [107], differing from more commonplace contraction PAMs as these increase in length with increased pressure rather than decreasing.

PAMs developed by FESTO are popular in industrial applications as their construction makes them more reliable. These PAMs have longer operating lives than typical nylon-braided McKibben muscles and a greater force output capability; thus, they are also studied in many research applications including modelling. A piecewise three-element model of a FESTO PAM is presented in [108] for improved MPC. The piecewise model uses multiple three-element systems for different pressure levels in the PAM in order to overcome the nonlinearity of the actuator. The MPC developed with this piecewise model, in comparison with PID control, has much better performance. Mathematical

models of FESTO PAMs are presented in [109, 110], and phenomenological models are shown in [111, 112].

In recent years, more research has gone into applying machine intelligence in the form of learning and optimisation to the problem of PAM modelling. This gives the advantage of potentially more accurate models with more sophisticated parameters as well as alleviating some of the need to measure the actuator's complex parameters and dynamics. Neural networks are a popular algorithm used in this application; neural networks can be tailored to the specific needs of the model, and their complexity can be varied easily. A modelling method using an artificial neural network as well as hybrid backpropagation algorithm and genetic algorithm for the learning stage is presented in [113] for modelling a novel pleated PAM with promisingly accurate results obtained in experiments. Various other neural network-based modelling approaches have been applied to FESTO PAMs, including a recurrent fuzzy-neuro approach in [114] and neural network approaches for antagonistic pairs of PAMs in [115, 116]. The architecture of each neural network used in these studies is widely similar, with multiple input nodes, a similar number of hidden nodes, and a single output.

Another common approach in applying intelligence in modelling is optimisation, with particle swarm optimisation (PSO) algorithms being a popular choice. PSO uses a swarm of particles that interact with each other as they move around a search space attempting to minimise some cost function. By using a large number of particles in the swarm, solutions can be found much faster. In the case of actuator modelling, each particle has a number of parameters that describe both its position in the search space as well as the parameters used in the equation describing the dynamics of the actuator. The objective function is typically some combination of errors between the actual behaviour of the actuator and the

approximated behaviour based on each particle's parameters. Using this method, the actual parameters can be approximated rapidly and accurately, with the calculation time being largely invariant to the complexity of the model. An empirical model of a McKibben muscle with parameters generated using PSO is presented in [117] with the aim of characterising the hysteresis behaviour of the muscle. The model was verified to be accurate; however, the nonlinearities of the PAM are mentioned for causing some inaccuracies, and more intelligent control strategies are suggested as a solution. An inverse model for a PAM is presented in [118], also based on an PSO algorithm for system identification.

Limitations exist for all modelling practices. As mentioned in [102], geometric modelling is difficult to apply to PAMs accurately as online measuring of their nonlinear dynamic properties is difficult to achieve accurately. The standard phenomenological model using mass–spring–damper approximation also suffers lower accuracy due to nonlinearity, as the linear model approximation does not account for hysteresis and disproportionate input-output relationships. Intelligent learning algorithms, such as neural networks and genetic algorithm as presented in [113, 114, 115, 116] and to an extent optimisation algorithms like PSO, can achieve highly accurate models of even complex nonlinear systems, but better approximations rely on sufficiently complex model parameterisation and learning datasets that can greatly increase the computational load and model generation time. This trade-off in model accuracy, complexity, and computation time must be accounted for.

This chapter will present a piecewise PSO modelling method for a FESTO DMSP-20- 400N PAM based on the phenomenological modelling approach. A three-parameter model based on the dynamics of the mass–spring–damper approximation for the PAM will be used as a template for the model, used for its

good approximation of PAMs as well as its simplicity and low parameter count, reducing model complexity and improving generation time. To compensate for the nonlinearity of the PAM, a piecewise modelling method will be used with multiple different models for different sections of the actuator's stroke length. Models generated in this manner will be compared experimentally with the PAM under different loads and inputs to validate their accuracy.

3.2 Materials and Methods

3.2.1 Phenomenological Model

The phenomenological model is commonly used in modelling PAMs due to their approximately similar behaviour to mass–spring–damper systems. A three-element model based on this will be used as a template for optimisation in this study. The equation of motion for this model is given as follows:

$$M\ddot{x}(t) + D\dot{x}(t) + Cx(t) = F_c - F_l \tag{3.1}$$

where M is the mass of the PAM, D is the damping element, C is the spring constant, F_c is the contractile force element applied by the internal pressure of the PAM, F_l is the force applied by external load to the system, and $x(t)$ is the displacement of the actuator from its nominal position at a given time step. This model is shown in Figure 3.1.

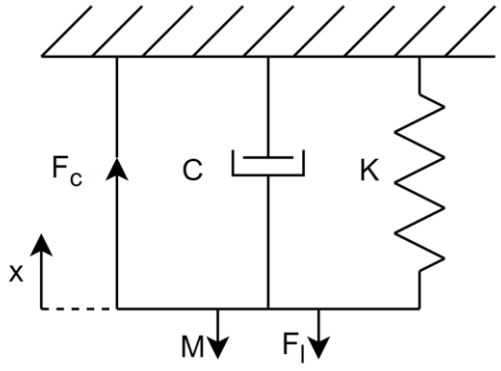


Figure 3.1: Phenomenological model of the PAM showing displacement x; contractile force element F_c; external load element F_l; and PAM parameters M, C, and K.

The contractile force applied by the PAM is proportional to the input pressure, making F_c proportional to the control input of the system, which will be henceforth denoted with U.

Using the displacement and velocity of the system as state variables, the following equations are obtained:

$$x_1(t) = x(t) \tag{3.2}$$

$$x_2(t) = \dot{x}(t) \tag{3.3}$$

$$\dot{x}_1(t) = x_2(t) \tag{3.4}$$

The equation of motion can be re-written in terms of these states:

$$U(t) = M\dot{x}_2(t) + Cx_2(t) + Kx_1(t) \tag{3.5}$$

$$\dot{x}_2(t) = -\frac{K}{M}x_1(t) - \frac{C}{M}x_2(t) + \frac{U(t)}{M} \tag{3.6}$$

The output of the system is the displacement of the actuator, so the output of the model y(t) is expressed as follows:

$$y(t) = x_1(t) \tag{3.7}$$

The state-space representation of this model in matrix form is given by the following:

$$\dot{X}(t) = \begin{bmatrix} \dot{x}_1(t) \\ \dot{x}_2(t) \end{bmatrix} = \begin{bmatrix} 0 & 1 \\ -\frac{K}{M} & -\frac{C}{M} \end{bmatrix} \begin{bmatrix} x_1(t) \\ x_2(t) \end{bmatrix} + \begin{bmatrix} 0 \\ \frac{1}{M} \end{bmatrix} U(t) \tag{3.8}$$

$$y(t) = \begin{bmatrix} 1 & 0 \end{bmatrix} \begin{bmatrix} x_1(t) \\ x_2(t) \end{bmatrix} + [0]U(t) \tag{3.9}$$

The unknown parameters of the system based on Equation (3.8) are $-\frac{K}{M}$, $-\frac{C}{M}$, and $\frac{1}{M}$. These three elements will be calibrated through optimisation using the PSO

algorithm and will be referred to henceforth as P_1, P_2, and P_3 respectively. The model equations for each state-space solution are given by Equations (3.9) and (3.10).

$$\dot{X}(t) = \begin{bmatrix} \dot{x}_1(t) \\ \dot{x}_2(t) \end{bmatrix} = \begin{bmatrix} 0 & 1 \\ P_1 & P_2 \end{bmatrix} \begin{bmatrix} x_1(t) \\ x_2(t) \end{bmatrix} + \begin{bmatrix} 0 \\ P_3 \end{bmatrix} U(t) \tag{3.10}$$

3.2.2 Particle Swarm Optimisation Algorithm

The classical PSO algorithm is referenced extensively in the literature [117, 118, 119, 120]. It uses a group of potential solutions (particles) to an optimisation function that iteratively updates their parameters in response to some fitness function, with these parameters acting as coordinates in a search space. The particles base their movement around the search space on both their own best fitness performance and the overall best fitness found in the swarm. This sharing of data between solutions allows for fast optimisation convergence. The following equations describe the velocity and position updates for the particles at each iteration of the algorithm:

$$\begin{aligned} V_i(k+1) = WV_i(k) + C1Rand\big(X_i best(k) - X_i(k)\big) \\ + C2Rand(Gbest(k) - X_1(k)) \end{aligned} \tag{3.11}$$

$$X_i(k+1) = X_i(k) + V_i(k+1) \tag{3.12}$$

where i is the current particle; k is the current iteration of the algorithm; V is the particle's velocity in the search space; X is a particle's position in the search space quantified by its parameters; $Rand$ is a random value between 0 and 1; $X_i best$ is the position of the current particle which achieved the best (lowest) fitness; $Gbest$ is the global best position of all particles in the swarm; and W, $C1$, and $C2$ are algorithm parameters that are tuned manually.

The parameters to be optimised using PSO algorithm in this study are P_1, P_2, and P_3 as described in Equation (3.10). As such the search space is three-dimensional. The optimisation function used to determine the fitness of each particle is the root mean squared error (RMSE) between the expected displacement of the PAM based on the model generated by a particle's parameters and the actual displacement of the PAM, measured over a period of one repeated sin wave motion, as described in Equation (3.13).

$$F_i = \sqrt{\frac{\sum_{t=0}^{N}(x - y_i(t))}{N}} \tag{3.13}$$

where F_i is the fitness value for particle i; t is the time step; N is the number of time steps in the measured motion sequence; x is the measured displacement of the PAM; and $y_i(t)$ is the output of the model based on Equations (9) and (10) using the three parameters of particle i as P_1, P_2, and P_3 at time step t.

Using this method, generated model solutions are iteratively improved based on how accurately they match the motion of the PAM. The update parameters of the algorithm are $W = 0.9$ to prevent divergent swarm motion and $C1 = C2 = 2$ to increase the efficacy of the algorithm and reach solutions in fewer iterations, while maintaining low enough velocities to keep the swarm coherent. The number of particles in the swarm is set to 50 as a balance between the time taken for each iteration and convergence time to a solution.

3.2.3 Piecewise Model

The nonlinear nature of PAMs makes them difficult to accurately approximate with linear models such as the three-element model described in Section 2.1. Nonlinear models of this nature are much more computationally complex and not feasible to generate using optimisation methods such as PSO. As such, a

compromise is made in the form of piecewise models. Multiple models will be generated using different reference target motions of the PAM, as well as different input ranges within those motions. These models are then put together, each operating during the specific range of inputs to the system as specified by how they were generated. The resulting piecewise model comprised of multiple linear models should better approximate the nonlinearity of the PAM than a single linear model.

The nature of the PAM's nonlinearity is twofold. Internal friction caused by the braided fibres in the outer mesh cause a hysteresis to occur, and the method of actuation in inflation by pressurised air makes the displacement not linearly proportional to input pressure, with displacement velocity gradually decreasing along the stroke length of the actuator. To account for the hysteresis, different models can be generated for the actuator's inflation and deflation. The disproportionate motion across the stroke length can again be accounted for by generating multiple models for different input ranges.

Each piecewise model is therefore comprised of multiple individual three-parameter solutions as described in Equation (3.10). In order to generate the whole piecewise model solution, the PSO algorithm is run once for each model section, generating three parameters per section.

The model output for each part of a piecewise model solution would therefore be described using Equations (3.14) and (3.15).

$$\dot{X}_J(t) = \begin{bmatrix} \dot{x}_{J_1}(t) \\ \dot{x}_{J_2}(t) \end{bmatrix} = \begin{bmatrix} 0 & 1 \\ P_{j_1} & P_{j_2} \end{bmatrix} \begin{bmatrix} x_{j_1}(t) \\ x_{j_2}(t) \end{bmatrix} + \begin{bmatrix} 0 \\ P_{j_3} \end{bmatrix} U(t) \tag{3.14}$$

With the specific model used based on the input $U(t)$ according to the following:

$$y(t) = \begin{cases} x_{1_1}(t)\ for\ \ 0 \le U(t) < K_1 \\ x_{2_1}(t)\ for\ \ K_1 \le U(t) < K_2 \\ x_{3_1}(t)\ for\ \ K_2 \le U(t) < K_3 \\ \cdots \\ x_{n_1}(t)\ for\ \ K_{n-1} \le U(t) \end{cases} \tag{3.15}$$

As well as differentiation of the inflating and deflating states according to the following:

$$y(t) = \begin{cases} x_{inf_1}(t)\ for\ \ \dot{U}(t) > 0 \\ x_{def_1}(t)\ for\ \ \dot{U}(t) \le 0 \end{cases} \tag{3.16}$$

where j is the model section, n is the total number of linear model sections of the piecewise model, and K_i is the input bound determining the upper bound of the model section $X_j(t)$ and the lower bound of the model section $X_{j+1}(t)$. Each model section j will have a set of P_{j_1}, P_{j_2}, and P_{j_3} that are independently generated for each j using the PSO algorithm for a total parameter count of $3j$ per piecewise model.

In cases where both the input ranges and inflating/deflating state differentiations are used, each model section $X_j(t)$ will constitute both an inflating and deflating state, resulting in both $X_{j_{inf}}(t)$ and $X_{j_{def}}(t)$, such that $y(t)$ would be given by the following:

$$y(t) = \begin{cases} \begin{cases} x_{1_{inf_1}}(t)\ for\ \ \dot{U}(t) > 0 \\ x_{1_{def_1}}(t)\ for\ \ \dot{U}(t) \le 0 \end{cases} for\ \ 0 \le U(t) < K_1 \\ \begin{cases} x_{2_{inf_1}}(t)\ for\ \ \dot{U}(t) > 0 \\ x_{2_{def_1}}(t)\ for\ \ \dot{U}(t) \le 0 \end{cases} for\ \ K_1 \le U(t) < K_2 \\ \begin{cases} x_{3_{inf_1}}(t)\ for\ \ \dot{U}(t) > 0 \\ x_{3_{def_1}}(t)\ for\ \ \dot{U}(t) \le 0 \end{cases} for\ \ K_2 \le U(t) < K_3 \\ \cdots \\ \begin{cases} x_{n_{inf_1}}(t)\ for\ \ \dot{U}(t) > 0 \\ x_{n_{def_1}}(t)\ for\ \ \dot{U}(t) \le 0 \end{cases} for\ \ K_{n-1} \le U(t) \end{cases} \tag{3.17}$$

However, there then exists a trade-off between accuracy and computational efficiency in using piecewise modelling. A greater number of models across the stroke length will ultimately cause the model to be more accurate as the nonlinearity is better approximated; however, this also results in the model being more complicated, taking longer to generate, and having more parameters. There is also the issue of reference motions becoming too small to properly approximate the overall motion of the PAM, potentially causing each individual model to be less accurate within its own input range. As such the piecewise models generated in this study will comprise of six input ranges, spaced across the stroke length of the actuator to best model the nonlinearity of motion, as well as different models generated for the inflating and deflating state.

3.2.4 Experimental Setup

The actuator to be used in this work is a FESTO DMSP-20-400N PAM. As previously discussed, PAMs provide compliant motion, which is desirable in a rehabilitation robot. They are also controlled with a single pressurised air input, meaning the only necessary control value is the air pressure flowing into the PAM. The main output measure of the setup is the actuator's displacement to be used to generate target references for the optimisation function as well as measure the error and calculate accuracy of the models. The load force applied to the PAM will also be measured to test the effects of external loads on the accuracy of the models. To measure each of these, a linear encoder and a load cell will be connected to the actuator.

The load cell used is a FUTEK LCM300 model and has a 300 Lb load limit and sufficient precision for any force changes required by the system. The displacement encoder connected to the bottom of the linear actuator is a FESTO

MLO-POT-300-TLF with a resolution of 0.01 mm and stroke length of 300 mm, both of which are sufficient for the system. The proportional pressure regulator used is a FESTO VPPM-6L-L-1-G18-0L6H. The system is held in place with a frame consisting of slotted aluminium extrusion, and the PAM is positioned vertically to ensure motion and forces are not adversely affected by the actuator's intrinsic compliance regarding gravity.

To control the system, a RoboRIO is connected to a desktop PC and coded using National Instruments LabVIEW. The outputs of the load cell and the displacement encoder are input to the RoboRIO to be measured on the display. The load cell is connected to a FUTEK IAA100 strain gauge voltage amplifier before the output is taken by the RoboRIO to allow for easier signal processing. Figure 3.2 shows a diagram of the experimental setup alongside the circuitry and computer communication systems used for data acquisition and actuator control. Figure 3.3 shows the PAM in the experimental setup.

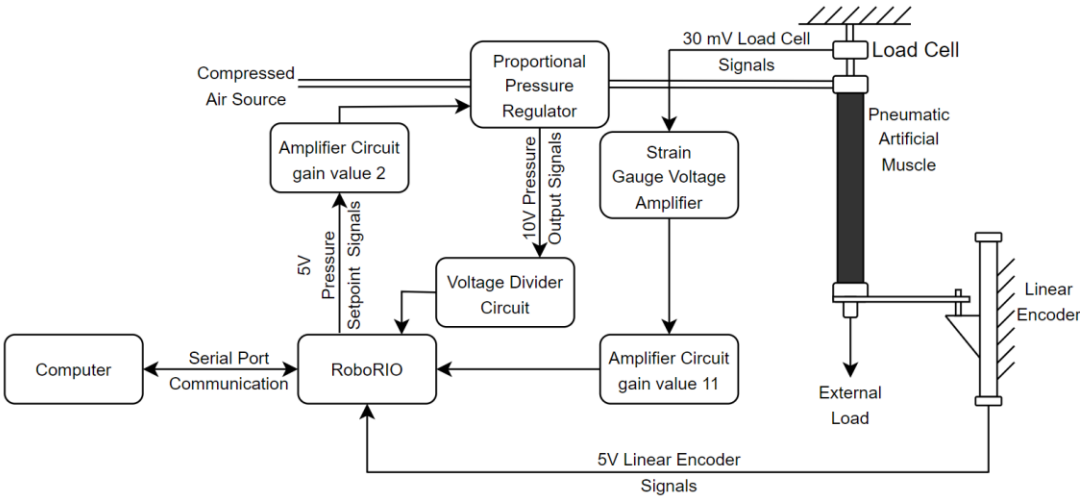


Figure 3.2: A diagram of the experimental setup, circuitry, and computer communications.



Figure 3.3: The experimental setup, showing the FESTO DMSP-20-400N PAM (1), FUTEK LCM300 load cell (2), FESTO MLO-POT-300-TLF displacement encoder (3), and external load attachment (4).

3.3 Results

3.3.1 Model Generation

To properly compare successes of the piecewise PSO modelling method, several different models were generated. As a benchmark comparison point, a linear phenomenological model was used. To properly justify the benefits of the piecewise modelling method, separate models were also generated using separate parameters for the inflating and deflating states, as well as six distinct ranges within the PAM's stroke length differentiated by input pressure. Four total

models were generated for experiments and comparison. Each individual state-space solution, comprised of the three optimised parameters, was generated using 20 iterations of the PSO algorithm, taking approximately five minutes per solution. The total number of iterations required for each model is shown in Table 3.1.

The linear model was generated using a single reference trajectory as comparison for the PSO's fitness function. This effectively gives Equation (3.15) a value of $n = 1$, and no K values are needed as model bounds. This reference was the displacement of the PAM measured using the displacement encoder as shown in Figure 3.3, over a single sin wavelength with an amplitude of the full stroke length of the actuator—approximately 10 cm total displacement from the resting point—and frequency of 0.25 Hz. The same reference trajectory was used to generate a model differentiating the inflating and deflating states of the PAM, hereafter referred to as the inflate/deflate model, using Equation (3.16) to describe the model section separation. To generate this model, the fitness function of the PSO algorithm was only calculated during periods where the reference trajectory was increasing or decreasing, thus two state-space solutions were generated.

The piecewise models used six separate reference trajectories, giving a value of $n = 6$ for Equation (3.15), chosen at intervals that would improve the model's approximation of the PAM's nonlinear motion across its stroke length. The full stroke length of the PAM is achieved using a range of input pressures from 0 to 6.3 Bar. To best split the piecewise model sections across the stroke length, a range of pressures were decided for this experiment of [0–1.5], [1.5–3], [3,4], [4,5], [5,6], and [6–6.3] Bar. These values were determined using manual tuning based on the full stroke value of the PAM being achieved at 6.3 bar, and the approximate pressure ranges across this length that show similar input-output

relationships. As the PAM shows increased nonlinear behaviour towards the upper limit of the stroke, the pressure ranges were chosen to decrease in size towards higher pressure values. The aim of these decisions was to best approximate the complex behaviour of the PAM using multiple linear approximations, leading to a more accurate model. There is potential to improve the performance of the models using more than six ranges as well as allocating the values to better represent the behaviour of the PAM, but this will require further experimentation.

At steady state, these pressure ranges are achieved by the following input voltages to the pressure regulator, $K_1 = 1.05$, $K_2 = 2.35$, $K_3 = 3.15$, $K_4 = 3.95$, and $K_5 = 4.75$. These values were therefore used as the piecewise model range boundaries in the model generation software.

Two piecewise models were generated using these input pressures as the operating ranges for each separate state-space solution. Each range was generated using a reference trajectory similar to that of the linear model, using a sin wave motion of the PAM, with the motion bounded by the lower and upper limits of each interval. Of the two models, one also used the inflation/deflation differentiation method described previously, resulting in what will hereafter be referred to as a piecewise model and a piecewise inflate/deflate model. The piecewise model has a total of six state-space solutions, one for each input interval, and the piecewise inflate/deflate model has a total of twelve state-space solutions. As previously discussed, this greater number of solutions is expected to result in better accuracy in comparison with the other models.

Table 3.1 shows the three parameters generated for each separate part of all four models. These parameters are then applied to Equation (10) to create a state-space solution for the input range and inflating/deflating state as specified by the

reference used for comparison in the PSO algorithm fitness function. Total iterations used for each model are included to show computational costs.

Table 3.1: Model parameters

Model	Total PSO Iterations	Model Section	P_1	P_2	P_3
Linear	20	Linear	0.451259	0.305468	0.519089
Inflate/Deflate	40	Inflate	0.204797	0.401668	0.821284
		Deflate	0.591312	0.224405	0.421155
Piecewise	120	1	0.0419824	0.717121	0.385334
		2	0.230325	0.428379	0.970208
		3	−0.194232	0.441082	2.05713
		4	0.129964	0.416894	1.11129
		5	0.343061	0.207203	1.00254
		6	−0.0147093	0.151612	1.74169
Piecewise Inflate/Deflate	240	Inflate 1	0.233221	0.522204	0.417219
		Deflate 1	0.04244	0.588327	0.628349
		Inflate 2	0.112168	−0.0255462	2.36332
		Deflate 2	0.0872913	0.681367	0.651491
		Inflate 3	0.0986908	0.638282	0.771687
		Deflate 3	0.632625	−0.0197651	1.0512
		Inflate 4	0.370783	0.399432	0.596057
		Deflate 4	0.616219	0.0665999	0.762527
		Inflate 5	0.480481	0.112959	0.900554
		Deflate 5	0.168957	0.648523	0.38119
		Inflate 6	−0.123881	0.612445	1.03806
		Deflate 6	0.651356	−0.126021	0.961433

3.3.2 Model Accuracy Experiments

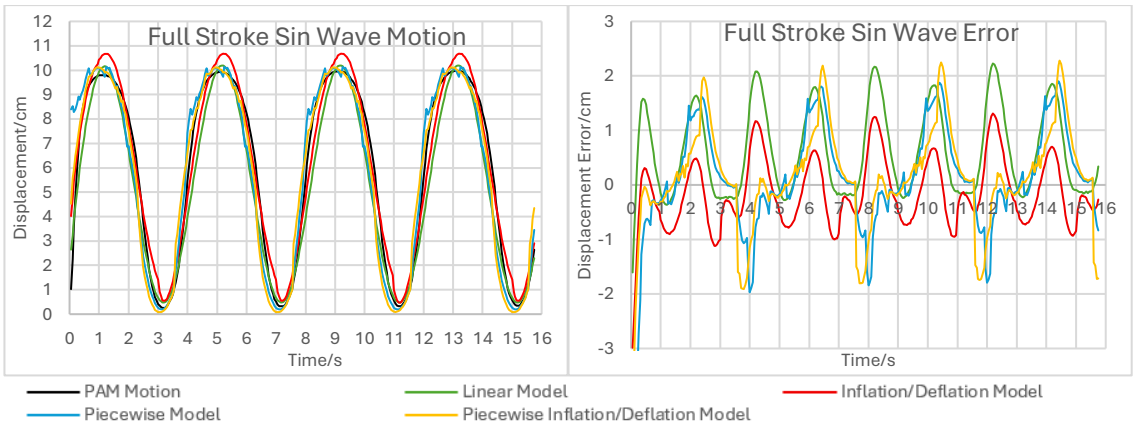
As PAMs are used in several small-scale and industrial applications, multiple experiments were performed to determine each of the four models' accuracy under different use cases. These experiments involved distinct repeated waveforms used as inputs to the pressure regulator controlling the PAM as well as to each of the four models in turn in order to measure the accuracy of the model to the PAM's actual motion. The parameters of each waveform were chosen to best demonstrate different use cases of the PAM. These included a sin wave

spanning the full length of the PAM's stroke length, both unloaded and with a 5 kg external load attached as shown in Figure 3.3. The same full stroke sin wave at a higher frequency was used to show the model's response to rapidly changing motion. Square and triangle waveforms, also spanning the full stroke length of the PAM, were used to test other possible operating procedures. Finally, two sin waveforms spanning the lower and upper ends of the PAM's stroke were used to validate the models' accuracy in smaller motions. The details of waveforms used for each experiment are outlined in Table 3.2. Each waveform is repeated for four wavelengths to ensure consistency and to mitigate potential unwanted disturbances, except for the rapid sin wave experiment which was repeated for eight wavelengths.

Table 3.2: Waveforms used in the model accuracy experiments

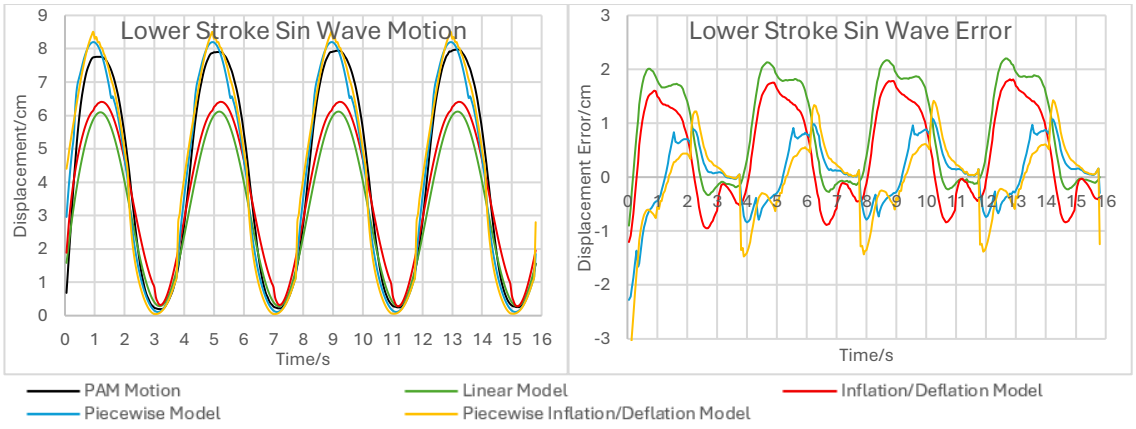
Experiment	Waveform Type	Amplitude (V)	Offset (V)	Frequency (Hz)	Additional Notes
Full Stroke Sin Wave	Sinusoidal	5	0	0.25	The maximum input giving a measurable output for the pressure regulator was 5 V
Lower Stroke Sin Wave	Sinusoidal	3	0	0.25	To determine accuracy at the lower stroke of the PAM
Upper Stroke Sin Wave	Sinusoidal	3	2	0.25	To determine accuracy at the upper stroke of the PAM
Triangle Wave	Triangle	5	0	0.25	To determine model response to constant velocity and rapid changes in velocity
Square Wave	Square	5	0	0.25	To determine model response to rapid changes in displacement
Rapid Sin Wave	Sinusoidal	5	0	1	Waveform repeated 8 times due to shorter wavelength to ensure consistency between experiments
Weighted Sin Wave	Sinusoidal	5	0	0.25	A 5 kg external load is applied to the unaffixed end of the PAM, as shown in Figure 3.3

The motion tracking results and displacement error values are shown for each of the models in each experiment in Figures 3.4–3.10. Specific error measures from each experiment are shown in Table 3.3.



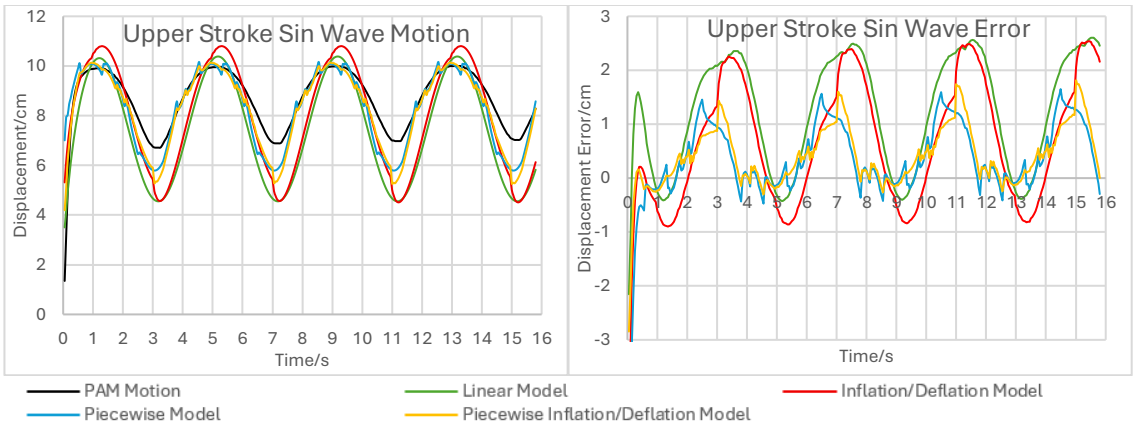
(a) (b)

Figure 3.4: Measurement values for the full stroke sin wave experiment. (a) shows the displacement readings, (b) shows the error values.



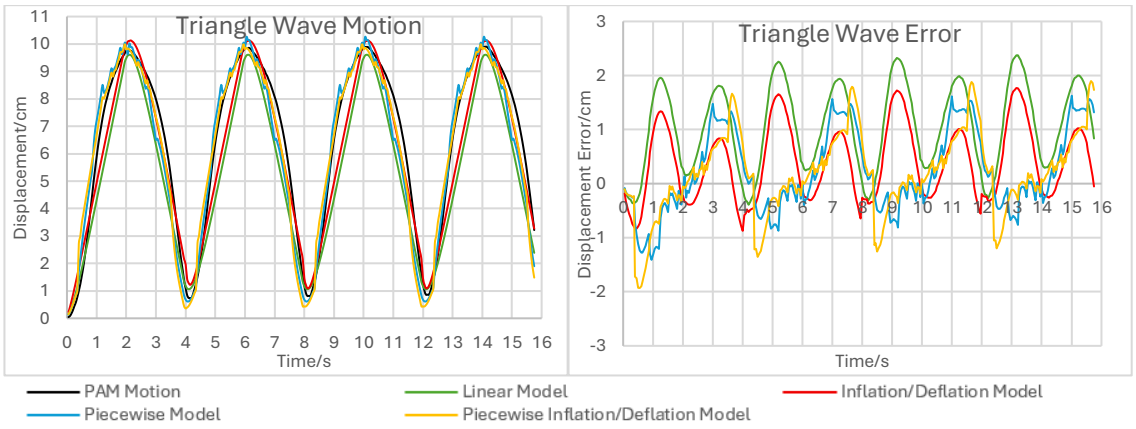
(a) (b)

Figure 3.5: Measurement values for the lower stroke sin wave experiment. (a) shows the displacement readings, (b) shows the error values.



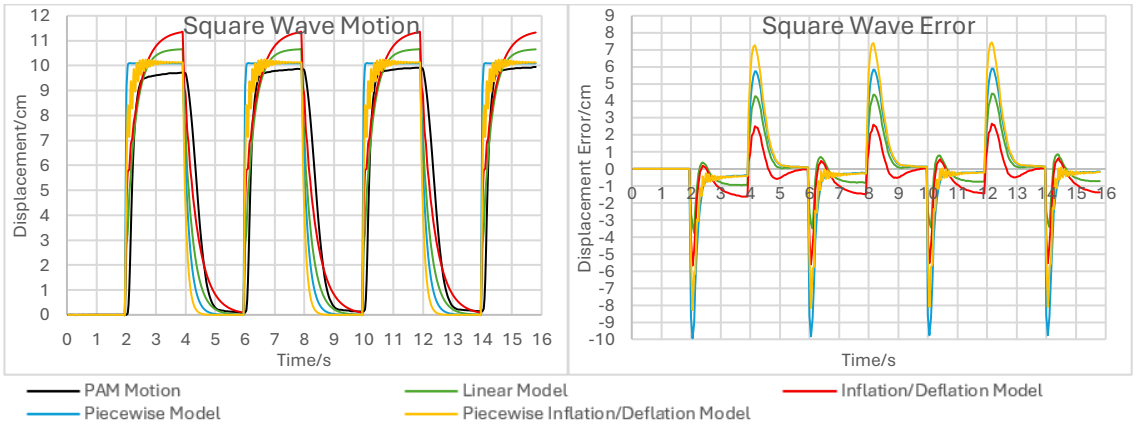
(a) (b)

Figure 3.6: Measurement values for the upper stroke sin wave experiment. (a) shows the displacement readings, (b) shows the error values.



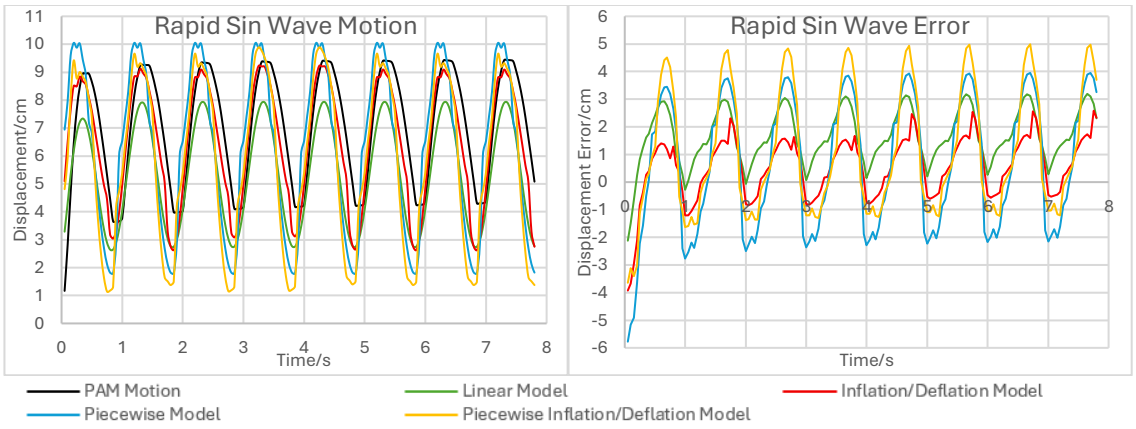
(a) (b)

Figure 3.7: Measurement values for the triangle wave experiment. (a) shows the displacement readings, (b) shows the error values.



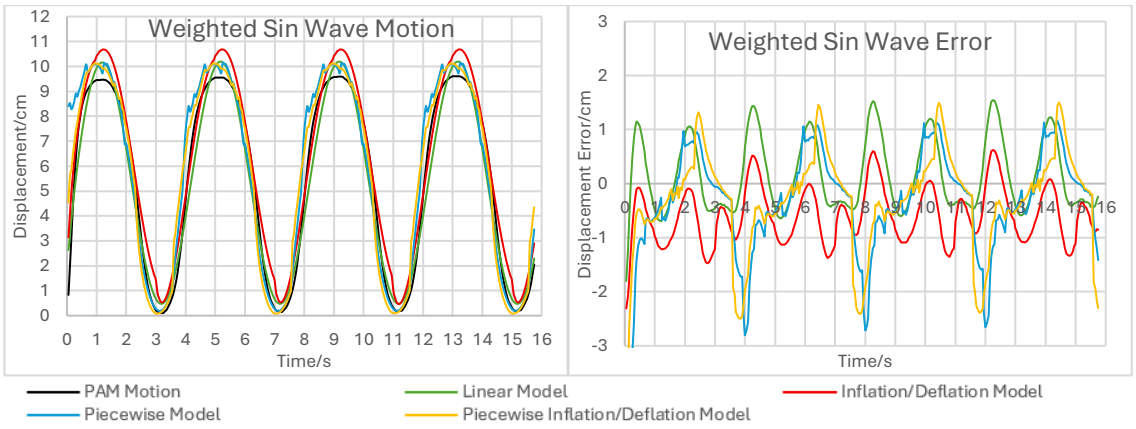
(a) (b)

Figure 3.8: Measurement values for the square wave experiment. (a) shows the displacement readings, (b) shows the error values.



(a) (b)

Figure 3.9: Measurement values for the rapid sin wave experiment. (a) shows the displacement readings, (b) shows the error values.



(a) (b)

Figure 3.10: Measurement values for the weighted sin wave experiment. (a) shows the displacement readings, (b) shows the error values.

Table 3.3: Experiment error values

Experiment	Error Measure	Linear Model	Inflate/Deflate Model	Piecewise Model	Piecewise Inflate/Deflate Model
Full Stroke Sin Wave Motion	Displacement RMSE	6.13633	4.56575	5.83597	5.65194
	Velocity RMSE	0.923337	0.864623	1.03032	1.01383
	Maximum Displacement Error	2.22815	1.31099	1.96861	2.28073
	Maximum Velocity Error	0.668612	0.981179	1.2318	1.30308
Lower Stroke Sin Wave	Displacement RMSE	7.92829	7.22548	3.99538	4.34249
	Velocity RMSE	0.530426	0.673029	0.497157	0.644981
	Maximum Displacement Error	2.20256	1.8153	1.08325	1.47484
	Maximum Velocity Error	0.401167	0.626442	0.751128	0.703432
Upper Stroke Sin Wave Motion	Displacement RMSE	10.9469	9.13923	4.26431	4.12044
	Velocity RMSE	0.641451	0.71235	0.74694	0.592489
	Maximum Displacement Error	2.6029	2.53934	1.6502	1.81496
	Maximum Velocity Error	0.907793	1.21929	1.55914	1.05378
Triangle Wave Motion	Displacement RMSE	9.16222	5.40654	5.33678	4.92422
	Velocity RMSE	0.906614	0.784657	0.840442	0.854697
	Maximum Displacement Error	2.37337	1.76919	1.62597	1.8976
	Maximum Velocity Error	0.220352	0.231343	0.381985	0.753218
Square Wave Motion	Displacement RMSE	8.83882	8.25559	13.2914	13.5085
	Velocity RMSE	2.0656	2.25246	3.37061	3.24101
	Maximum Displacement Error	4.40405	5.5969	9.74115	8.26315
	Maximum Velocity Error	1.67346	2.81359	4.95761	4.13536
Rapid Sin Wave Motion	Displacement RMSE	7.00625	4.20318	9.08059	7.81292
	Velocity RMSE	1.09764	1.25888	2.54982	2.60158
	Maximum Displacement Error	3.19252	2.58384	3.95251	4.98838
	Maximum Velocity Error	0.994197	1.51908	2.13284	1.89554
Weighted Sin Wave Motion	Displacement RMSE	4.89103	5.96969	6.03493	5.67446
	Velocity RMSE	0.824754	0.804333	1.00429	0.954394
	Maximum Displacement Error	1.54481	1.47573	2.80113	2.50223
	Maximum Velocity Error	0.668612	1.04407	1.62628	1.30308

3.4 Discussion

Performance criteria for real-time operating models of actuators such as the ones presented here are numerous; thus, a consensus on the best performing model is difficult to reach. These criteria include accuracy to the physical system, robustness to external forces including both load and environmental noise and to different operating modes and input sequences, and computational complexity in generation and during runtime.

In general, the absolute error values in each experiment reach a maximum of around 2 cm for all models, except during the square wave experiment in which the maximum error was much higher due to the very rapid change in displacement of the PAM that exacerbates the model's slight lag/lead of the real motion. The rapid motion experiment also showed larger error values, see Figure 3.9, again due to rapid motion of the PAM but also due to the hysteresis effect in the actuator altering the dynamics more during faster motion. The linear and inflate/deflate models have similar error functions with time in most experiments, with the inflate/deflate model having generally lower error values. However, as particularly evident in the upper stroke sin wave, see Figure 3.6, and rapid sin wave experiments, see Figure 3.9, the changing between inflating and deflating states can cause the inflate/deflate model to have a sharp spike in error as it switches between parameters. Both of these models do not properly follow the nonlinearity of the PAM towards the peak of its displacement. They also suffer much larger error values during the lower- and upper-stroke tests than in the full stroke test, as the use of a single reference trajectory in the model generation causes the PSO algorithm to overfit to the specific motion used to calculate fitness. The use of piecewise models reduces this effect as both the piecewise and

piecewise inflate/deflate models have generally lower error values during the upper- and lower stroke tests. In terms of displacement RMSE, the piecewise model has the lowest error in each experiment as shown in Table 3.3 except during the rapid motion and square wave tests, where both the RMSE and maximum displacement error is greater than that of the linear and inflate/deflate models. This is slightly mitigated by the piecewise inflate/deflate model.

The error values listed in Table 3.3 for the square wave test show much higher values for the piecewise and piecewise inflate/deflate models than for the linear and inflate/deflate models. While this suggests the piecewise method severely reduces the model accuracy when performing instantaneous changes in input, these values are somewhat misleading. Figure 3.8a shows the actual predicted motion of each model, and the two models using the piecewise method show a general shape much closer to that of the actual motion, flattening out at the peak, whereas the two models which do not use the piecewise method predict smoother, continuous motion that overshoots the actual maximum displacement. This effect is more noticeable in Figure 3.8b, where the inflate/deflate model shows the lowest peak error in both directions but does not flatten out at the peak/trough of motion, whereas the piecewise and piecewise inflate/deflate models stabilise to a consistent low value outside of the large errors present at the switching points of the input.

Figure 3.4 shows the jumps between input ranges in the piecewise model's output; while this model does exhibit lower error values than the piecewise inflate/deflate model, these sharp jumps are undesirable in online operation. Thus, the piecewise inflate/deflate model may be more suited to real time applications.

In comparison with other PAM models in literature, especially those pertaining to the FESTO PAMs, the piecewise PSO modelling method shows similar motion prediction behaviour to other mathematical models. Results from [109] show similar model accuracy in online comparative displacement tests, with models overshooting at higher displacement values of the PAM, similar to that of the linear and inflate/deflate models presented here. Hysteresis is also not properly accounted for. The phenomenological model presented in [112] shows lower RMSE values and closer fitting motion prediction than the piecewise PSO models here; however, the experiments were conducted over much smaller contraction ranges, making accurate comparisons difficult. Models presented in [110, 111] are also difficult to compare as experiments focus on force output estimation over pressure input range rather than displacement over time. Neural network-based models, such as those presented in [113, 114, 115, 116], have very low error values in motion estimation experiments; however, the results in [115, 116] utilise an antagonistic pair of PAMs and measure angle rather than displacement. The algorithm used in [113] for model generation uses a hybrid genetic algorithm and backpropagation neural network. There are several mentions of both algorithms having slow convergence times, and the model used in experiments required 3000 iterations of the backpropagation learning function. In [114], the error values converged to a satisfactory value after 250 iterations of the fuzzy neural network training. Exact generation time is not mentioned; however, the large number of iterations required for neural network-based modelling alongside the computational complexity and required training data make the piecewise PSO modelling method presented here a favourable option in terms of the model generation stage. The PSO-based empirical model presented in [117] shows similar motion tracking results to those presented here, although accuracy is

generally better. However, this empirical model is based on a McKibben muscle, and as mentioned in the paper, the model would not apply to other compliant or soft actuators. Therefore, the simple three-element estimation used here may be more generally useful in modelling various PAMs and other similar soft actuators. Table 3.4 shows a brief comparison of important points between the proposed piecewise PSO modelling method and those more commonly used modelling techniques.

The error values in the weighted test are generally similar to those in the unweighted full stroke test. This is mainly due to the FESTO PAM's high load tolerance causing the weight to have little effect on the motion. In order to properly determine the effects of larger loads on the model's accuracy, a more sophisticated experimental setup is required. As the piecewise PSO modelling method does not include any real-time measurement in the parameters, the models do not change dynamics based on external factors and do not respond to loads and noise that would impact their robustness in an industrial setting. The inclusion of measures from the attached load cell to the parameter calculation could improve this and have the models respond to loads and environmental factors affecting the PAM's motion.

Table 3.4: FESTO PAM modelling method comparisons

Modelling Method	**Comparison References**	**Accuracy Comparison**	**Computational Cost**	**Model Complexity**
Mathematical Model	[108, 109]	Similar accuracy, the piecewise model shows smaller overshoots at higher stroke lengths	Similar or slightly higher than the PSO method	Similar or slightly higher than the PSO method
Phenomenological Model	[112]	Better accuracy than the PSO method, different	More measurements	Similar model complexity

		experiment procedures make comparison difficult	required than the PSO method	
Neural Network-Based Model	[113, 114, 115, 116]	Much higher than the PSO method	Much higher than the PSO method	Much higher than the PSO method
PSO-Base Empirical Model	[117]	Similar motion tracking results, generally better accuracy than the PSO method	More measurements required than the PSO method	More model parameters and templates required than the PSO method

The three-element phenomenological model used as the template of the piecewise PSO modelling method makes it computationally simple, and the use of state-space solutions for each individual model mode makes for fast runtime operation and simple implementation when compared to more involved methods such as deep learning modelling. The use of an optimisation function for parameter estimation also removes the need to measure these parameters manually, and as such this modelling method could be applied to other linear actuators for which the mass–spring–damper approximation is a good estimation of their dynamic properties. Under a different dynamic model template, the proposed PSO modelling method could be applied to other types of actuators, but this would require further testing to properly validate. The PSO algorithm has fast optimisation time and requires very little training data when compared to deep learning methods, as only a single trajectory is required to calculate model fitness for each set of parameters. The piecewise inflate/deflate model, being the most complicated with 12 separate state-space solutions, takes approximately one hour to generate using the algorithm parameters mentioned previously. With further tuning of the C1 and C2 parameters, as well as swarm size and number of iterations used, this time can be reduced at little cost to the model's accuracy.

3.5 Chapter Conclusion

A piecewise PSO modelling method for pneumatic artificial muscles is presented in this chapter. A phenomenological model was adopted as a model template, based on the approximation of the PAM as a mass–spring–damper system, with three parameters based on the spring constant, damping constant, and mass of the muscle. Models were generated using reference trajectories from a displacement encoder connected to a FESTO PAM with sin waveform inputs to a pressure regulator forming a constant sin motion, and the RMSE calculated between each particle solution was used as the fitness function for the PSO algorithm. Four different models were generated for testing using this method: a linear model using a single three-element solution, an inflate/deflate model with two solutions differentiating between the PAM's inflating and deflating states, a piecewise model using six pressure ranges for six different solutions, and a piecewise inflate/deflate model using both the inflation/deflation modes as well as input pressure ranges. Experiments show that these models have good accuracy, with the piecewise PSO modelling method effectively accounting for the nonlinearity present in the PAM. Compared to other PAM models in literature, results show similar motion behaviour and similar or slightly worse prediction accuracy to mathematical and physical models. When comparing to neural network and genetic algorithm-based models, the error values from the piecewise PSO modelling method are noticeably higher; however, the use of deep learning algorithms greatly increases the time to generate models as well as the computational requirements and complexity. The use of the phenomenological model approximation of the PAM could also allow for more generalised use cases than other model examples, including other PAM types and some other actuators

with similar operating principles for which the phenomenological model used here is applicable.

Improvements can be made to the robustness of these models. Measurements of external forces applied to the PAM during operation could be incorporated into the model parameters to allow for dynamic adjustment of the model in response to load and environmental factors. Improvements to the accuracy, as well as generation time, can be made in fine-tuning the PSO algorithm parameters. Accuracy can also be improved using a greater number of pressure ranges for piecewise model generation, as well as more efficient spacing of these ranges within the PAM stroke length. This does come with a trade-off of modelling time and complexity as each additional model requires further optimisation, but the simple phenomenological model template makes the increase in complexity minimal.

The contributions of this chapter are the PSO-based modelling method and piecewise modelling approach. The modelling method is computationally efficient, using a three-parameter approach to modelling a complex actuator, and produces accurate dynamic models quickly. The piecewise method also allows for nonlinearities and time variance in the system to be accounted for. Based on comparisons between the developed method and other commonplace modelling methods in the literature, the developed method has similar model accuracy to others, less in the case of deep learning methods, but with greatly reduced complexity and time to generate, and removes the need for dynamic parameter measurements.

CHAPTER 4

MODEL PREDICTIVE CONTROL WITH OPTIMAL MODELLING FOR ACCURATE PNEUMATIC ARTIFICIAL MUSCLE MOTION

This chapter presents a novel MPC based on dynamic models generated using the PSO method, as well as a particle-swarm optimised proportional-integral-derivative controller (PSO-PID), an ILC, and classical PID control, for accurate motion control of the PAM. Experiments using predetermined series of waveform inputs and external loading to the system are used to validate each controller, and the results compared to determine successes and failings of each.

The work presented in this chapter is published in Biomimetics as:

- Brown DF, Xie SQ. Model Predictive Control with Optimal Modelling for Pneumatic Artificial Muscle in Rehabilitation Robotics: Confirmation of Validity Though Preliminary Testing. Biomimetics (Basel). 2025 Mar 28;10(4):208. doi: 10.3390/biomimetics10040208.

4.1 Introduction

The type of actuator used in a rehabilitation robot is important for several reasons. They must be capable of repeated, accurate motion to provide the treatment necessary for patients requiring rehabilitation and be able to apply sufficient torque to the patient to move their limb along the required motion, or to resist their motion in the case of active resist exercises but be controllable such that the torque output does not exceed safe values. Specifics of actuator design and control for rehabilitation robotics are detailed in [121]. Another desirable factor is intrinsic compliance, which can help increase safety and comfort, allow users a degree of freedom of motion, as well as increase the transparency of the system by reducing patient–machine interaction forces. Several compliant actuators exist which are popular in the field of rehabilitation robotics, including Series Elastic Actuators (SEAs) and PAMs, but controlling these actuators comes with its own problems. Due to the nonlinear nature of intrinsically compliant actuators, they act dynamically to input rather than linearly. This makes more traditional controllers like PID less effective in providing accurate motion. Reviews of soft and compliant actuators in rehabilitation robotics are presented in [122, 123].

The use of pneumatic actuators in lower-limb rehabilitation robots has grown over the past few years, as explored in the review presented in [124]. Various pneumatic actuators are popular in the field for their compliant dynamics and interactive nature, including McKibben artificial muscles, rubbertuators, air muscles, pneumatic artificial muscles, and pneumatic muscle actuators. It is also mentioned in this review that while PID controllers are suitable for controlling pneumatic actuators, the nonlinear dynamics and complexity of the actuators

may not be accurately controlled without further integrated control paradigms. Among those mentioned are various adaptive controllers using PID, a neuro-fuzzy network controller, neural-network based control and sliding mode control. One final suggestion states that a more complicated controller may not be the best approach to this problem, as additional sensors and impedances would increase the overall complexity of the system and make it more difficult to use, and a simpler controller is preferred.

This sort of compliant actuator is used for various purposes in the field, and in different configurations. The robot presented in [125] uses an antagonistic pair of pneumatic muscles to control a finger rehabilitation robot. This system also uses a magnetorheological dampener, and in experiments both open- and closed-loop PID control systems are implemented. A powered ankle–foot orthosis (PAFO) using a pair of PAMs to provide two degrees of freedom is presented in [126]. This system uses a sliding-mode controller for actuator control. The system presented in [42] consists of three separate pneumatic subsystems for body weight support, postural support, and gait orthosis. This system is a full-body gait rehabilitation system and uses an Interval Type-2 Fuzzy Sliding Pulse-Width Modulation Control to allow for proper control of the nonlinear pneumatic systems. A control system is developed in [127] which incorporates the RBF neural network and sliding mode control to ensure adaptive and disturbance-resistant control of a single-degree-of-freedom rehabilitation robot using a pair of antagonistic PAMs. The robot is designed to function for multiple different limbs. A neural network-based controller is also used in [128] for a hand rehabilitation robot utilising flexible pneumatic muscles. The intelligent controller has adaptive elements allowing it to accurately control the position of the orthosis despite interference forces and the nonlinearity of the actuators. Another control scheme designed to

accurately control pneumatics is presented in [67] with a multiple-input single-output model free-adaptive control scheme. This controller is applied to a single DOF multi-joint rehabilitation robot which uses two PAMs similar to [126]. Experiments presented in [104] aim to determine the dynamic characteristics of PAMs with the intention of accurate servo control. Nonlinear pressure flow values are compensated for using a lookup table, and position control is achieved using a model-based PID controller. This simple control structure achieved good closed-loop regulation and position tracking.

As shown in the literature, there is sufficient interest in pneumatic actuators in the field of rehabilitation robotics to make it an area of growing research, particularly the problem of accurate control. Accurate, reliable, and flexible motion tracking in a rehabilitation robot is essential for its effective use in a real rehabilitation setting. As professional therapists set the desired exercise motions, it is important to have them be properly followed to ensure proper rehabilitation outcomes for patients, as well as ensure their safety in using a robot. A control system able to perform well under many different input requirements also makes the robot more flexible in the conditions and stages of recovery it can treat. However, while good control performance is shown in many studies, there is a lack in comparison data between different intelligent control approaches in PAM-actuated rehabilitation robotics.

To address this limitation and investigate a novel application of prediction and optimisation algorithms, this chapter presents preliminary implementation and testing of an MPC scheme utilising the PSO modelling method, tested experimentally on a single-PAM setup in a simple hanging position as a feasibility study for eventual application of the controller to a PAM-driven rehabilitation robot. This approach involves a phenomenological approximation of the PAM to

a mass-spring-damper system, optimising the three parameters using a PSO algorithm in a three-dimensional search space. Based on preliminary testing, the linear model generation method, in which a single model is used to approximate the PAM's motion over a specific pressure input range, will be used here. The switching issue present in the piecewise and inflate–deflate modes has a magnified effect when used in conjunction with a control algorithm; as such, the linear method was considered the best approach for motion accuracy.

In order that this controller is properly validated in comparison with other controllers commonplace in the field, two other intelligent control strategies were applied to the system, as well as one classical control strategy: ILC, Particle Swarm Optimised Proportional Integral Derivative Control (PSO-PID), and classical PID control. While PID control is generally regarded as unsuitable for use with nonlinear systems based on its linear nature and poor approximation of time-variant systems, its use is prevalent in control theory as a computationally and mathematically efficient algorithm. As such it will be included in this study as a comparison point to demonstrate the improved effectiveness of intelligent control on the PAM system.

MPC uses a dynamic model of the system to predict over a finite period the behaviour of the system and calculates the control output required to best optimise some cost function over that period. Using this predictive method, the time-variant characteristics of the system are accounted for, and nonlinearities can be included in the model of the system. This makes MPC a suitable controller for PAMs. However, the need for a model of the system makes it difficult to apply to complex systems and actuators. This is especially true for systems including uncertainties and multiple nonlinear factors such as PAMs, as models for such systems tend to include multiple assumptions and simplifications, giving model-

based controllers an inherent trade-off between accuracy and computational efficiency. In [108], a switching model predictive controller is developed for a PAM for the purpose of testing a novel modelling method using PieceWise Affine model approximation. The PAM is initially estimated as a spring-damper system with a second-order differential equation of motion, but in the piecewise modelling estimation the second-order element is ignored. A single PAM is set up vertically to measure displacement with no load attached. The controller, in comparison with the PID control of the same system, is found to have lower motion error values and faster convergence. A 2 DoF robot actuated by two antagonistic pairs of PAMs as presented in [129] which uses MPC for motion control. Simulations show that the controller provides accurate motion control with small errors and stable steady-state behaviour, with the model used for the system dynamics being a nonlinear eighth-order set of differential equations, with polynomial functions serving as the characteristics of the PAMs. A discrete-valued model-predictive controller is presented in [130], and improved upon in [131], for motion control of a novel hybrid-pneumatic electric actuator and a double-acting pneumatic cylinder, respectively. Results from both studies show that novel controllers outperform the state-of-the-art sliding mode control by a significant margin. A lower limb orthosis powered by PAMs and controlled by a neural network-based nonlinear MPC is presented in [132]. In online experiments, the system meets requirements for each different participant, and the major concerns for inhibited system performance are the PAM's intrinsically slow rate of motion owing to the maximum allowed air flow into and out of it, and human–machine interaction sensing. MPC has been proven suitable for accurate motion control of PAMs; however, the modelling required for this control method produces another level of complexity, as this in itself is a separate area of study.

ILC is popular for use with nonlinear actuators as it does not rely on a complex model of the system, rather measuring the desired and actual outputs and iteratively calculating the best control signal based on the difference. This makes it suitable for time-varying systems, and there are many examples of its use in rehabilitation robotics using PAMs. The system RUPERT presented in [79] uses ILC for assistive reach-to-grasp tasks actuated by a series of PAMs, where its use is attributed to the need for a suitable controller for a nonlinear and time-varying system, as well as the repetitive nature of attempting the same task multiple times. Another rehabilitation/assistive robot utilising PAMs is presented in [133], which uses an improved PID controller, has issues with phase lag relieved using ILC to iteratively adjust control parameters, fixing this lag issue and reducing output error. A simulation of a PAM presented in [134], utilising ILC to account for the nonlinear and time-varying nature of the actuator, shows results proving the algorithm is capable of accounting for these characteristics, as well as uncertainties in the system. Based on the widespread use and research into ILC in the field of rehabilitation robotics and specifically its usefulness in controlling PAMs, it was chosen as a comparison for the developed MPC in this study.

Similarly to learning algorithms, optimisation is often used to improve the performance of controllers for complex systems, with PSO being a popular optimisation algorithm. PID is often the target of such optimisation as its functionality is heavily tied to how well the small number of parameters are tuned to the system it is to control. An upper limb exoskeleton robot using this method of optimised control is presented in [27] alongside a method using an improved version of classical PSO, Artificial Bee Colony Optimisation. A lower limb rehabilitation robot presented in [37] also uses improved PSO-PID control. Both these studies found their optimised controllers to be robust and have more

accurate motion control. The study presented in [135] develops a dynamic neural network and PID controller for control of PAMs, the parameters of which are optimised using the PSO algorithm with Integral Time Absolute Error as the objective function. Another study using a similar technique is presented in [136] with adaptive and classical synergetic controllers developed for a robotic arm actuated by a PAM.

The experiments presented in this chapter aim to test and compare the developed MPC with classical ILC, PID, and PSO-PID in controlling the actuation of a single PAM in online control experiments, for future implementation to a complete PAM-driven rehabilitation robot. The main results for determining effectiveness will be motion tracking accuracy, response to disturbance, and smoothness of motion, as these are necessary for the controller to function well as part of a rehabilitation robot utilising PAMs for actuation. The experiments will take place on a single PAM set up to accurately measure displacement. Weights will be used to apply resistive force to the actuator, as well as to simulate disturbances to the system. Each controller will be implemented and tested with the same test scheme, and the displacement error values will be measured and analysed to determine how well they perform comparatively.

The contributions of this chapter include development and implementation of a model predictive controller for accurate PAM motion using the PSO-based modelling method presented in chapter 3 to generate dynamic models of the system, experimental data for comparison of the performance of the developed MPC as well as other popular controllers in the field of rehabilitation robotics—ILC, PID, and PSO-PID—using an experiment plan designed to simulate the motion and load requirements of PAMs in a rehabilitation robot, as well as a comparative discussion comparing the relative strengths and weaknesses of each

controller. Based on the limited examples of comparative studies, this experiment including multiple commonplace controllers will help in quantifiably demonstrating the relative benefits and shortcomings of these controllers and help fill this gap in the literature. The overall aim of this research is to determine the feasibility of the developed MPC, as well as classical ILC and optimised PID controller, for accurate motion control of PAMs in a rehabilitation robot setting, with the aim to implement the developed algorithms in a PAM-driven rehabilitation robot.

4.2 Materials and Methods

4.2.1 Controllers

4.2.1.1 Model Predictive Control

MPC uses a model of the system as well as prior knowledge of the input sequence to predict the movement of the actuator in advance for a given future time period. This allows for accurate control of nonlinear systems for any input sequence and is therefore usable for various applications. MPC also has the option of constraining many aspects of the control sequence, including minimum and maximum control values for both the control output and the predicted control output, as well as minimum and maximum values for the rate of change of control values. However, the necessity of a mathematical model of the system can cause issues in development, especially for a complex system such as a PAM, as these models often include simplifications and assumptions resulting in inaccuracies. The controller also requires that the entire input sequence be known beforehand, and the predictive nature prevents it from being used in modes other than passive

movement, such as resistive training in rehabilitation. The structure of the MPC algorithm is shown in Figure 4.1.

At each sampling period t the state of the system is taken and via an optimization function, a cost-minimising control output is calculated for a time horizon defined by the prediction period T. Once a cost-minimal control trajectory starting at the sampled state and for the time period $[t, (t + T)]$ is found, the first step of this strategy is applied to the system. The remainder of the calculated control trajectory is discarded, and the process is repeated from the new system state. While MPC is an optimal control strategy as it uses a cost optimisation method for control, the process by which it calculates this control is not optimal as a great many calculations are discarded.

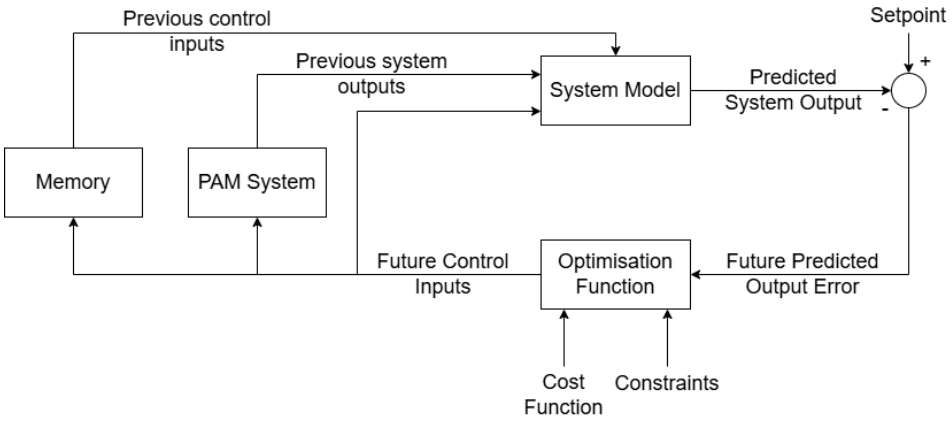


Figure 4.1: MPC Structure. The system model is generated according to the methods described in chapter 3.

The optimisation algorithm used here is linear quadratic programming, the cost function of which is described by Equation (4.1):

$$J = \sum_{t}^{T} q(\hat{y} - s)^2 + \sum_{t}^{T} r\Delta u^2 \qquad (4.1)$$

Where J is the cost function, t is the current time step, T is the prediction period, q is the output error weight parameter, $\hat{y}$ is the predicted system output, s is the

setpoint, r is the control weight parameter, and Δu is the predicted change in the control value such that $\Delta u = u_k - u_{k-1}$ with u_k being the control value taken at time step k. For this MPC implementation, the output error weight was set to 1 and the control weight was set to 20.

Based on the value of J as determined by the cost function in Equation (4.1), the optimal control value u for a given time period T is achieved by solving Equation (4.2):

$$\frac{\delta J}{\delta u} = 0 \tag{4.2}$$

This allows for the minimum possible J to be calculated, and the associated optimal value of u to be found.

As MPC relies heavily on the accuracy of the model of the system to properly optimise potential control solutions, it is important the model used approximates the PAM as closely as possible. As discussed in chapter 3, modelling PAMs is particularly challenging due to their dynamic behaviour. The PSO-based modelling method used there will be employed here to generate mathematical models for the MPC based on the proposed mass-spring-damper approximation. To get a more accurate model response without the undesirable jumping from a piecewise model, a single linear phenomenological model will be generated for each required motion, accounting for the position- and time-variant behaviour of the PAM over different stroke lengths and pressure input ranges.

4.2.1.2 Iterative Learning Control

The ILC improves tracking performance over multiple iterations of the same input sequence, thereby progressively reducing errors. Using this control algorithm, long-term stability and performance is improved; however, the initial learning period is generally unstable and inaccurate. Therefore, reducing this

initial period by speeding up the learning rate can improve the functionality of the controller. This control method is model-free, as the controller output is calculated using error feedback. This is a desirable trait for controllers of nonlinear systems as it removes the need for a complex mathematical model, which would likely include simplifications and assumptions.

The standard equation for control output for ILC is shown in Equation (4.3):

$$u(t) = u_{old}(t) + pe_{old}(t) \tag{4.3}$$

Where $u(t)$ is the new control signal, $u_{old}(t)$ is the control signal at the same time step within the previous learning period, $e_{old}(t)$ is the error at the same time step within the previous learning period, and p is the learning rate parameter which is manually tuned.

4.2.1.3 Particle Swarm Optimised PID Control

PID control is generally regarded as unsuitable for nonlinear systems such as PAMs as it treats the input–output relationship of the system as position- and time-invariant. Introducing PSO algorithms to optimise the parameters of the PID controller can improve this shortcoming by calculating optimal parameters based on the behaviour of the PAM over the required motion. Standard PID requires the three control parameters to be tuned manually based on trial and error of the system output which can result in poor performance due to human error. The use of an optimisation technique allows for control parameters specific to the plant to be generated, resulting in a control system specialised for the system to be controlled, and thus more accurate motion. The optimisation algorithm is run offline to generate parameters for the PID controller for online experiments.

The equations for velocity and position update in the PSO algorithm are given in Equations (3.11) and (3.12).

To use PSO to optimise parameters for PID control, a 3-dimensional search space is used, optimising the parameters K_c, T_i, and T_d. To converge on an optimal solution, the objective function used for swarm fitness is the RMSE of motion tracking over a single input wavelength. Offline parameter generation is performed using an unloaded PAM with an input sequence of a sin wave with an amplitude of the full stroke length, meaning the generated parameters are optimal only for the specific use case of this study. In the case that PSO-PID of this nature is used for control of other systems or under different experimental parameters, the optimisation would need to be performed for each specific case to find optimal control parameters. As the optimisation technique used here is specifically performed offline, it would be unsuitable for use with a potential user or a system which changes during online motion.

4.2.2 Experimental Setup

The system setup used for these comparative experiments is the same as that used in chapter 3. See section 3.2.4 for a detailed description of the setup, Figure 3.2 for the flowchart diagram of physical and data connections, and Figure 3.3 for a labelled picture of the setup.

4.2.3 Experiment Plan

The intended outcome of these experiments is to gather motion tracking data for each of the four control schemes such that their overall accuracy including average error, smoothness of motion, and factors such as overshoot can be analysed and compared. Through this analysis, the most suitable controller(s) for the application of PAM motion control can be determined and brought forward

for further work. Experiments are designed to exhaustively test the output capabilities of the PAM to allow for the best possible comparison.

Each experiment will involve a specific motion as input to each controller, along with the addition of external weights applied to the PAM, and adding/removing them at certain points during motion. Table 4.1 shows the experiment outline as well as the main purpose of each set of experiments. Each experiment, including input motion setpoints and weights used, will be performed unaltered for each controller to ensure the results are comparable.

Table 4.1: Experiment Outline

Experiment	Experiment Purpose	Motion and Weights
Continuous Motion	Determine controller's motion accuracy with no disturbance for different types of motion	Sin wave, 0cm – 10cm Sin wave, 0cm – 5cm Sin wave, 5cm – 10cm Sin wave, 0cm – 10cm, rapid motion Triangle wave, 0cm – 10cm Square wave, 0cm – 10cm
Continuous Motion with Weights	Determine the effect of added weight to controller's motion accuracy	Sin wave, 0cm – 10cm, 5kg load Sin wave, 0cm – 10cm, 10kg load Square wave, 0cm – 10cm, 5kg load Square wave, 0cm – 10cm, 10kg load Sin wave, 0cm – 10cm, rapid motion, 10kg load Sin wave, 0cm – 5cm, 10kg load Sin wave, 5cm – 10cm, 10kg load
Continuous Changing Motion	Determine the controller's response to a change in continuous motion, how quickly they can adapt Changes made after 6 wavelengths	Sin wave, 0cm – 4cm changed to 0cm – 8cm Sin wave, 0cm – 10cm changed to 2.5cm – 7.5cm Sin wave, 0cm – 5cm changed to 5cm – 10cm Sin wave, 0cm – 10cm, slow motion changed to rapid motion Sin wave, 0cm – 10cm, rapid motion changed to slow motion
Static with Disturbance	Determine controller's response to disturbance with no noise or motion Performed with static 5cm setpoint, weights added/removed at 5 seconds	5kg load added 10kg load added 5kg load removed 10kg load removed
Continuous Motion with Disturbance	Determine controller's response to disturbance during motion	Sin wave, 0cm – 10cm, 10kg load added after 4 waveforms Sin wave, 0cm – 10cm, 10kg load removed after 4 waveforms Sin wave, 0cm – 10cm, 5kg load added and removed after each waveform

4.2.4 Algorithm Parameters

4.2.4.1 MPC Model Generation

The PSO-based modelling method presented in chapter 3 is used here to generate dynamic models of the PAM for use in the MPC algorithm. A PSO algorithm with a swarm size of 50, $W = 0.9$, $C1 = C2 = 2$, and run for 20 iterations was used to generate each model. The fitness value was calculated using the actual PAM motion with a sin wave voltage input to the pressure regulator, the amplitude of which was based on the steady-state displacement of the PAM at certain voltage inputs, as shown in Figure 4.2, such that the required displacement upper and lower bounds for the comparative experiment were reached during model generation. Using this method, a set of model parameters were generated which best described the PAM's behaviour for each required motion in the experiment plan, allowing for more accurate control through the MPC algorithm. The parameters of these models are shown in the MPC model parameters column in Table 4.2.

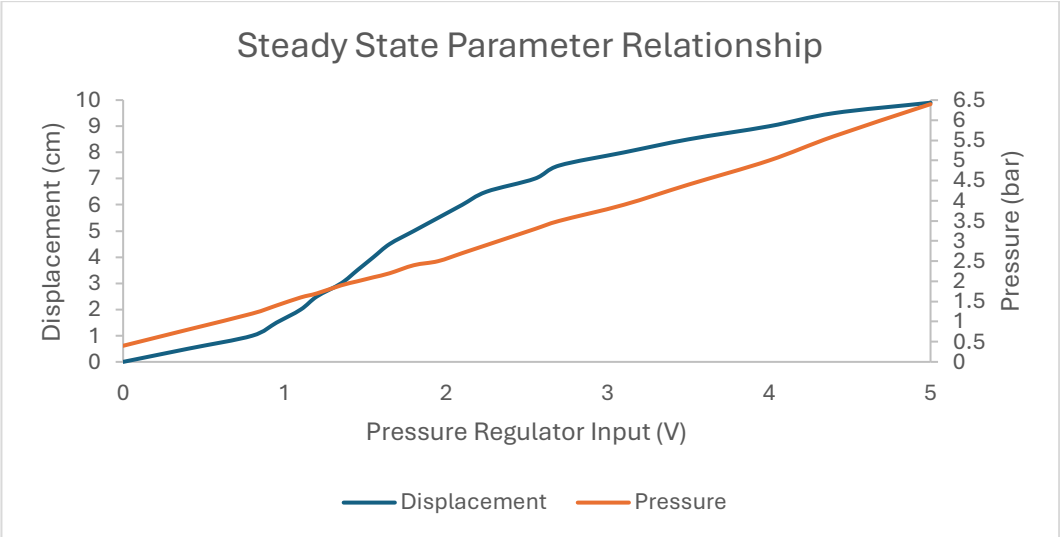


Figure 4.2: Steady-state relationships between voltage input to the pressure regulator, internal air pressure in the PAM, and actuator displacement.

Table 4.2: PID control parameters and MPC model parameters

Waveform	Amplitude (cm)	Offset (cm)	Frequency (Hz)	PSO-PID Parameters			MPC Model Parameters		
				K_c	T_i	T_d	P_1	P_2	P_3
Sinusoidal	10	0	0.25	0	0.801752	0.0191877	8.18E-06	0.182535	0.534393
Sinusoidal	5	0	0.25	0	0.34711	0.00266562	0	0.460018	0.191448
Sinusoidal	5	5	0.25	0	1.0466	0.0187886	3.45E-06	0.741741	0.012203
Sinusoidal	10	0	1	0	0.801752	0.0191877	8.18E-06	0.182535	0.534393
Triangular	10	0	0.25	0	0.570082	0.00962227	9.15E-06	0.182535	0.534393
Square	10	0	0.25	0	0.885228	0.00971446	4.96E-06	0.182535	0.534393
Sinusoidal	10	0	0.25	5	0.801752	0.0191877	8.18E-06	0.182535	0.534393
Sinusoidal	10	0	0.25	10	0.801752	0.0191877	8.18E-06	0.182535	0.534393
Square	10	0	0.25	5	0.885228	0.00971446	4.96E-06	0.182535	0.534393
Square	10	0	0.25	10	0.885228	0.00971446	4.96E-06	0.182535	0.534393
Sinusoidal	10	0	1	10	0.801752	0.0191877	8.18E-06	0.182535	0.534393
Sinusoidal	5	0	0.25	10	0.34711	0.00266562	0	0.460018	0.191448
Sinusoidal	5	5	0.25	10	1.0466	0.0187886	3.45E-06	0.741741	0.012203
Sinusoidal	4	0	0.25	0	0.442617	0.00526149	5.98E-06	0.101338	0.626386
	8	0	0.25	0	0.756974	0.00641648	5.38E-06	0.503874	0.154515
Sinusoidal	10	0	0.25	0	0.801752	0.0191877	8.18E-06	0.182535	0.534393
	5	2.5	0.25	0	0.626517	0.00597624	7.00E-06	-0.10410	0.890396
Sinusoidal	5	0	0.25	0	0.34711	0.00266562	0	0.460018	0.191448
	5	5	0.25	0	1.0466	0.0187886	3.45E-06	0.741741	0.012203
Sinusoidal	10	0	0.25	0	0.801752	0.0191877	8.18E-06	0.182535	0.534393
	10	0	1	0	0.801752	0.0191877	8.18E-06	0.182535	0.534393
Sinusoidal	10	0	1	0	0.801752	0.0191877	8.18E-06	0.182535	0.534393
	10	0	0.25	0	0.801752	0.0191877	8.18E-06	0.182535	0.534393
Constant	0	5	0	5	0.632498	0.0134572	1.10E-05	-0.10410	0.890396
Constant	0	5	0	10	0.632498	0.0134572	1.10E-05	-0.10410	0.890396
Constant	0	5	0	5	0.632498	0.0134572	1.10E-05	-0.10410	0.890396
Constant	0	5	0	10	0.632498	0.0134572	1.10E-05	-0.10410	0.890396
Sinusoidal	5	2.5	0.25	10	0.626517	0.00597624	7.00E-06	-0.10410	0.890396
Sinusoidal	5	2.5	0.25	10	0.626517	0.00597624	7.00E-06	-0.10410	0.890396
Sinusoidal	5	2.5	0.25	5	0.626517	0.00597624	7.00E-06	-0.10410	0.890396

4.2.4.2 PID Parameters

The parameters used for the classical PID controller were $K_c = 0.6$, $T_i = 0.01$, and $T_d = 1e^{-5}$. These parameters were tuned manually for fast response while minimising instability.

4.2.4.3 ILC Parameters

The learning rate used for the ILC in each experiment was p = 0.2. This value was tuned manually to optimise rate of convergence to the setpoint while minimising overfitting.

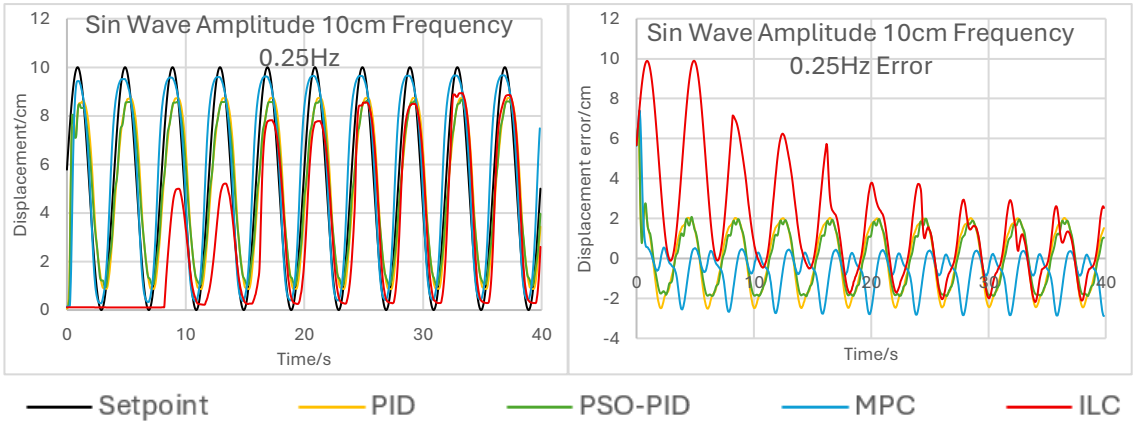
4.2.4.4 PSO-PID Parameters

To improve on the classical PID algorithm, PSO was used to generate optimal parameters for the three control values. Based on the dynamic behaviour of the PAM across its stroke length, as well as keeping the controller as computationally simple as possible while maintaining accurate motion tracking, a set of parameters, each of which included values K_c, T_i, and T_d, was generated for each motion required by the comparative experiment plan. This allowed for the most optimal PID control available based on the algorithm for each experiment.

Each set of parameters was generated using a PSO algorithm with a swarm size of 10, $W = 0.9$, $C1 = C2 = 2$, and run for 10 iterations. The position values of each particle corresponded to the K_c, T_i, and T_d parameters of the PID controller. The fitness of each particle was calculated as the RMSE between the desired setpoint motion of the PAM displacement and the actual PAM displacement under PID control, using that particle's parameter values, over two wavelengths of motion. The resulting parameter sets are shown in the PSO-PID parameters column in Table 4.2.

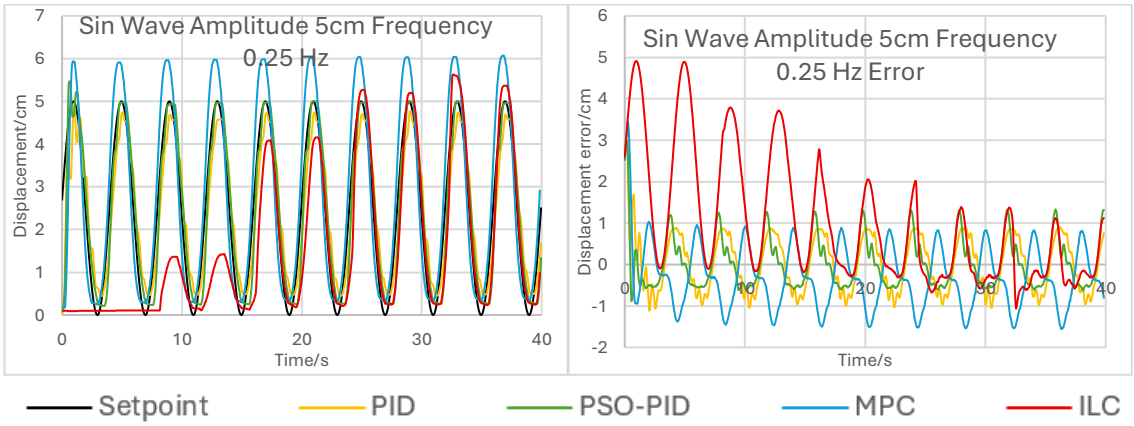
4.3 Results

The displacement of the PAM under each control scheme was measured for each experiment and overlaid for comparison. The displacement error for each experiment was also calculated and overlaid for each experiment. Figures 4.3-4.27 show graphical results of the experiments.



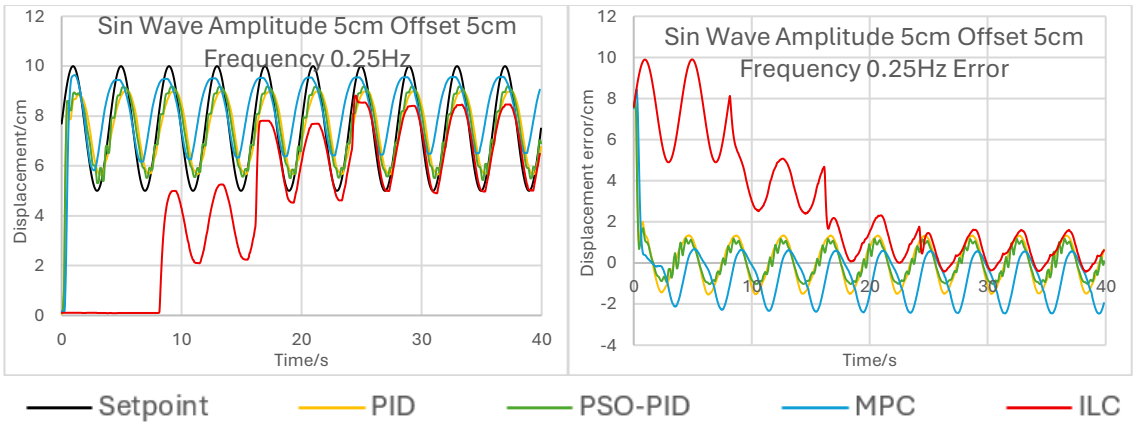
(a) (b)

Figure 4.3: Measurement values for the 0cm-10cm sin wave experiment. (a) shows the displacement readings, (b) shows the error values.



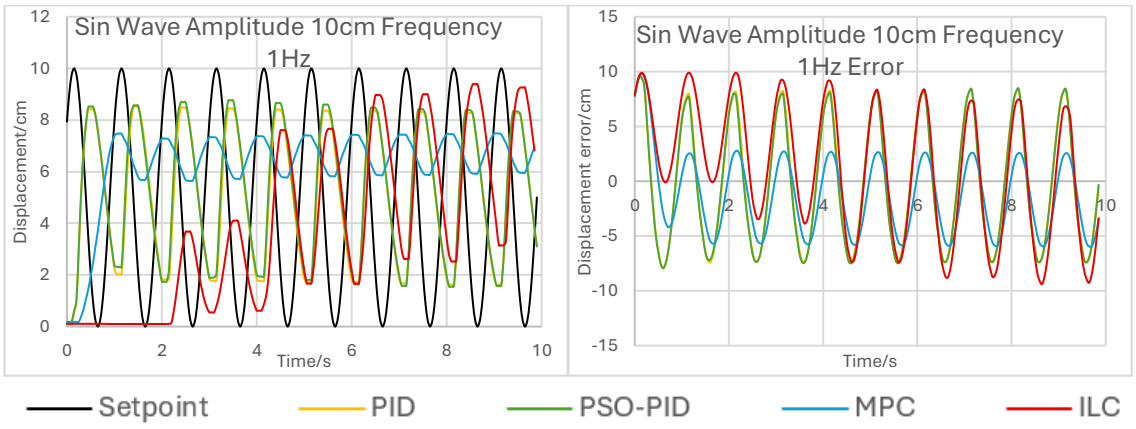
(a) (b)

Figure 4.4: Measurement values for the 0cm-5cm sin wave experiment. (a) shows the displacement readings, (b) shows the error values.



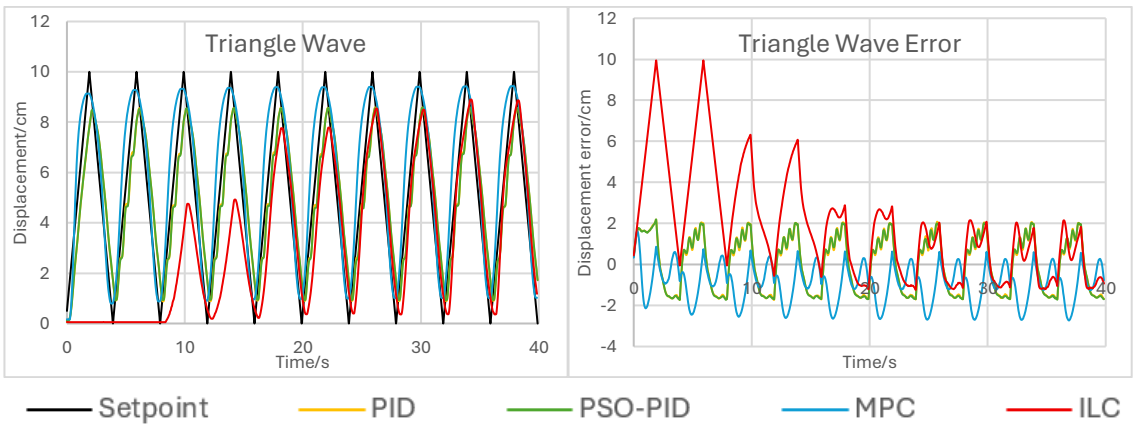
(a) (b)

Figure 4.5: Measurement values for the 5cm-10cm sin wave experiment. (a) shows the displacement readings, (b) shows the error values.



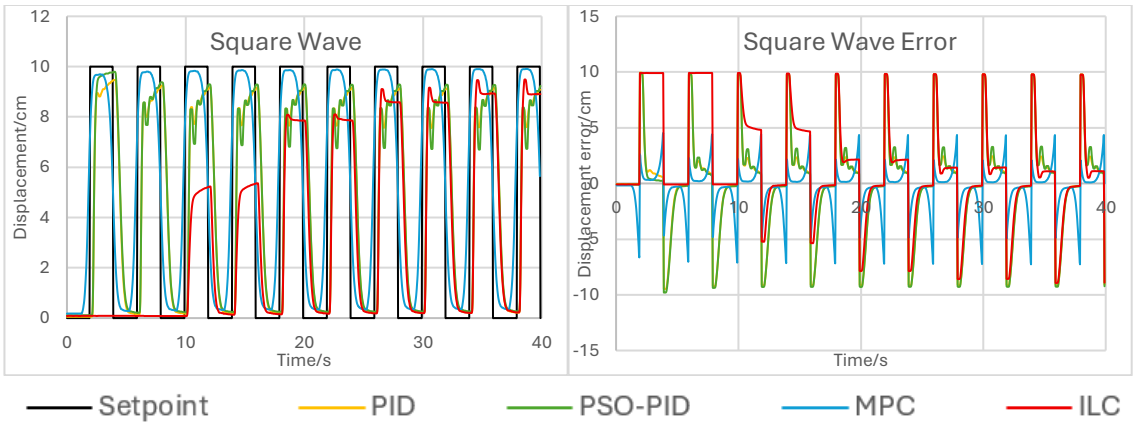
(a) (b)

Figure 4.6: Measurement values for the rapid motion sin wave experiment. (a) shows the displacement readings, (b) shows the error values.



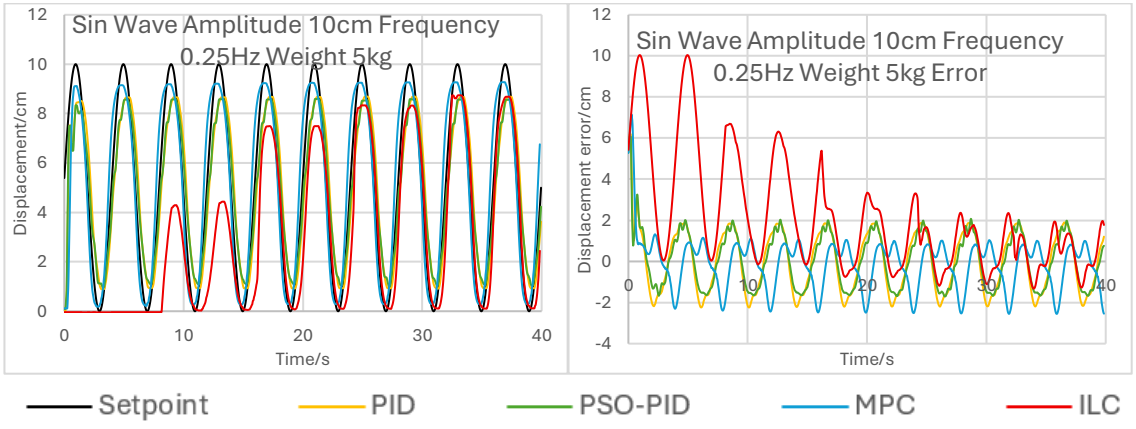
(a) (b)

Figure 4.7: Measurement values for the triangle wave experiment. (a) shows the displacement readings, (b) shows the error values.



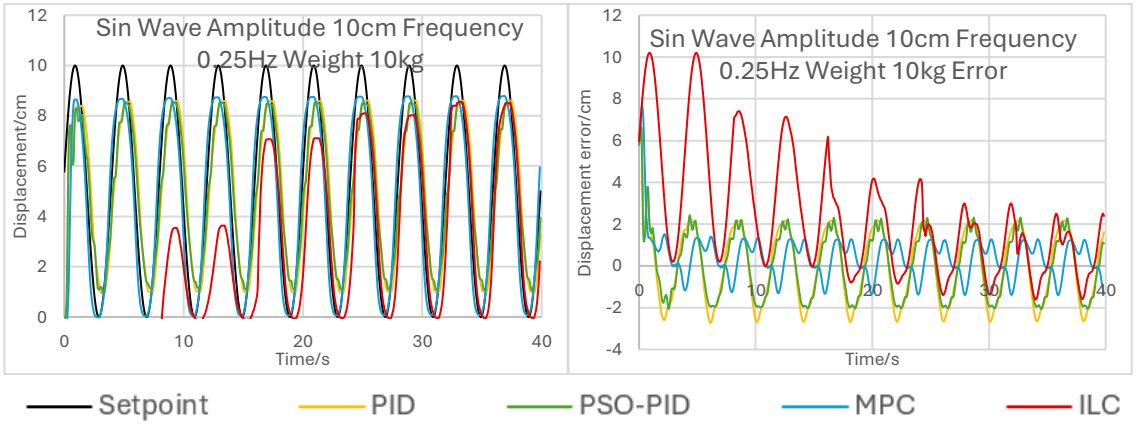
(a) (b)

Figure 4.8: Measurement values for the square wave experiment. (a) shows the displacement readings, (b) shows the error values.



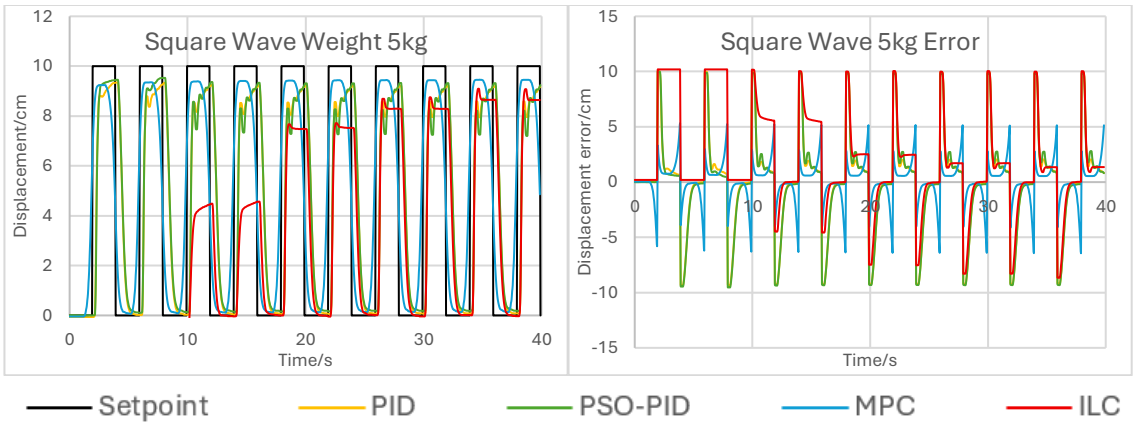
(a) (b)

Figure 4.9: Measurement values for the 5kg weighted 0cm-10cm sin wave experiment. (a) shows the displacement readings, (b) shows the error values.



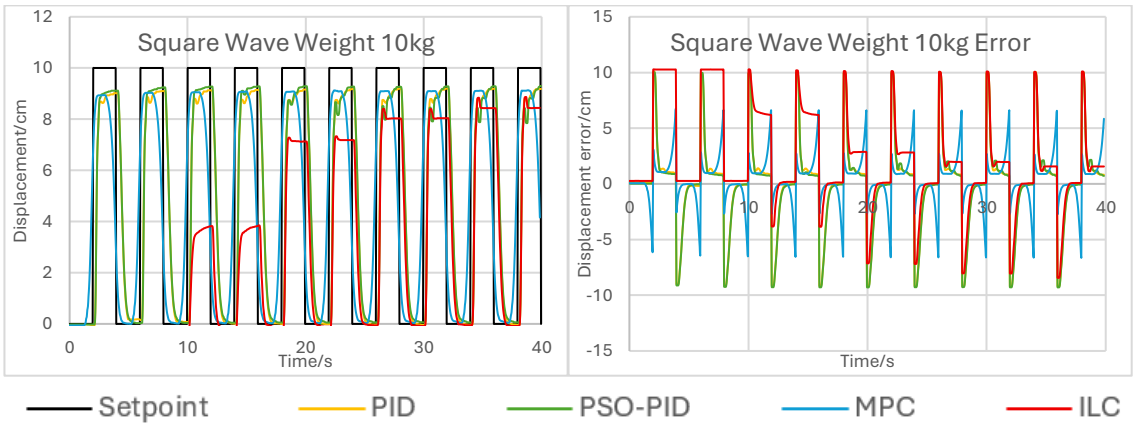
(a) (b)

Figure 4.10: Measurement values for the 10kg weighted 0cm-10cm sin wave experiment. (a) shows the displacement readings, (b) shows the error values.



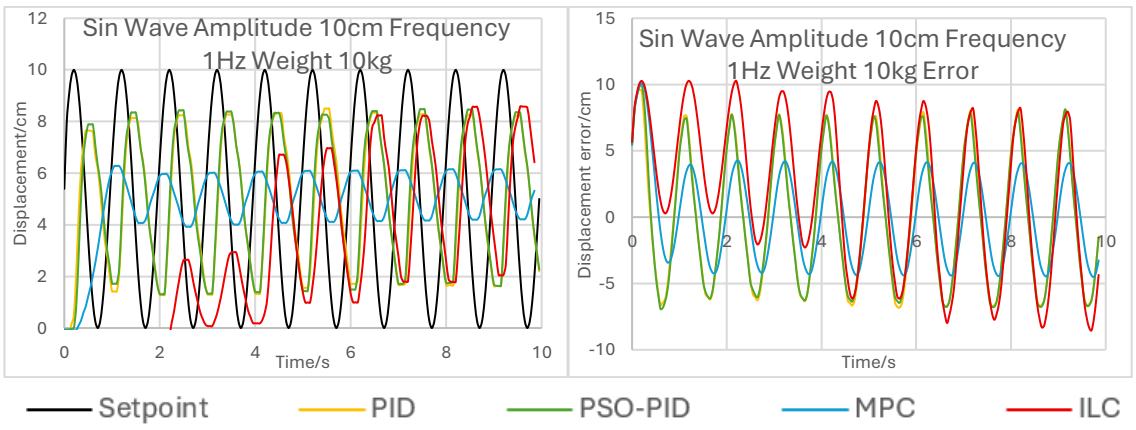
(a) (b)

Figure 4.11: Measurement values for the 5kg weighted square wave experiment. (a) shows the displacement readings, (b) shows the error values.



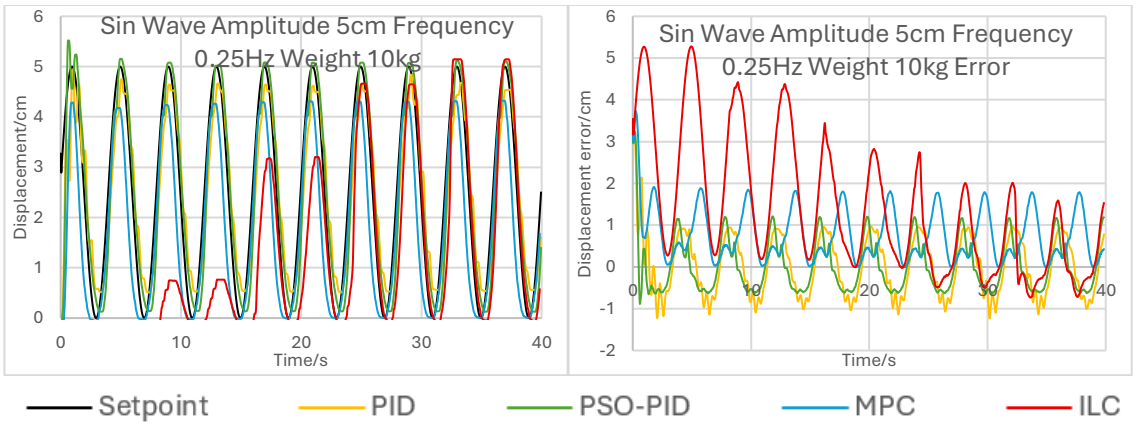
(a) (b)

Figure 4.12: Measurement values for the 10kg weighted square wave experiment. (a) shows the displacement readings, (b) shows the error values.



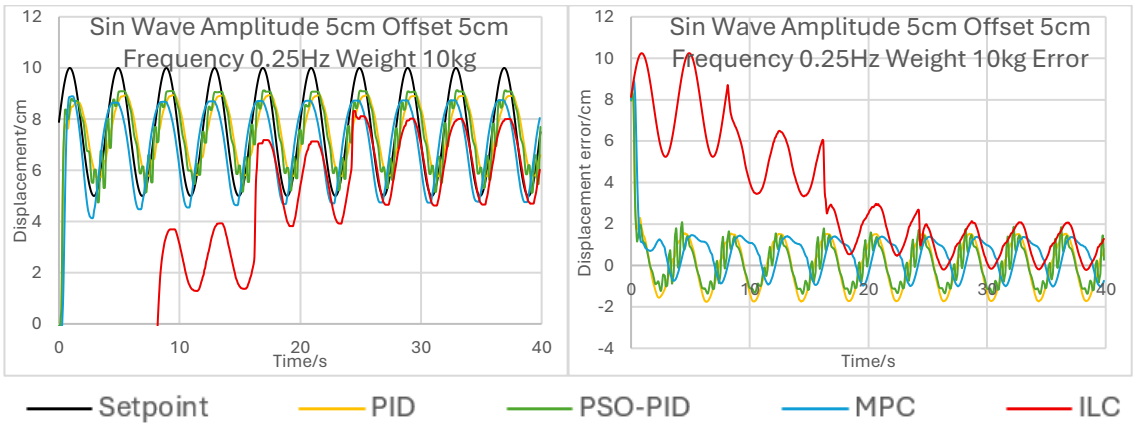
(a) (b)

Figure 4.13: Measurement values for the 10kg weighted rapid sin wave experiment. (a) shows the displacement readings, (b) shows the error values.



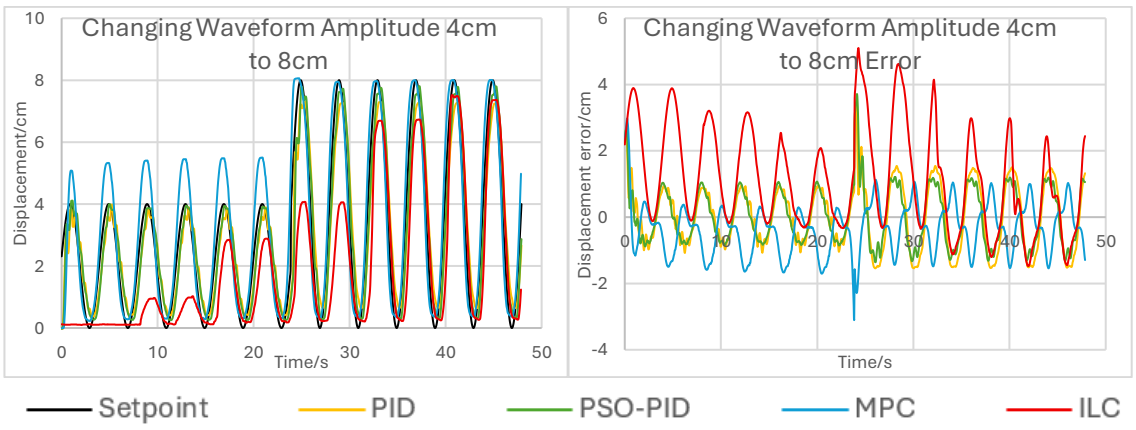
(a) (b)

Figure 4.14: Measurement values for the 10kg weighted 0cm-5cm sin wave experiment. (a) shows the displacement readings, (b) shows the error values.



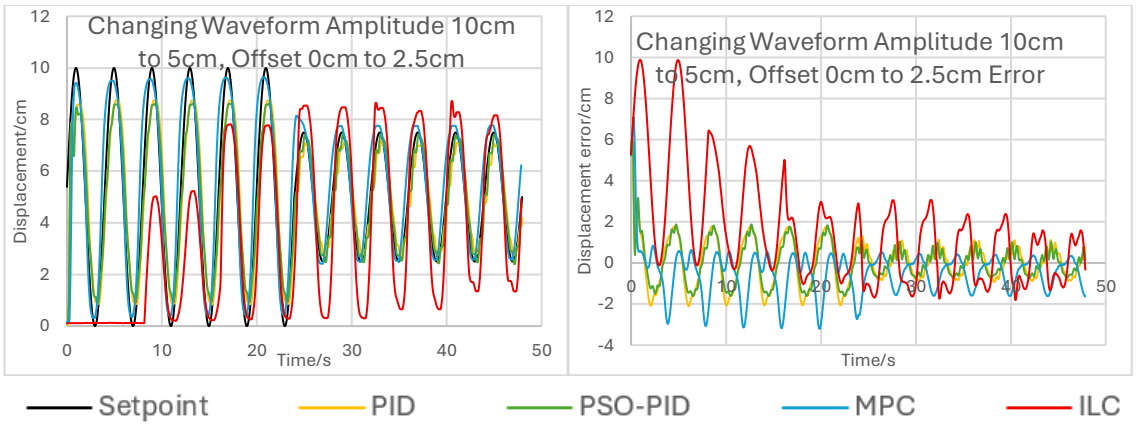
(a) (b)

Figure 4.15: Measurement values for the 10kg weighted 5cm-10cm sin wave experiment. (a) shows the displacement readings, (b) shows the error values.



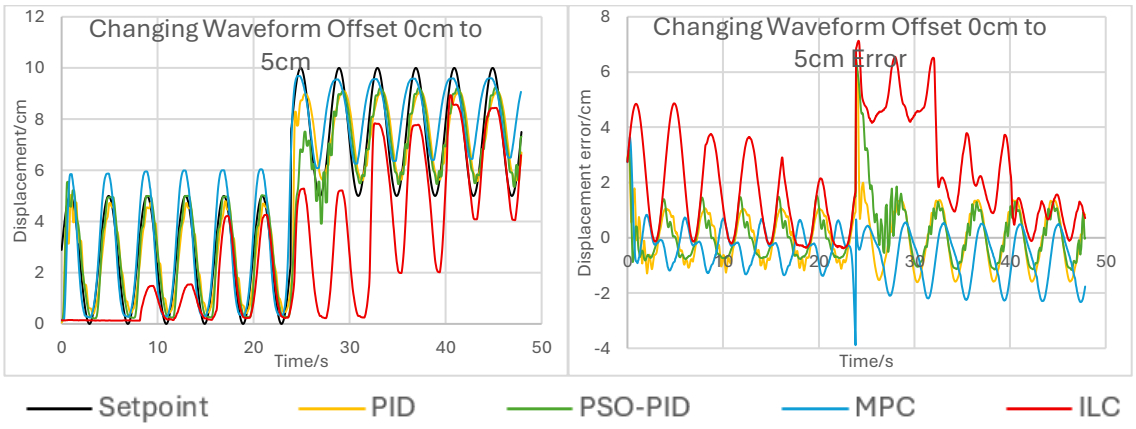
(a) (b)

Figure 4.16: Measurement values for the 0cm-4cm changing to 0cm-8cm sin wave experiment. (a) shows the displacement readings, (b) shows the error values.



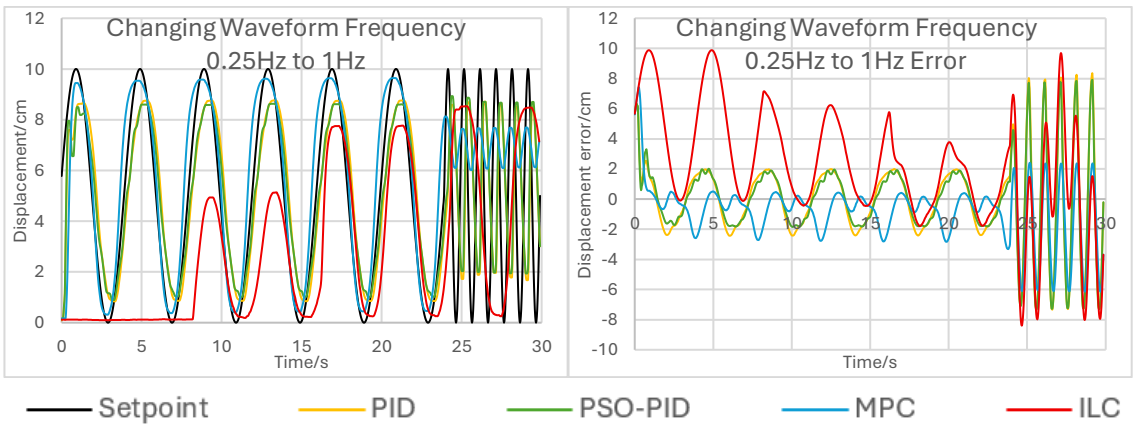
(a) (b)

Figure 4.17: Measurement values for the 0cm-10cm changing to 2.5cm-7.5cm sin experiment. (a) shows the displacement readings, (b) shows the error values.



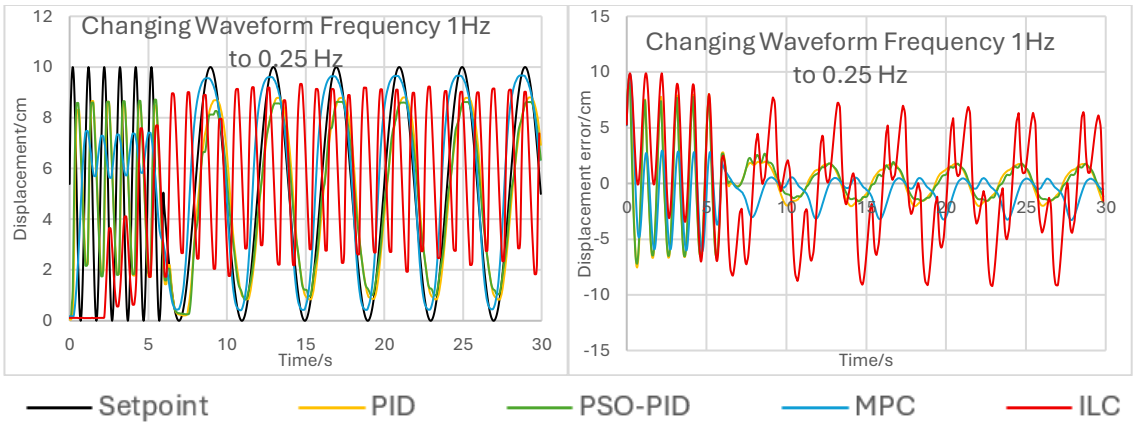
(a) (b)

Figure 4.18: Measurement values for the 0cm-5cm changing to 5cm-10cm sin experiment. (a) shows the displacement readings, (b) shows the error values.



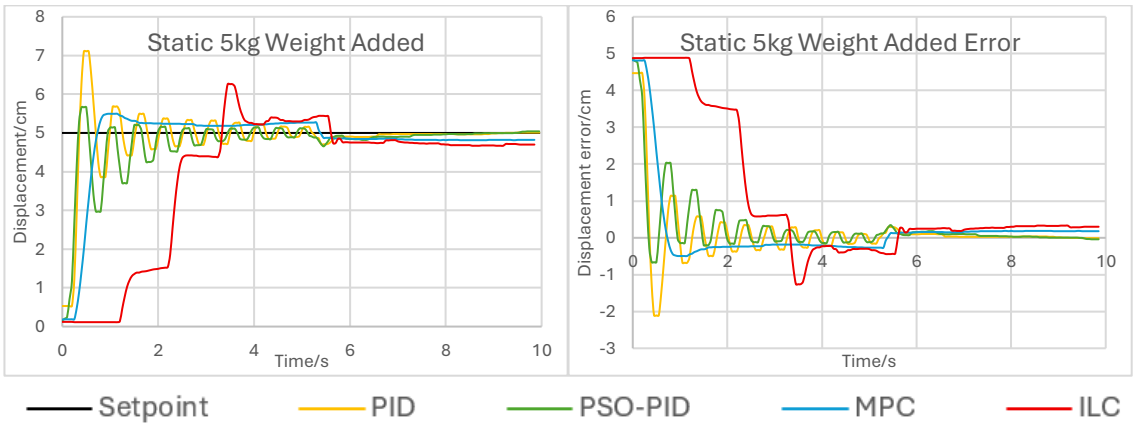
(a) (b)

Figure 4.19: Measurement values for the slow changing to rapid sin experiment. (a) shows the displacement readings, (b) shows the error values.



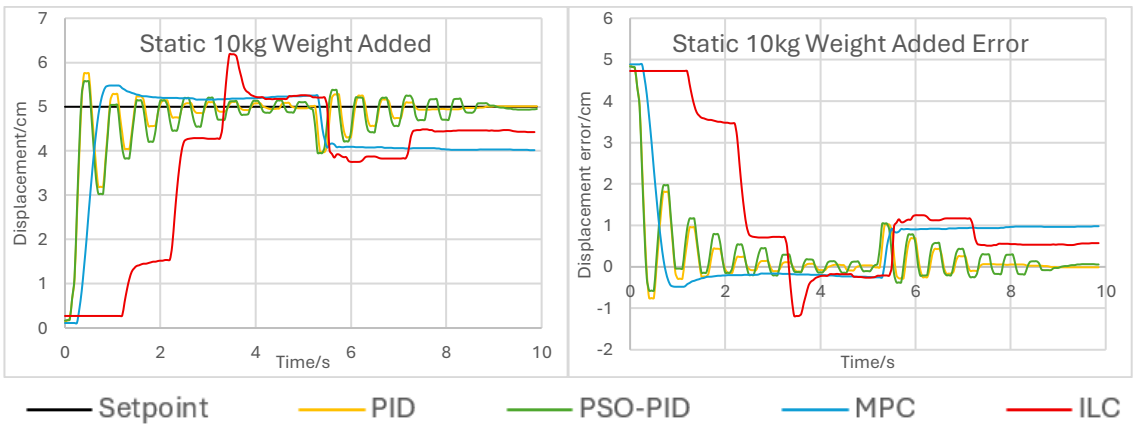
(a) (b)

Figure 4.20: Measurement values for the rapid changing to slow sin experiment. (a) shows the displacement readings, (b) shows the error values.



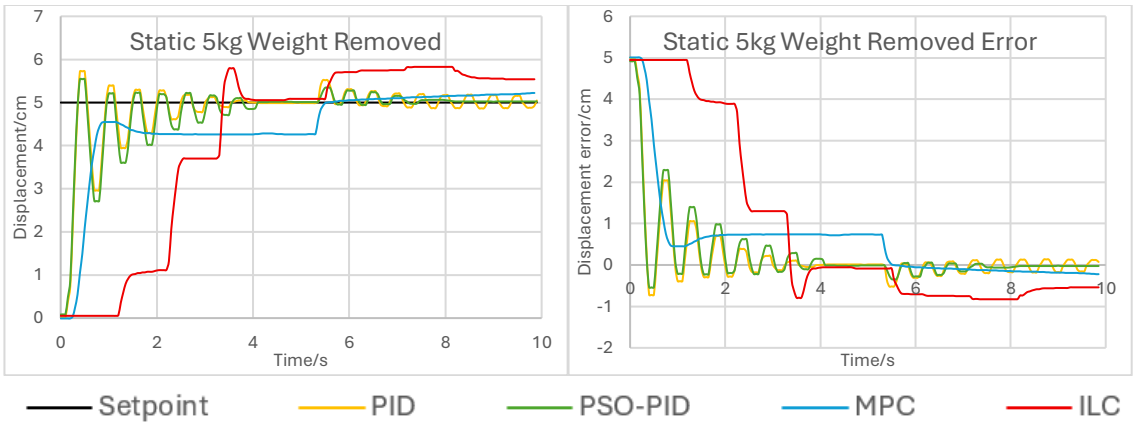
(a) (b)

Figure 4.21: Measurement values for the 5kg weight added experiment. (a) shows the displacement readings, (b) shows the error values.



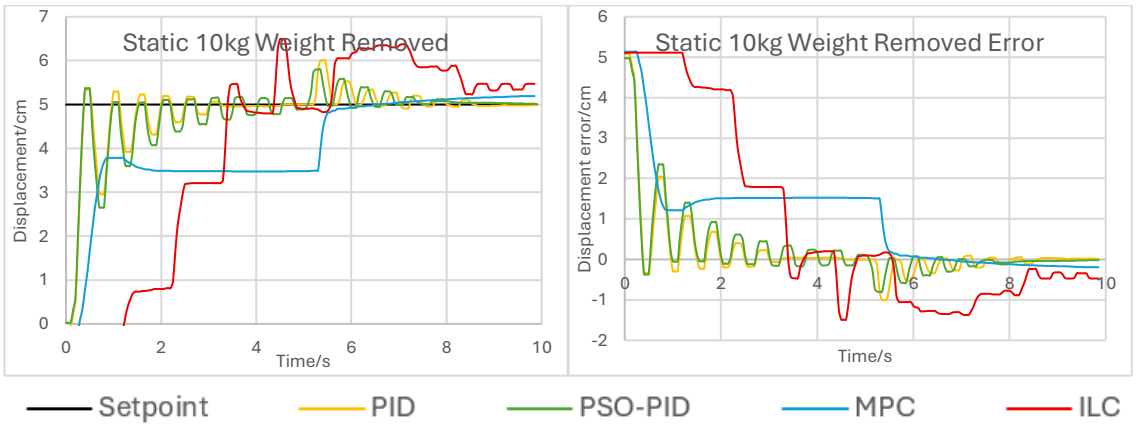
(a) (b)

Figure 4.22: Measurement values for the 10kg weight added experiment. (a) shows the displacement readings, (b) shows the error values.



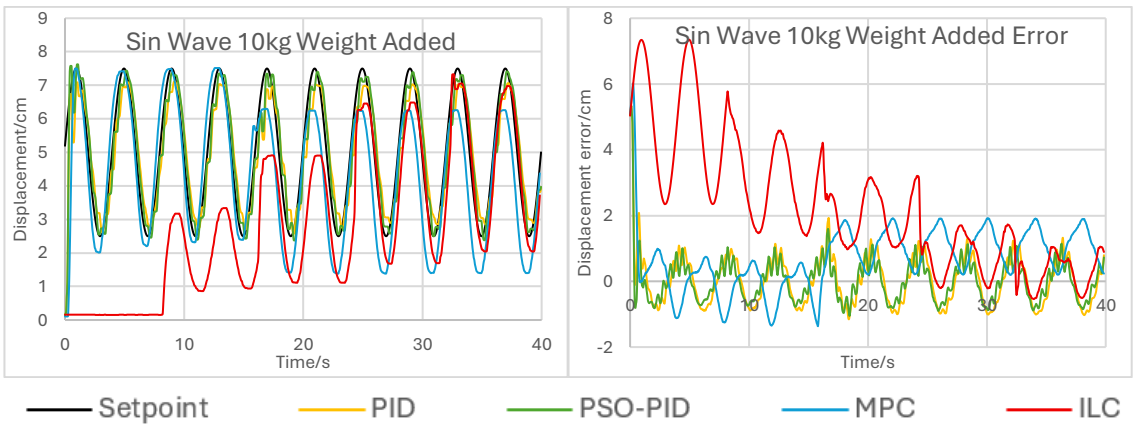
(a) (b)

Figure 4.23: Measurement values for the 5kg weight removed experiment. (a) shows the displacement readings, (b) shows the error values.



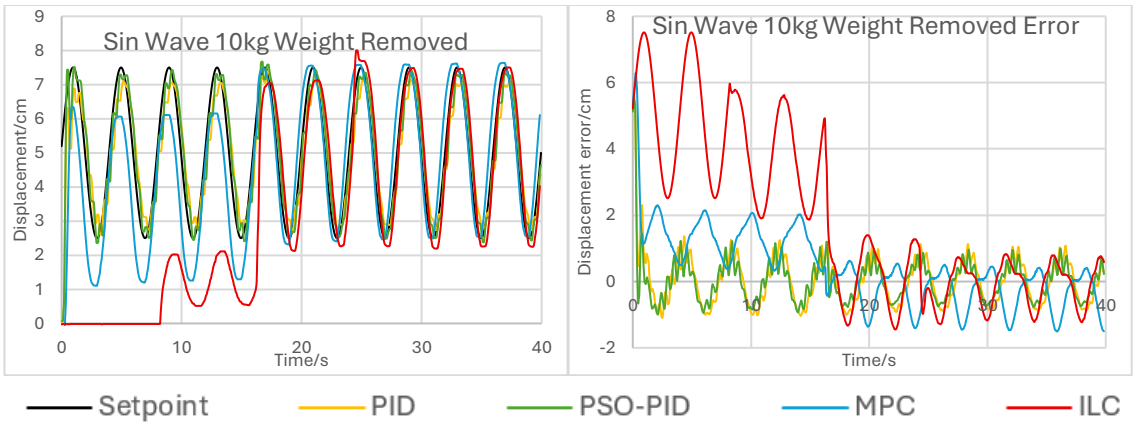
(a) (b)

Figure 4.24: Measurement values for the 10kg weight removed experiment. (a) shows the displacement readings, (b) shows the error values.



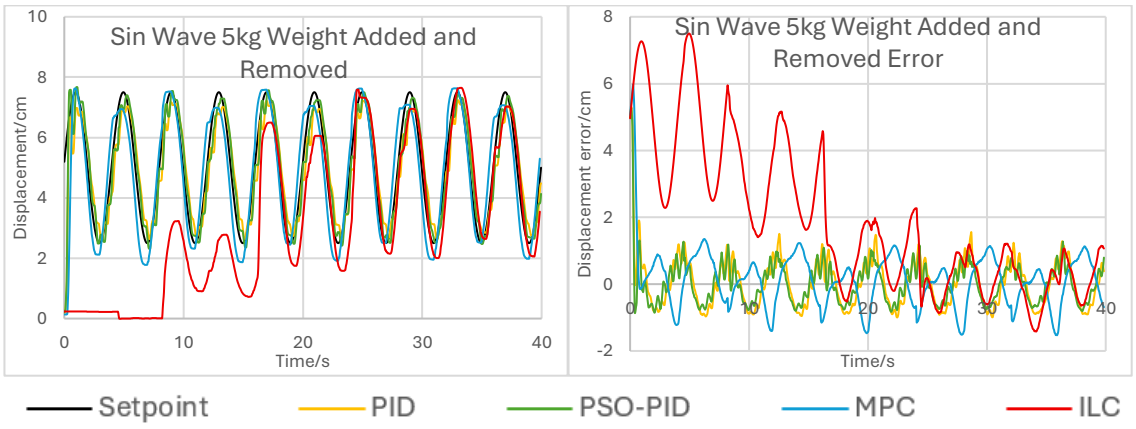
(a) (b)

Figure 4.25: Measurement values for the 10kg weight added experiment. (a) shows the displacement readings, (b) shows the error values.



(a) (b)

Figure 4.26: Measurement values for the 10kg weight removed sin wave experiment. (a) shows the displacement readings, (b) shows the error values.



(a) (b)

Figure 4.27: Measurement values for the 5kg weight added and removed sin wave experiment. (a) shows the displacement readings, (b) shows the error values.

4.4 Discussion

The dynamic properties of the PAM heavily impact the accuracy of motion under all control schemes at a high-velocity input, such as during the rapid sin wave experiments, in which a 1 Hz setpoint waveform is used rather than the 0.25 Hz used in the other experiments, as well as the square wave experiments. Rather than a fault in the controllers, this is mostly a reflection of the maximum change in displacement the actuator is capable of achieving. This also has an effect under a triangle wave setpoint, as constant velocity is difficult to achieve with dynamic

input/output behaviour. The higher frequency experiment, while not an accurate representation of actuator requirements in a rehabilitation setting, was performed to test the higher limits of speed response for the PAM and controllers. The error values for these experiments were generally the highest; however, the comparisons between the controllers is still useful and will be discussed.

The performance of the PID and PSO-PID controllers were generally consistent with each other. Both exhibited oscillating behaviour during most motions, including during constant displacement experiments and during the stationary points of the square wave setpoints. This was exacerbated with the addition of external loads, especially noticeable in the static experiments where the oscillation was mostly present before the weights were removed and after they were added. Both PID control schemes had a poor response time under square wave setpoints compared to the other controllers, with noticeably larger errors at the changing points in the waveform as well as slower settling time; however, the steady-state error at the static points was generally small. The poor response time can also be seen in the sin wave experiments with the PAM motion lagging behind the setpoint. The PSO-PID controller showed lower error values in all experiments than classical PID, and the oscillating behaviour was less pronounced, except during the upper stroke length of the PAM and during the triangle wave setpoint. This behaviour is likely due to a closer fitting to the setpoint at points where the nonlinear nature of the PAM is most pronounced, causing the controller to quickly switch between increasing and decreasing pressure input in an attempt to meet the desired displacement.

The behaviour of the ILC was as expected in all experiments in terms of learning, with convergence to a steady state reached after eight wavelengths, or four iterations of the learning algorithm. Once a steady state is reached the error is

typically similar in magnitude to that of the PSO-PID controller, but with no evidence of oscillation about the setpoint. Motion under the ILC is generally smoother than under PID control. ILC suffers from similar response-time issues to PID control, with the PAM motion lagging behind the setpoint even after a steady state is reached. The response time during square wave motion is slightly better than that of PID, with lower settling time and notably no oscillation at the static points, but instantaneous errors are similar in magnitude at the changing points of the waveform. Under external load the ILC performs well, with little impact on the learning rate or the overall motion accuracy. Addition and removal of weights during motion and during static displacement is accounted for by the learning algorithm; however, with a constant setpoint the steady state error under ILC is the worst of the controllers tested here. Under changing setpoints the ILC can respond to the change in a similar time to the initial learning period, but this does result in worse overall error. The learning algorithm does not respond properly to changes in the frequency of the setpoint during motion, with the initial frequency maintained throughout without changing to match the setpoint. This is due to the learning period being based on the wavelength of the setpoint. A more sophisticated learning algorithm could improve on this with a better-defined learning period.

Overall, based on average error values across the experiments' runtimes as well as maximum error magnitudes, the motion of the PAM under MPC is the most accurate. The response time issue present in the other controllers tested here is removed by the predictive algorithm, although in some cases the actual motion precedes the setpoint, which is a unique issue. With square wave input this is most noticeable, as the PAM motion under MPC changes direction before the changing points of the waveform, resulting in overall lower error values. Under

most setpoints the error is lowest under MPC with smoother motion than PID and, as to be expected, a faster settling time than ILC. One major downside of this implementation of MPC is that the model used does not consider external loads to the system, and as such the controller does not change input based on additional loads to the PAM, resulting in larger error values when weights are added. Under rapid motion the predictive algorithm works somewhat against the PAM motion. The system itself is incapable of changing velocity at the rate required by the setpoint, usually resulting in a lagging motion which attempts to reach the peak of the sin wave input. The MPC predicts rapid changes in the setpoint before they occur and changes the direction of motion in advance. While this does result in overall lower error values under MPC than other controllers, the maximum displacement of the PAM is much smaller in practice due to this interaction, which is usually undesirable when displacement accuracy is the priority. The predictive algorithm is capable of adjusting to changes in setpoint waveforms seamlessly. PAM motion immediately before the change in waveform is adjusted to best fit the requirements after the change, so error values are only minorly affected, there is little or no increase in error between the different setpoints, and motion after the change is just as accurate as before.

While the predictive and learning control systems used in this study show promise in accurate motion control for a single actuator, alternative control methodology is required in many rehabilitation robotics applications. Impedance control, such as that presented in [137, 138], uses force sensor measurements to determine actuator motion. This feedback system is required in active rehabilitation, in which a user applies force to the robot and the motion is assisted or resisted by the system. This would be impractical for the controllers used here

to achieve in their current configuration, so they are not sufficient for every control need of a rehabilitation robot.

4.5 Chapter Conclusion

This chapter presents an intelligent control scheme designed to overcome the nonlinearity of PAMs, Model Predictive Control using PSO-based dynamic modelling, which was implemented on a single PAM setup to test for validity. Three other controllers which are popular in the field of rehabilitation robotics, ILC, PID, and PSO-PID, were also investigated for quantifiable comparison of their performance.

An experiment scheme was designed to test the behaviour of each control scheme under conditions as would be required in a rehabilitation setting. Displacement of the PAM was measured for each different experiment setpoint and external loading under each of the four control schemes, and the displacement error calculated and compared. Based on these comparisons, it was found that the PID controller performed worst in terms of error magnitude and response time, with undesirable oscillating behaviour in many cases, which was worsened by the addition of weights. Optimised parameters using PSO slightly improved the error values and response times but did not remove the oscillations. The ILC reached a steady state after learning for four iterations in each experiment, with smoother motion and smaller error values than PID. Performance was also not inhibited by external loading, and changes to the setpoint and external loading during motion were accounted for in the next learning iteration. Response time was still slow, however, and the algorithm was incapable of adjusting to changes in frequency. The MPC had the best performance, with smooth motion during all experiments and the overall lowest error values. The prediction algorithm allowed motion in

advance of changing setpoints and maintained low error values after changes as well. Due to the method of model generation for the MPC and the lack of feedback, the algorithm was unable to adjust for external loads, and error values were negatively affected by weights.

The results gained in these experiments prove conclusively that machine intelligence can greatly improve the performance of control systems for PAMs in terms of tracking accuracy, response time, and motion smoothness. Both learning and predictive control methods show excellent performance in most scenarios. Despite being a standard implementation of learning control, the ILC algorithm used in this study showed rapid convergence to accurate motion as well as the ability to sufficiently reject external load and disturbance. The use of additional learning parameters and robust elements could further improve its performance. The predictive nature of MPC especially shows promise as it mitigates many issues which arise in controlling complex actuators like PAMs, including lagging behind the setpoint caused by a limited flow rate of air into the actuator, and the PAM's tendency to oscillate about setpoint values as it repeatedly attempts to over-adjust. These preliminary results suggest that this implementation of MPC is suitable for further study and future application to a PAM-driven rehabilitation robot. It could also be suitable for other robotics applications, such as in more complex actuator arrangements [139]; however, this is outside the scope of the current research. The overall performance of MPC depends heavily on the accuracy of the model used, and as such a more accurate dynamic model of the PAM would further improve the controller's performance.

The contributions of this chapter are the development of a predictive control algorithm, MPC, for accurate motion control of a PAM and experimental comparison results for validation of its performance alongside other intelligent

controllers ILC and PSO-PID, with traditional PID as a benchmark. The MPC allows for accurate and effective motion tracking of the actuator, with the predictive algorithm and models accounting for much of the nonlinearity present in the PAM. Results from comparative experiments give useful data on the performance of predictive, learning, and optimised parameter controllers, allowing for detailed comparison of the controllers used here.

CHAPTER 5

MODEL PREDICTIVE CONTROL WITH PSO MODELLING APPROACH FOR POSITION CONTROL OF COMPLIANT ANKLE REHABILITATION ROBOT

This chapter introduces the Compliant Ankle Rehabilitation Robot (CARR) for research objective 2, in which the control strategies developed in chapters 3 and 4 are validated on a full ankle rehabilitation robot setup. Using the mechanical structure and kinematics of the CARR the MPC system and PSO modelling methods developed previously are applied for motion tracking control. Two separate dynamic models of the PAMs used to actuate the CARR are generated using the PSO method, one assuming all four operate on the same parameters and one assuming the upper and lower pairs have different parameters based on their orientation. These models are then used in MPC systems for motion tracking control of the robot. To properly validate the controllers on a much more complex

system, ILC and PID are used for comparison. A series of experiments utilising the X and Y axis motions of the robot are performed, and the results analysed to confirm good performance of the MPC on the CARR and validate it for further use in experiments with participants.

The work presented in this chapter is published in Biomimetics as:

- Brown DF, Xie SQ, Tu Y. Model Predictive Control with a PSO Modelling Approach for Position Control of a Compliant Ankle Rehabilitation Robot. Biomimetics. 2026; 11(5):349. doi: 10.3390/biomimetics11050349

5.1 Introduction

The field of rehabilitation robotics has seen rapid increases in both research and applications [140], with the global market expected to grow by $5 billion by 2032 [141]. With the ever-increasing interest and usage of these robots in both research and clinical environments, it is becoming increasingly important that they are safe, reliable, and are held to a high standard of functionality. To this end, a great deal of research in the field concerns intelligent algorithms and control structures [142, 143], with many designs mentioning user comfort and safety as a measure of success alongside more commonplace measures for robotics like motion and force tracking accuracy [144, 145]. The use of compliant actuators and structures in the design of rehabilitation robots is an effective way to improve patient comfort and safety by allowing for some freedom of motion during usage as well as increasing the transparency of the robot by reducing interaction torques between the robot and patient. Flexible pneumatic actuators, such as PAMs, allow for compliant actuation with sufficient torque capability to apply proper force output for rehabilitation exercises, making them a suitable and increasingly popular choice for actuation in the field. However, their elastic construction and

actuation method relying on pressurised air makes them more complicated to control than traditional actuators, often leading to less accurate motion and force tracking. Intelligent control strategies are generally more suitable than traditional control for these dynamic actuators, as their unique properties can be better accounted for. A great variety exists in the literature concerning the specific intelligent algorithms used in control systems, even within the field of rehabilitation robotics. Learning control methods such as ILC allow for improved performance over time using system feedback and measured error values, making them applicable to systems with repeated, predictable input sequences. However, this necessarily means that the initial motion accuracy is poor before the algorithm has had a chance to learn, and adjusting learning parameters to speed up learning often leads to instability. Adaptive controllers are specifically suitable for rehabilitation as they allow for dynamically adjusted control parameters based on certain feedback or measurements, helping improve both motion accuracy and comfort for users. These algorithms can be applied to many different control schemes, but therefore only increase the complexity and computational load of whatever algorithm to which they are applied. The use of fuzzy logic is also common in control algorithms, as it allows for heuristic decision making and easy grouping of continuous data. However, some accuracy is inevitably lost in the fuzzification of data. Neural network control methods are an increasingly popular algorithm in many fields based on high performance and decision-making capabilities, but the very large required sets of training data and resulting computational complexity make them unsuitable for more user-specific applications. MPC produces optimal predicted control outputs for both current and future inputs. The consideration of future control inputs allows for accurate time-dependent control, and the use of optimisation algorithms in the generation

ensures consistently accurate motion. The main drawbacks of MPC are the requirement of an accurate system model and knowledge of future input sequences, but as rehabilitation robots use predetermined sets of motions to provide therapeutic exercises this second requirement is already fulfilled. As such, this chapter will present the development, implementation, and experimental testing of an MPC scheme designed for a platform-based ankle rehabilitation robot driven by four parallel PAMs, as well as an optimisation-based modelling method to account for the requirement of a system model in the controller.

Using a dynamic model of the plant, MPC predicts the optimal control input sequence to achieve a given output. So long as an accurate model of the system can be calculated, this allows for accurate and reliable control of even complex systems, accounting for time-variance, position dependence, and other nonlinearities. There are several examples of MPC used in rehabilitation robotics, even aside from those systems which use PAMs for actuation [142]. Some examples of walking-based patient following rehabilitation robots using MPC are presented in [146, 147]. In [146] a robot is designed to automatically follow patients at a set distance allowing for walking aid, using MPC to maintain distance and speed. A similar system focused on stroke rehabilitation presented in [147] uses a weight-bearing support structure to assist lower-limb impaired patients in following predefined paths, using MPC with quadratic regression to accurately track the desired motion. Other examples of MPC used in lower-limb rehabilitation include powered orthoses and exoskeletons, such as those presented in [148, 149]. An impedance controller uses MPC to calculate optimal joint stiffness in a wearable lower-limb rehabilitation exoskeleton developed in [148], while a position controller for a nonlinear knee exoskeleton using a

linearization technique and MPC is developed and compared with several other MPC methods is presented in [149]. Upper limb rehabilitation also benefits from the use of MPC, such as the system presented in [150]. A portable upper-limb rehabilitation robot is tested using MPC and PID control for comparison. In fact, PID is often used as a comparison point in control system development for rehabilitation robotics, with results in [147, 149, 150] showing comparative data verifying the performance of MPC in their respective applications.

The biggest difficulty in developing MPC is the requirement for a model of the plant. As the predicted control inputs are calculated based on the behaviour of the model, a more accurate model necessarily results in more accurate control. In the case of complex, nonlinear systems, accurate models become difficult to calculate, often resulting in a significant trade-off between accuracy and complexity. PAMs, with the presence of hysteresis as well as the nonlinear input-output relationship and time variance, are notoriously difficult to accurately model. Many different applicable modelling techniques exist for rehabilitation robots, with unique and novel methods present throughout literature as well. The parallel upper-limb rehabilitation robot developed in [151] uses a kinematics-based model approximating the system as a series of chains, as well as discussing the Lagrangian method. Another upper limb rehabilitation robot shown in [152] uses a multi-domain modelling method in SimScape multibody, developed to assist with tracking the patient's recovery process. In [153], a fuzzy inference system is used to accurately calculate the forward kinematics of an ankle rehabilitation robot. The fuzzy inference system was optimised using several optimisation methods for comparison of their effectiveness.

Optimisation algorithms are often used for the purpose of dynamic modelling, as they are an ideal choice for calculating parameters of complex systems without

themselves becoming more complicated. Particle Swarm Optimisation (PSO) is a popular optimisation method, based on its comparatively fast convergence through the usage of a large “swarm” of potential solutions, or particles, which communicate their respective fitness according to the objective function allowing for informed changing of parameters, resulting in fewer required iterations to reach an optimal solution compared with other optimisation algorithms. An example of a 3 DoFs cylindrical manipulator is presented in [154], with inverse kinematics identification performed using least squares and recursive least squares, and dynamic parameter identification performed by PSO. With a dynamic model generated using Lagrange equation, it was found that PSO parameter identification was more accurate than the least squares methods. Another instance of PSO being used comparatively with a least squares identification method is shown in [155] with a desktop Phantom Omni haptic device. There are many examples of PSO being used for parameter identification in rehabilitation robotics as well. An upper limb rehabilitation device driven by two antagonistic PAM pairs is modelled using a neural network trained using PSO algorithm in [156], with results suggesting the method is suitable for modelling and control of various multi-input multi-output (MIMO) systems. Another upper limb rehabilitation device as shown in [157] uses an advanced PSO algorithm with variable parameters for dynamic modelling. Results showed that the proposed method outperformed least-squares as well as basic PSO, with significantly reduced tracking errors and chattering. A full dual lower-limb exoskeleton as shown in [158] uses a PSO-optimised Support Vector Regression system to identify walking modes in users, and in experiments with three users this method was proved to be effective.

In this chapter, a platform-based compliant ankle rehabilitation robot, the CARR,

actuated by four FESTO PAMs, is used for development of a novel intelligent control system. The robot is designed to allow for compliant and comfortable rehabilitation of the ankle joint on three rotational DoFs. The aim of this control system is to provide more accurate, stable, and consistent motion to the CARR to make it more suitable for the safe human-robot interaction required when undergoing robot-assisted physical rehabilitation. The actuation method of the CARR, using four PAMs arranged to act as antagonistic pairings on each of the three axes of motion, creates difficulty in accurately modelling and controlling the system by introducing significant nonlinearity and time-dependence. To account for this, a PSO-based modelling method was developed for dynamic parameter identification of PAMs using a phenomenological model template in chapter 3. Using this method, a series of dynamic models will be generated to approximate behaviour of the actuators of the CARR. These developed models will then be applied to an MPC strategy. Two methodologies will be used; a single-model setup in which each of the four PAMs in the system are assumed to have the same dynamic properties, and a dual-model setup in which the upper- and lower-pairs will be modelled separately. These single-model and dual-model MPCs will then be experimentally compared, alongside traditional PID control and ILC, to confirm validity of the proposed method. The CARR has been experimentally validated in multiple experiments including a case study in the treatment of drop-foot [159] and has had multiple different control strategies developed and tested [160, 161].

This study aims to demonstrate a computationally simple and adaptable modelling method in combination with an intelligent control strategy for accurate, smooth and predictable motion of the CARR which would allow for suitable and safe clinical usage with patients with impaired motor function of the

ankle. The main contributions are summarized as follows:

1. Real-world application and validation of a computationally efficient algorithm to generate dynamic models of complex, nonlinear systems in the PSO modelling method.
2. Two sets of dynamic models proposed for the CARR in the single-model and dual-model setups.
3. Development of two MPCs using each of the generated model sets.

5.2 Robot Design

5.2.1 Layout and Functionality

The CARR is shown in Figures 5.1 and 5.2. It consists of two platforms: a fixed platform, the frame, and a mobile one, the footplate. The platforms are connected in two places: by four FESTO DMSP-20-400N PAMs fixed with one end at points around the footplate and the other at the upper section of the frame as shown in Figure 5.1(a), and via a bar linkage serial mechanism with three rotational DoFs as shown in Figure 5.1(b). This mechanism includes rotary encoders on each of the rotational axis. The PAMs are actuated using four FESTO VPPM-6L-L-1-G18-0L6H proportional pressure regulators. This configuration allows for the CARR to achieve three rotational DoFs, corresponding to dorsiflexion/plantarflexion, inversion/eversion, and abduction/adduction motions of the ankle joint, by actuating the PAMs in opposed pairs. The use of four PAMs connected at each corner of the footplate end effector and angled outwards in relation to the plane of motion allows for antagonistic force to be applied across the three axes, with the upper and lower pairs acting to operate the X axis, the left- and right-hand

pairs acting to operate the Y axis, and diagonally opposed pairs acting to operate the Z axis.

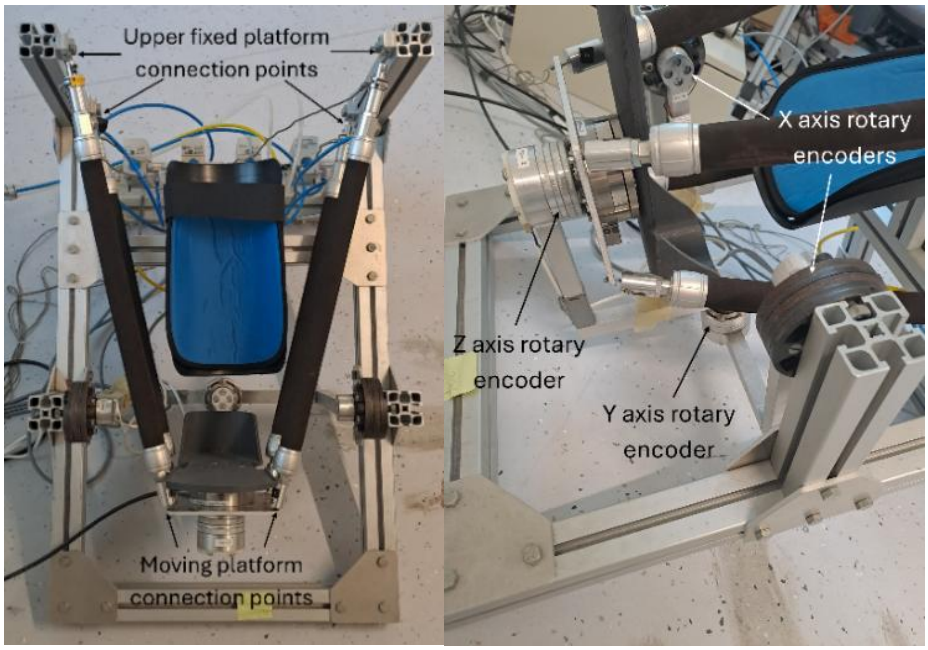


Figure 5.1(a) and 5.1(b): Images of the CARR. Figure 5.1(a) shows the PAMs and connection points. Figure 5.1(b) shows the bar linkage mechanism for the footplate and the rotary encoders used to measure angular displacement.

Shown in Figure 5.2 is the coordinate system used to describe the CARR. The system consists of fixed coordinates describing the fixed platform denoted as $O_f X_f Y_f Z_f$ and moving coordinates describing the mobile platform denoted as $O_m X_m Y_m Z_m$. The upper connection point on the fixed platform where the actuators are connected is denoted as UFP, while the lower connection point of the fixed platform where the linkage mechanism of the mobile platform is connected is denoted as LFP. The mobile platform consisting of the linkage mechanism and footplate is denoted as MP. The connection point of the ith PAM on the UFP and MP are referred to as UFP_i and MP_i respectively. With O_f referring to the centrepoint of UFP and O_m referring to the rotational centre of MP, O_e refers to the centrepoint of the footplate such that it is equidistant from each of

$MP_i, i = 1\ to\ 4$. H refers to the distance $\overline{O_f O_m}$ and h refers to the distance $\overline{O_m O_e}$. These coordinate systems and definitions are displayed graphically in Figure 5.2 and were originally defined in [162].

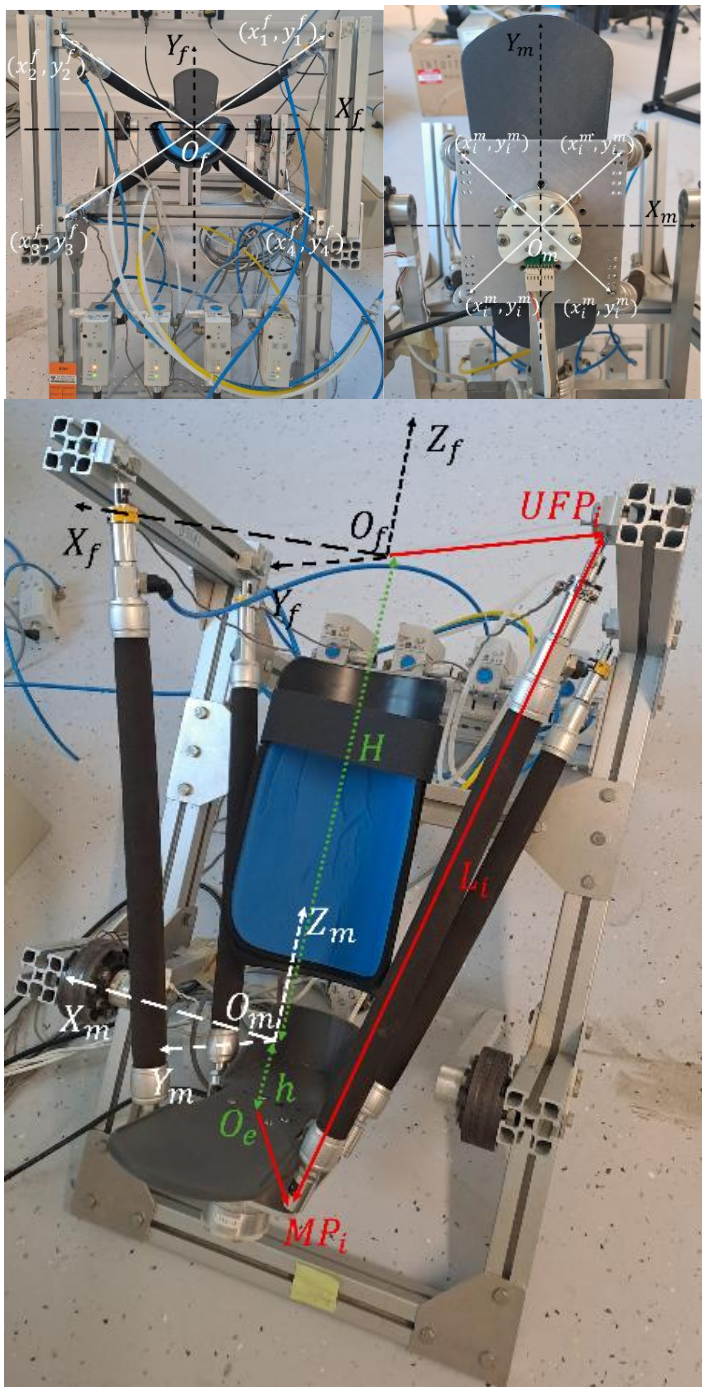


Figure 5.2(a), 5.2(b), and 5.2(c): Coordinate system of the CARR. Figure 5.2(a) shows the upper fixed platform coordinates, Figure 5.2(b) shows the moving platform coordinates, and Figure 5.2(c) shows the combined coordinate systems along with the measured values H, h, and the muscle length L_i.

A flaw of the system's current configuration is that while the actuator configuration allows for proper control of the X and Y axis in both directions using opposed pairs of PAMs, the methodology for actuation of the Z axis is fundamentally lacking. Using diagonally opposed PAMs at small angles to the footplate results in difficulty accurately controlling the axis due to the force vectors being mostly parallel with the axis of motion. This combined with the necessary interaction with the other axis while in motion causes the Z axis of the system to be unstable and inaccurate, a fault not currently rectifiable by software control. Discussion on the potential redesign of the CARR to better control the Z axis will be made towards the end of this chapter, but as this is outside the scope of the study presented here the experiments will focus on the X and Y axis motion for better validation of the developed modelling and control algorithms.

5.2.2 Kinematics

In order that the CARR be properly modelled and controlled using the methods described in the next section, the length of each PAM must be known throughout online motion. Therefore, the kinematics of the CARR are calculated.

The length of the ith actuator is given by the distance $\overline{UFP_iMP_i}$. The coordinates of UFP_i in relation to O_f are described as $[x_i^f, y_i^f, z_i^f]$, and the coordinates of MP_i in relation to O_m are described as $[x_i^m, y_i^m, z_i^m]$. Therefore, the length of the ith actuator, denoted as L_i, can be calculated per equation 5.1.

$$L_i = \sqrt{\overline{x_i^f x_i^m}^2 + \overline{y_i^f y_i^m}^2 + \overline{z_i^f z_i^m}^2} \tag{5.1}$$

These cartesian distances can be calculated using the angular displacement measured by the rotary encoders on the linkage mechanism of the mobile platform θ_x, θ_y, and θ_z, as defined in equations 5.2 – 5.4.

$$\overline{x_i^f x_i^m} = x_i^f + h\big(\sin(\theta_x)\sin(\theta_z) + \cos(\theta_x)\sin\big(\theta_y\big)\cos(\theta_z)\big) + y_i^m\big(\cos(\theta_x)\sin(\theta_z) - \sin(\theta_x)\sin\big(\theta_y\big)\cos(\theta_z)\big) - x_i^m\cos\big(\theta_y\big)\cos(\theta_z) \quad (5.2)$$

$$\overline{y_i^f y_i^m} = -y_i^f + h\big(\sin(\theta_x)\cos(\theta_z) - \cos(\theta_x)\sin\big(\theta_y\big)\sin(\theta_z)\big) + y_i^m\big(\cos(\theta_x)\,cos(\theta_z) + \sin(\theta_x)\sin\big(\theta_y\big)\sin(\theta_z)\big) + x_i^m\cos\big(\theta_y\big)\sin(\theta_z) \quad (5.3)$$

$$\overline{z_i^f z_i^m} = H + x_i^m\sin\big(\theta_y\big) + h\cos(\theta_x)\cos\big(\theta_y\big) - y_i^m\sin(\theta_x)\cos\big(\theta_y\big) \quad (5.4)$$

Measured values of the coordinates of each of UFP_i and MP_i are shown in Table 5.1. The values of H and h are $H = 415$ and $h = 120$. All values are measured in millimeters relative to the centrepoints O_f and O_m.

Table 5.1: Coordinates of PAM Connection Points

Actuator Affixed Point	x_i	y_i	z_i
UFP_1	202.5	140	0
UFP_2	-202.5	140	0
UFP_3	-202.5	-140	0
UFP_4	202.5	-140	0
MP_1	65	60	-120
MP_2	-65	60	-120
MP_3	-65	-60	-120
MP_4	65	-60	-120

The length outputs calculated from equation 5.1 were scaled to the range [0-10] to allow for simpler calculations in the modelling and control stages.

5.3 Modelling and Control

5.3.1 Modelling Methodology

The developed PSO-based dynamic modelling method was adapted and used here to generate dynamic models of the PAM used in actuating the CARR. Given a comparison point generated by applying a predetermined sequence of inputs to the plant, the fitness of each particle in the PSO algorithm is calculated using the error value between the behaviour of the model using that particle's parameters

in place of the unknown values, and the behaviour of the plant. As the CARR uses four PAMs, a simple waveform-based pressure adjustment would not work as the intended outputs of the robot are the angles of the footplate. Therefore, a sin wave input with amplitude 2 and frequency 0.05Hz and repeated twice was used as input to the upper pair of PAMs, with the same waveform inverted and used as input for the lower pair. This results in a constant and smooth sinusoidal changing of the X angle of the system. The values for the amplitude and frequency were tuned manually based on the requirements of the system in a rehabilitation setting to best model for the intended application, keeping range, speed, and acceleration of motion within expected operational limits. Using the measured output of the CARR joint angles, the inverse kinematics equations of the system were used to calculate the length of each PAM. The resulting length measurements were used as setpoints to calculate the RMSE of each particle. These values were used as the fitness values of the particles in the PSO algorithm. Two separate modelling setups were used for comparative experiments, a single-model setup and a dual-model setup. In the single-model setup, the four PAMs used in the CARR were assumed to have the same dynamic properties and a single set of three parameters were calculated using the PSO method, forming a single dynamic model which was used to model all four PAMs. The fitness of each particle was calculated by summing the RMSE calculated for each of the four PAM setpoint motions. In the dual-model setup, the upper pair of actuators was assumed to have different properties to the lower pair based on their angle to the ground and position in the structure of the CARR, so two separate sets of parameters were calculated using separate PSO algorithms running alongside each other, one summing the RMSE values for the upper two PAMs to calculate fitness values and the other summing the RMSE values for the lower two to

calculate fitness. Using this setup, two independent models were generated for each pair of PAMs. The parameters used for the PSO algorithm were $W = 0.9$ to prevent divergent learning of the swarm, $C1 = C2 = 2$ to increase the optimisation rate and reduce the number of iterations required to reach an optimal solution, a swarm size of 50 as a trade-off between optimisation rate and computational complexity, and each model setup was run for 20 iterations as this was the point by which local optimal solutions were most often reached. The parameters for the models generated for these experiments are shown in Table 5.2.

Table 5.2: Coordinates of PAM Connection Points

Model Setup	P1	P2	P3
Single-Model Setup	0.547499	0.124483	0.445087
Dual-Model Setup – Upper PAMs	0.778931	0.032553	0.387574
Dual-Model Setup – Lower PAMs	0.134703	0.595939	0.335659

5.3.2 Control Methodology

Using the models generated by the proposed PSO modelling method, an MPC strategy can be created for position control of the CARR. MPC uses an optimisation algorithm together with prior knowledge of the intended input sequence and a model of the plant to predict an optimal control signal. At each time period t, an optimisation function calculates a cost-minimising control output for the defined prediction period T based on the input sequence for that period and the predicted behaviour of the plant from the model. The first stage of this control output is applied to the system, and the rest is discarded for the process to be repeated at the next time step. MPC is therefore suitable for

application in nonlinear systems due to the predictive nature, as well as for unusual or time-variant input sequences so long as they are known beforehand. The use of the PSO modelling method also allows this implementation of MPC to accurately control complex systems while remaining computationally efficient.

The optimisation function and internal parameters used for the MPC is the same as that presented in chapter 4, see section 4.2.1.1 and equations 4.1 and 4.2. The models generated by the PSO method as detailed earlier described the dynamics of the individual PAMs rather than the CARR as a whole. Therefore, four separate MPCs were used for controlling the system. While a MIMO or centralised control algorithm accounting for the CARR as a combined system would allow for cooperative action of the PAMs and may improve accuracy, this would also necessitate a far more complex model of the CARR than is required of the PAMs individually. It may also introduce further nonlinearities and time variance to the MPC and would make relative force output readings more complicated. This potential alternate control architecture is therefore left as future work in the case of this study. The input of the system was defined as the desired angles on the X, Y and Z axes for the footplate. While the Z axis will not be implemented as part of the controller validation due to instability as previously discussed, it is a necessary measure for the kinematics equations of the system and must therefore be included in the control architecture, so all input values for the Z axis will be set to 0 for the purposes of this study. Input sequences for each actuator were calculated using the inverse kinematics equations of the system. Figure 5.3(a) shows a diagram of the MPC for the four PAMs and the overall control structure for the CARR. Figure 5.3(b) shows the structure of the PAM MPC blocks.

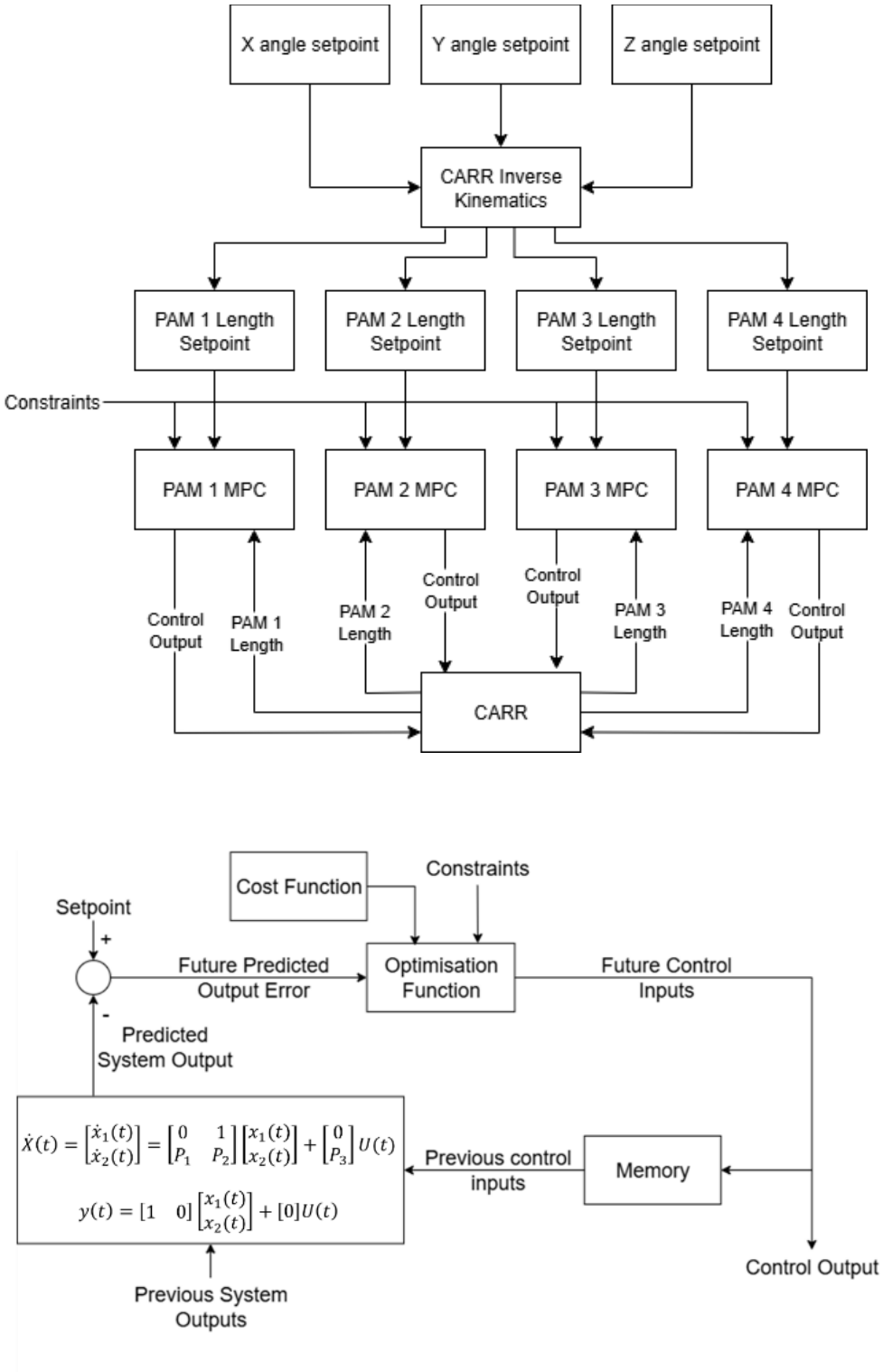


Figure 5.3(a) and 5.3(b): Control structure for the CARR, including setpoint calculation, and structure of the MPC loop including application of the PSO dynamic model.

For experimental comparison of the developed MPC strategies, a traditional PID controller and ILC were developed for the CARR. Similarly to the functioning of the MPC, a separate controller was used for each of the four PAMs in all cases, and the setpoint length for each was calculated using the inverse kinematics of the system.

As neither PID control nor ILC require that the entire input sequence be known by the controller beforehand, the setpoints for each PAM were calculated online during motion. The parameters of the PID controller used in this study were $K_c = 20, T_i = 0.009, T_d = 0.00225$. These values were tuned manually for fast response to the setpoint while minimising instability.

The ILC used in this study was a classical implementation. The control output of the algorithm is given in equation 5.5.

$$u(t) = u_{old}(t) + pe_{old}(t) \qquad (5.5)$$

Where $u(t)$ is the control output, $u_{old}(t)$ is the control output of the previous iteration, $e_{old}(t)$ is the measured error during the previous iteration, and p is the learning rate, which was set to 20, again tuned manually for fast convergence to the setpoint in a low number of learning periods while minimising instability, overfitting, and divergent behaviour. The length of each learning iteration was a single wavelength of the input for each experiment.

5.4 Experiment Methodology

The intended outcome of these experiments is motion tracking data for the X and Y axes of the CARR which can be used to compare the accuracy performance of the developed MPC strategies with each other and the PID and ILC strategies. Data gathered will be analysed to determine relative strengths and weaknesses of the controllers, discuss potential improvements to be made to their performance,

and if applicable decide which is most suitable to bring forwards to later stages of the project.

Each experiment uses a set waveform setpoint to the X, Y, or both axes of the CARR. As previously discussed, the Z axis will not be implemented as part of these experiments due to shortcomings of the CARR mechanical design. Table 5.3 shows the parameters for each waveform in each experiment. Amplitude values are normalised based on the motion range of the CARR on each of the X and Y axes and the direct voltage outputs from the angular encoders.

Table 5.3: Setpoint waveform Parameters

Experiment	X axis frequency /Hz	X axis amplitude	Y axis frequency /Hz	Y axis amplitude
X axis	0.05	0.2	0	0
Y axis	0	0	0.05	0.2
X and Y axes	0.05	0.1	0.05	0.1
Rapid X axis	0.1	0.1	0.05	0.1
Rapid Y axis	0.05	0.1	0.1	0.1

For each experiment, each of the single-model MPC, dual-model MPC, PID and ILC controllers will have the same unaltered waveform input as the setpoints for each axis, allowing for comparable results. For the MPC and PID algorithms each experiment will be run for 5 waveforms, except in the cases of the rapid motion experiments where they will be run for 10 waveforms. As the first wavelength of each experiment for the ILC is necessarily only learning and no control output can be calculated, each experiment will be run for 6 waveforms with the first omitted from the results, or for 12 waveforms in the case of rapid motion with the first 2 omitted.

5.5 Results

The measured X and Y angles for each experiment under each control scheme were measured and overlaid for comparison. The angle error for each motion was calculated and overlaid with each other to demonstrate the relative performance of each controller. The measured angle results for each experiment are shown here in Figures 5.4 – 5.8. Key comparison metrics were calculated and are shown in Table 5.4.

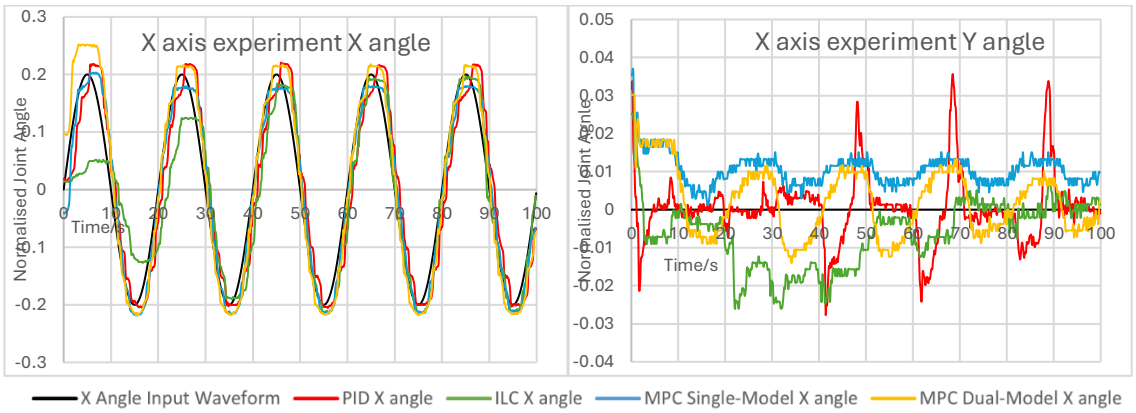


Figure 5.4: Measured angle values for the X and Y axis of the CARR during the X axis experiment.

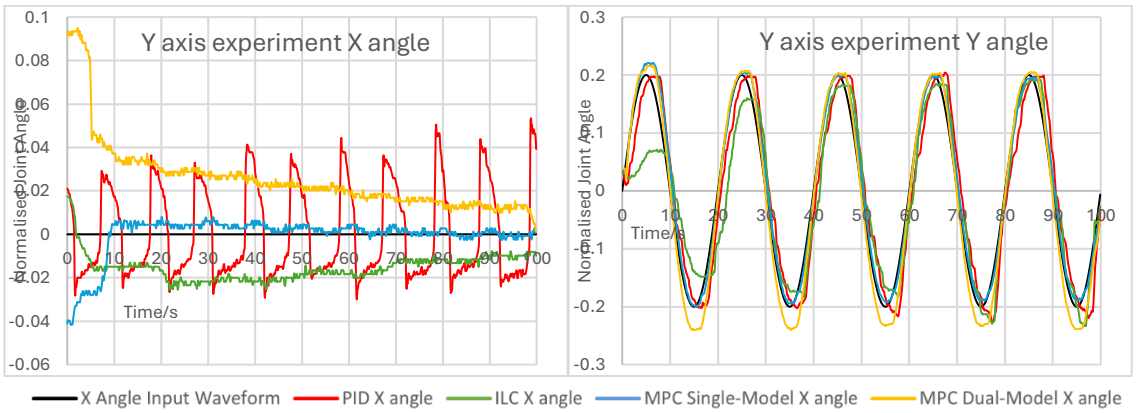


Figure 5.5: Measured angle values for the X and Y axis of the CARR during the Y axis experiment.

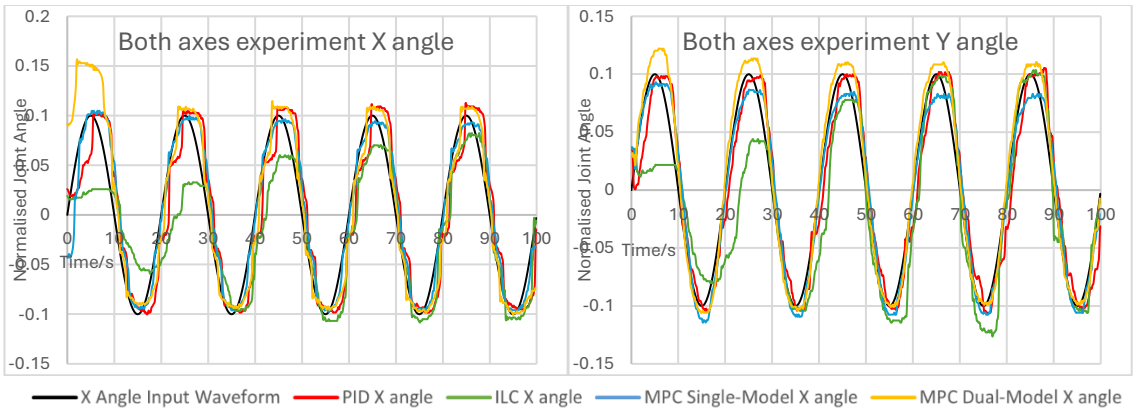


Figure 5.6: Measured angle values for the X and Y axis of the CARR during the X and Y axis experiment.

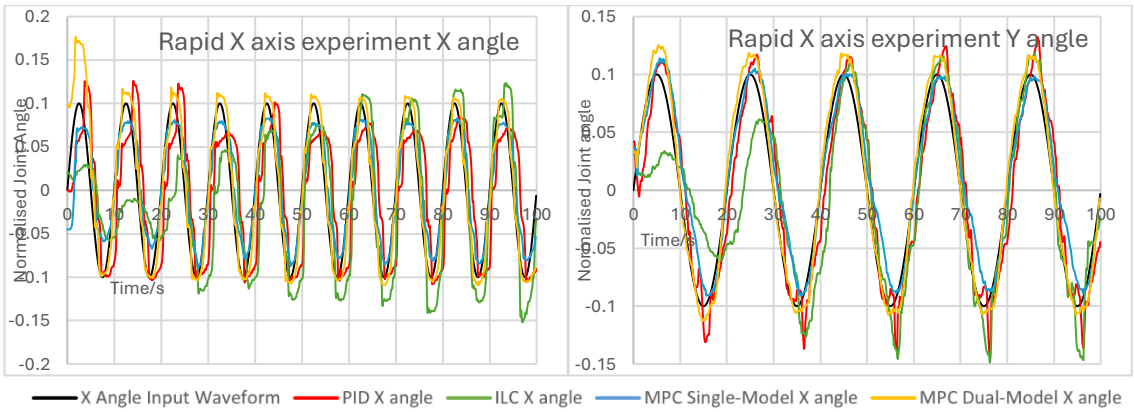


Figure 5.7: Measured angle values for the X and Y axis of the CARR during the rapid X axis experiment.

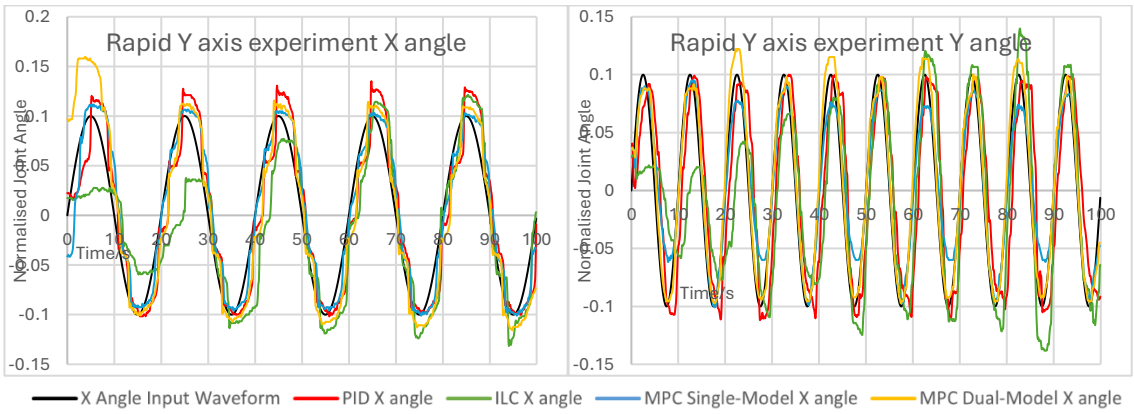


Figure 5.8: Measured angle values for the X and Y axis of the CARR during the rapid Y axis experiment.

Table 5.4: Result Metrics

Experiment	Controller	RMSE		Peak Error		Percentage Overshoot	
		X axis	Y axis	X axis	Y axis	X axis	Y axis
X axis	PID	0.0485	0.0088	0.1081	0.0356	10.4	N/A
	ILC	0.0598	0.0109	0.1309	0.0261	8.2	N/A
	MPC Single-Model	0.0294	0.0112	0.0654	0.0151	8.6	N/A
	MPC Dual-Model	0.0366	0.0092	0.0728	0.0140	9.1	N/A
Y axis	PID	0.0211	0.0461	0.0534	0.1077	N/A	13.5
	ILC	0.0166	0.0527	0.0255	0.1349	N/A	16.7
	MPC Single-Model	0.0092	0.0182	0.0080	0.0459	N/A	2.7
	MPC Dual-Model	0.0308	0.0275	0.0307	0.0565	N/A	20.1
X and Y axes	PID	0.0301	0.0214	0.0614	0.0542	12.9	6.9
	ILC	0.0370	0.0354	0.0947	0.1076	8.4	26.4
	MPC Single-Model	0.0192	0.0142	0.0431	0.0286	-0.3	9.4
	MPC Dual-Model	0.0270	0.0152	0.0670	0.0363	14.8	13.7
Rapid X axis	PID	0.0553	0.2545	0.1148	0.0541	22.8	41.3
	ILC	0.0554	0.0389	0.1408	0.1023	51.9	48.8
	MPC Single-Model	0.0248	0.0213	0.0436	0.0462	-10.7	5.1
	MPC Dual-Model	0.0230	0.0131	0.0767	0.0249	18.2	18.6
Rapid Y axis	PID	0.0277	0.0440	0.0571	0.1058	35.2	11.9
	ILC	0.0407	0.0481	0.1049	0.1213	31.7	39.8
	MPC Single-Model	0.0217	0.0199	0.0459	0.0463	6.6	-1.1
	MPC Dual-Model	0.0306	0.0129	0.0669	0.0331	15.8	22.2

5.6 Discussion

The experiments run in this study were designed to approximate the requirements of the CARR in a rehabilitation setting. The frequency and amplitude of the input waveforms were selected based on the speed and angle of exercise requirements during ankle rehabilitation. The rapid motion experiments used frequency values on the extreme upper end of required values in rehabilitation, which usually requires slow, measured motions. This was primarily a test for the capability of the controllers and the CARR to perform well

during faster motion, and to determine the system's ability to perform two simultaneous motions with different speeds. In experiments where both X and Y angles were in motion, the chosen amplitude of motion was smaller as the CARR exhibits some accuracy issues at the extremes of motion while the footplate is undergoing multiple angle motions simultaneously. In order that each controller performed as well as possible, some recalibration of the rotary encoder on the X axis was required for each which resulted in some temporary inaccuracy at the immediate start of each experiment on this axis, especially noticeable in the two MPC implementations. Specific performance metrics in RMSE, peak error, and overshoot percentage values are listed for both axis in Table 5.4 and will be referenced throughout this discussion.

Validation for each controller was performed by comparing motion responses with each other and identifying points at which motion deviated from the setpoint. This included general waveform shape, any consistent deviations such as lead or lag, overshooting, and smoothness of motion. Similar analysis was performed on the error waveforms. The key comparison metrics shown in table 5.4 were also used to provide direct numerical comparison between certain performance parameters including average and peak error and maximum overshoot. In general, each controller is validated in comparison with each other controller, with PID used as a baseline for improvement.

In general, the performance of the PID controller was the worst of the controllers, with higher RMSE and peak error in the majority of experiments than the MPC implementations, and the least consistent motion of all controllers. Where an axis was expected to remain at 0 angular displacement the peak error under PID was invariably highest and significant motion was observed. In several examples, namely the Y axis experiment and both rapid motion experiments, the percentage

overshoot of the Y axis under PID control was significant, and in the rapid motion experiment the X axis suffered both over- and undershooting at different points by a significant margin. In terms of smoothness of motion, an important metric for safety and comfort in rehabilitation exercises and often regarded as a more important measure of success in such a device than motion tracking, all control schemes showed evidence of some chattering. This is likely due to the construction of the CARR and the inherent friction present in the actuators and joints on the footplate mechanism. However, the chattering was most significant under PID control and in many cases the motion would briefly change direction at a chatter point, most noticeable in the X axis when both X and Y axis are in motion.

As is to be expected, ILC began each experiment with poor accuracy and improved over the course of the waveform, with each wavelength reducing the tracking error in most cases. This includes cases where an axis was expected to remain at 0, and in the case of the X axis resulted in small peak error and RMSE values. However, there is evidence of overfitting in some experiments, mostly during rapid motion where overshooting of the setpoint becomes more common and significant towards the end of the waveform as indicated by the very high overshoot percentage values, suggesting instability. In terms of motion smoothness, the ILC had similar but less severe chattering than PID with fewer examples of fully changing direction of motion.

Both MPC implementations performed similarly, however there were some defining features of both that caused them to outperform each other in certain scenarios. The single-model MPC converged quickly to 0 under experiments where an axis was to remain at 0 and maintained a steady value consistently, evidenced by the lowest RMSE and peak error values in the X axis and

comparably low values for the Y axis. The percentage overshoot values were the lowest of all controllers in almost every case by a significant margin, however it did show the only cases of negative overshoot indicating that while both axes are in motion the maximum rotational values were never fully reached. The chattering effect under single-model MPC is lower than under PID control and ILC, resulting in smoother motion.

The dual-model MPC, while having generally similar behaviour to the single-model MPC, did show the closest motion to the setpoint under rapid motion, with the lowest RMSE values of all controllers, as well as either lowest or nearly lowest RMSE and peak error for the Y axis in every experiment. Chattering behaviour was best accounted for under this control scheme, with very little evidence of this unwanted motion in all experiments other than in the X axis while both X and Y axes were in motion. The main drawback of the dual-model MPC was overshooting, which was present in every experiment and noted in the percentage overshoot values, however unlike the overshooting present under PID and in some cases under ILC this motion remained smooth and consistent.

PID performed significantly worse than both MPC implementations in terms of RMSE, peak error, and smoothness of motion. After converging to a steady state, the ILC performed well for the X axis but less so for the Y axis and was especially impacted by rapid motion as well as evidencing overfitting towards the end of these experiments.

Single-model MPC performed well on the X axis and had the best results for maintaining a constant 0 displacement as well as the lowest overshoot values, but did suffer from undershooting, which was most significant under rapid motion.

The dual-model MPC showed consistently low error while both X and Y axis were under motion, as well as the smoothest motion and lowest RMSE under rapid

motion. However, it also had evidence of overshooting. MPC control has proven to be significantly more effective than traditional control like PID for nonlinear, complex systems like the CARR, and capable of more reliably accurate motion in more specific use cases than ILC, although the fact that both MPC implementations have drawbacks suggest there is still work to be done in developing robust controllers.

5.7 Chapter Conclusion

In this chapter, an ankle rehabilitation robot actuated by four antagonistic PAMs, the CARR, was used as the platform for development and testing of a PSO-based dynamic modelling method and two MPC schemes for more accurate and smooth motion of the device in a rehabilitation setting. The modelling method was adapted for use with the MIMO system, and uses a phenomenological model template of PAMs and the PSO algorithm to calculate computationally efficient, yet accurate, models of the nonlinear actuator. Two different setups were used in both modelling and control of the CARR; a single-model setup in which each of the four PAMs in the robot were assumed to have the same dynamic properties and were therefore modelled with the same parameters, and a dual-model setup in which the top pair of PAMs were assumed to have different dynamic properties to the bottom pair, resulting in two different models.

These models were then used in MPC schemes in experiments to test for their motion tracking accuracy and motion smoothness with the CARR. A traditional PID controller and classical ILC were also used as comparison points to determine the relative increase in effectiveness of these MPC algorithms. An experiment scheme was devised using standard sin wave input setpoints for the angular displacement of the X and Y axis of the CARR, and each of these setpoints

were used in the PID controller, ILC, and both the single-model MPC setup and the dual-model MPC setup to allow for comparison of their behaviours. The experiments included actuating the two axes separately, as well as simultaneously and at different speeds to test a range of applications. It was found that the MPCs both outperformed PID in terms of absolute error values, as well as smoothness of motion, as did ILC after sufficient learning periods. PID control exhibited the worst chattering effect and either over- or undershot the setpoint in most cases. ILC could converge to accurate and smooth motion in most cases but showed some evidence of overfitting towards the end of experiments involving both axes and especially under rapid motion. The single-model MPC had the best behaviour when only a single axis was in motion at once, keeping the unmoving axis consistently stable. It however suffered from some decrease in accuracy at higher frequency motion, as well as when both axes were moving simultaneously. The dual-model MPC had the best performance for the Y axis and better accuracy while both axes were in motion. The dual-model MPC had the least evidence of chattering, only apparent in the X axis with both axes in motion, resulting in the smoothest tracking results. It did however show overshooting, although not as significant or sharp as under PID control.

The primary successes of the developed MPC controllers over other controllers are stability, with lower chattering than PID and no divergent learning as with ILC, and the ability to respond well to complex MIMO situations as with both axes of the CARR moving at once and at different speeds. These successes prove the validity and accuracy of the proposed PSO-generated models for complex MIMO systems as well. As such, based on their accuracy and motion smoothness in the experiments presented here, both the PSO-based modelling method and the resulting MPC schemes are suitable for further research in clinical trials with

the CARR. The relative successes of the single-model and dual-model MPCs can be used to the system's advantage with the addition of a switching-mode or adaptive controller, allowing the shortcomings and benefits to counteract each other in certain cases where one may be preferred over the other.

The CARR itself will require a mechanical redesign to rectify the issues with the Z axis motion, as the current PAM configuration makes this axis unstable and inaccurate. This could be done with the addition of a rotary actuator on the footplate to assist with motion, or a repositioning of the PAMs to better apply force in the required direction.

The primary contribution of this chapter is the development of two MPC algorithms for use with the CARR, a MIMO system with inherent compliance and nonlinearity introduced by the actuation method of PAMs. Comparative experiments confirm the validity of the developed controllers in comparison with ILC and PID, in which accuracy and stability are improved by the predictive algorithm. The intended use case for the CARR, providing rehabilitative exercises to patients with impaired ankle motion, requires steady and stable motion to keep the user comfortable and to maintain safety, therefore predictable and smooth motion is essential to the better functioning of the device.

CHAPTER 6

USER STUDY OF INTELLIGENTLY CONTROLLED COMPLIANT ANKLE REHABILITATION ROBOT

Experimental results have proven the effectiveness of the developed MPC strategies in motion tracking for the CARR; however, the intended function of a rehabilitation robot is to apply these motions to a human user. As such, this chapter presents online experiments with human participants to realise research objective 3. The results of these experiments are twofold: to validate and compare the two implementation of MPC, single-model and dual-model, in terms of response to the disturbance and torque requirements associated with the addition of a user to the system; and to gather results from the participants concerning the comfort and usability of both the CARR and the motion applied by the two controllers. These sets of results will help validate the system as a whole, both in terms of motion tracking accuracy and disturbance rejection but also comfort and usability from a potential patient standpoint.

6.1 Introduction

With the field of rehabilitation robotics becoming more prominent in advancing medical technology, and with some devices becoming available for clinical and home use, it is imperative that newly developed systems are properly verified to be safe to use and be able to provide the care needed to patients experiencing limited range of motion. With the ankle joint being a common point for loss of motion due to neurological conditions like stroke, cerebral palsy, and multiple sclerosis, as well as a commonly injured joint accounting for 5% of UK emergency department visits annually [163], research into ankle rehabilitation robots is an important aspect of this growing field of research. Many novel ankle rehabilitation devices have been produced in recent research and their functionality in a real rehabilitation setting must be properly verified before they can be found conclusively safe and fit for purpose.

There are many examples of ankle rehabilitation robots used in clinical trials in literature for differing purposes. Some, for example, look to prove the effectiveness of robot-aided rehabilitation over traditional manual rehabilitation exercises. The trial presented in [164] shows results from 20 post-stroke inpatients over a 2-week period in which one group used a seated platform-based ankle rehab robot, and another was treated manually. Results showed similar results in ankle properties and balance between both groups but found that dorsiflexion spasticity and stiffness was better improved by the robot-aided group. A similar study is shown in [165] in which a group of 34 stroke-unit inpatients were divided into two groups, with 18 assigned to a modular Anklebot and 16 receiving passive manual stretching exercises, for an hour a day over a period of 10 days. Results showed that both groups improved, however those

using the Anklebot had greater improvements to gait symmetry and motor control than those receiving manual treatment.

With the effectiveness of robot-assisted vs manual rehabilitation exercises as a common purpose of clinical trials, there are also examples of more specific comparisons being made. The trial presented in [166] compares robot-guided therapy in a hospital environment vs at home. 41 children with cerebral palsy were divided into two groups and received six weeks of robot-assisted passive training exercises for their impaired ankle in the respective environments. With very little difference between the results for each group found, it was concluded that the robot-aided training benefits can be achieved in both a clinical and home environment. Two different arrangements for robot-assisted gait therapy are experimentally compared in [167] with task-specific rehabilitation performed using treadmill-integrated ankle robotics and individual joint-targeting seated ankle robotics. A group of 26 chronic hemiparetic gait patients were randomly assigned to one of the two treatment programs over a six-week period, with results finding that the treadmill-integrated training proved more effective in supporting range of motion and gait velocity than seated training. Optimal training protocols for robot-assisted ankle rehabilitation are explored in [168], with four groups of 9 stroke patients with drop-foot receiving different intensity and frequency training over a period of 3 weeks with a dua-foot ankle rehabilitation robot. While all groups showed improved dorsiflexion range of motion after the trials, the groups receiving higher frequency and higher intensity training sessions showed a greater level of improvement.

As is proved in the literature, real-world effectiveness of rehabilitation devices can only be properly validated in trials under the intended use case, and offline experiments with no participants can only do so much to prove a system may be

suitable for the intended application. The experiments using the developed MPC systems with the CARR were performed as an initial verification of the motion accuracy of the control schemes in comparison with other popular controllers, but the potential effectiveness of the CARR and the controllers in an actual rehabilitation environment must be validated in online experiments with human participants. System validation is a common goal of clinical trials with rehabilitation devices, and the primary measure of success is usually improvement of a patient's ankle range of motion, strength, and control. A platform-based ankle rehabilitation robot ARBOT alongside admittance, position, and admittance-based assistive control strategies are developed and validated in [169] in experiments with a group of healthy subjects. Results from various controller setups prove their effectiveness, with future work planned to improve the EMG sensor integration and develop rehabilitation exercises with the system. Another proposed ankle-foot rehabilitation system was validated in experiments with seven post-stroke patients in [170] over a 3-month training period. Each participant's impaired ankle was used as the experimental group, while their unimpaired ankle was used as the control group. After the training period it was found that the experimental group improved in muscle strength and range of motion, and walking speed increased. A pilot study for robot-guided passive ankle training on multiple sclerosis patients was conducted in [171], with six patients completing the 6-week course. Results showed a significant increase in ankle range of motion and motor performance in all participants. Participants also completed a short questionnaire about the experience, and they reported that the training was good in both passive and active exercises. They also stated that the video game aspect of the training was fun and engaging, and that they would be willing to use the robotic system at home if possible. The CARR itself has been

the focus of several clinical trials including the one presented in [159] in which a patient suffering from drop foot engaged in a 15-minute exercise session. The patient gave positive feedback on the experience and motion tracking results proved the device is capable of providing accurate motion while rejecting external disturbance.

This chapter aims to validate the comfort and usability of the CARR in a set of experiments designed to generally approximate the actual use case of a rehabilitation robot. The two developed MPC systems, the single-model setup and dual-model setup, will both be used in these experiments to determine which is most suitable for use with participants in terms of comfort and disturbance rejection. Each participant will complete a short questionnaire detailing their experience with the CARR as well as with both MPC setups. The angular displacement measurements from the X and Y axis of the CARR will also be measured and discussed. The motivations and contributions of this research are as follows:

- To experimentally validate the function of the developed MPC systems in online experiments with participants, ensuring good response to disturbance and increased torque output requirements in line with those expected in a real rehabilitation scenario.
- To compare the performance of the single-model and dual-model MPC setups under a variety of user-involved tests, for comparable results and a conclusive answer on which is most suitable for use in a rehabilitation setting.
- To gather participant survey results on the comfort, usability, and motions of the CARR under MPC, giving direction for future mechanical development of the robot.

6.2 System Setup

6.2.1 Ankle Rehabilitation Robot Setup

The CARR is set up as shown in Figure 6.1. As the CARR must be used in a sitting position, an adjustable chair was used to allow participants of different height to be as comfortable as possible while using the device. The emergency stop button was kept within reach of the participant for safety purposes. The participant is sat with their chosen foot resting on the footplate of the CARR and their calf strapped to the calf rest. The chair is positioned such that the participant is comfortable, with the sole of their foot firmly on the footplate but not applying unnecessary pressure. From here the participant is given a questionnaire to document their experience of using the CARR, and then motions are performed by the robot to apply force to the participant's ankle joint on the plantar/dorsiflexion and ab/adduction axes.



(a) (b) (c)

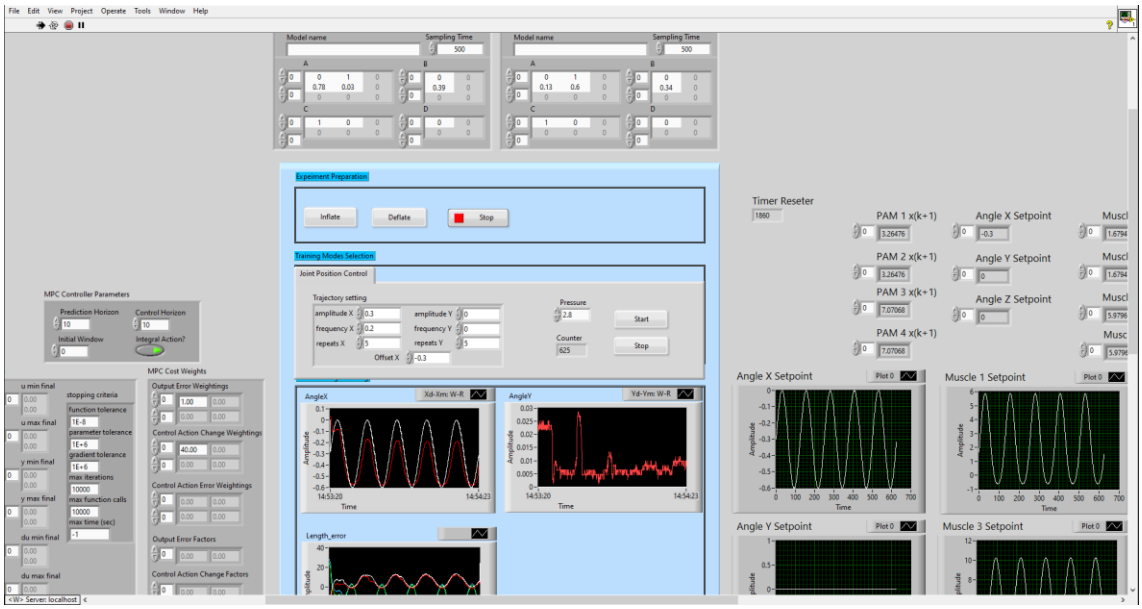
Figure 6.1: Setup of the CARR for experiments with participants. (a) and (b) show the setup without a participant, (c) shows the setup with a participant in the chair with their foot in the footplate and calf strapped to the calf rest.

6.2.2 Model Predictive Controller Setup

The control system used for these experiments is the MPC algorithm developed during this research project. Both the single-model and dual-model setups will be used to determine which is better suited for use with participants, in terms of both user comfort and disturbance rejection. The model parameters used here are the same as those used in chapter 5, presented in Table 5.2. Figure 6.2 shows the user interface for the two controller implementations in National Instruments LabVIEW after running the plantar/dorsiflexion motion.



(a)



(b)

Figure 6.2: The user interface for the MPC systems in NI LabVIEW. (a) shows the interface for the single-model setup, and (b) shows the interface for the dual-model setup.

6.3 Experiment Methodology

6.3.1 Participants

Ethical approval for these experiments was gained through the University of Leeds Ethical Approval Committee, reference EPS FREC 3587. See appendix A. Exclusion criteria for participants were that they must have no recent leg/ankle injury that would affect their ability to walk unaided, as this would both negatively affect their experience with the robot and the forces applied during experiments could potentially exacerbate injurie and cause unintended discomfort. 15 participants took part in this study, aged 22±4. Two had experienced knee injury, one with a medial meniscus tear 2 years prior and one sprained 1 month prior, and one had flat feet. Otherwise, the participants were all healthy, with no adverse condition to the functioning of the ankle joint.

6.3.2 Experiment Protocol

Each participant was positioned with one of their feet, participant's choice, on the footplate of the CARR with their lower leg resting on and strapped into the calf rest. The CARR then performed a set of two motions, firstly actuating plantar/dorsiflexion followed by ab/adduction. Each motion was mapped to a sin wave, the parameters of which are shown in Table 6.1, and were repeated for 5 wavelengths. This motion is initially performed under the single-model setup MPC and then repeated under dual-model MPC, resulting in four separate motions for each participant. This allows for both controllers to be tested under the same conditions using the same input setpoint and the same user, as well as getting separate sets of participant responses to each controller. This allows for directly comparable results for both controllers in terms of motion tracking

accuracy and user experience. The separation of the motions into groups also allows for a short break between each for the participant to rest and readjust their sitting position, ensuring fatigue experienced from the first set of motions does not negatively impact the second. Each participant was given a short questionnaire about the experience detailing how comfortable and stable they felt using the device, as well as how fatigued they felt afterwards.

Table 6.1: Motion Parameters

Motion Parameter	**X-axis – Plantar/Dorsiflexion**	**Y axis – Ab/Adduction**
Amplitude	0.3	0.3
Frequency/Hz	0.08	0.08
Offset	-0.3	0

The experiments performed in this study were designed to test the ability for the developed MPC systems to perform accurate motion control when used with a participant and the associated disturbances, as well as to gather data on participant's experiences using the CARR in terms of comfort and stability. The amplitude parameters for the setpoint waveforms were based on comfortable RoM for a human ankle joint, causing slight stretching in the muscles but not overextending in any direction, while the frequency was kept low to mimic early-stage rehabilitation passive exercises. The addition of an offset of the X axis is due to the relative resting positions of the ankle and the footplate of the robot, keeping motion centred on the participant. Each exercise was repeated 5 times resulting in a 62.5 second runtime for each motion. While a standard rehabilitation session in a clinical environment would typically last several hours, the results from this experiment were focused on motion accuracy and patient comfort and stability which are unlikely to change over the course of a longer period. Fatigue and effort applied would likely increase over a longer period, however in the interest of time

spent for each participant the duration of just over a minute for each motion was deemed appropriate to give the experience of using the CARR for its intended purpose. Figure 6.3 shows the different motion and footplate positions for plantar/dorsiflexion motion, and Figure 6.4 shows the different motion and footplate positions for ab/adduction motion.



(a) (b) (c)

Figure 6.3: Motion undertaken by the footplate during plantar/dorsiflexion motion. (a) shows the footplate at the equilibrium position and the directions of motion are indicated, (b) shows the footplate at its most downward extended position, and (c) shows the footplate at its most upwards extended position.



(a) (b) (c)

Figure 6.4: Motion undertaken by the footplate during ab/adduction motion. (a) shows the footplate at the equilibrium position and the directions of motion are indicated, (b) shows the footplate at its rightmost extended position, and (c) shows the footplate at its leftmost extended position.

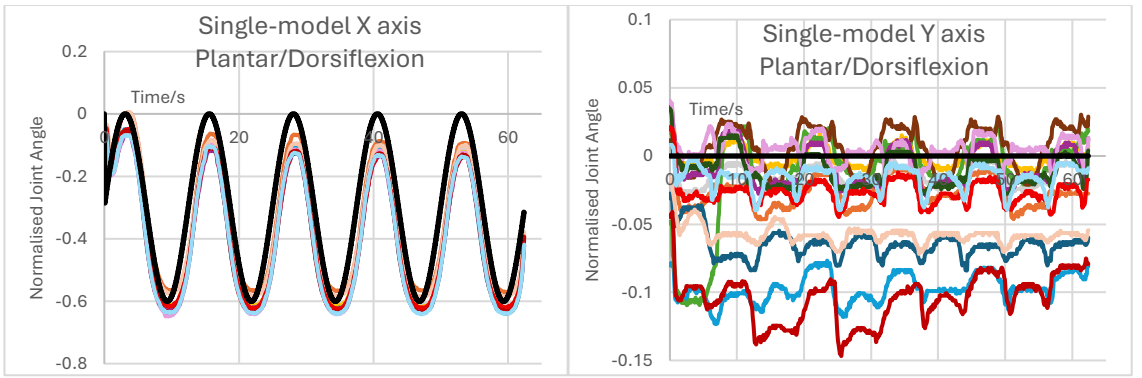
6.4 Motion Tracking Results

6.4.1 Displacement Measures

Figures 6.6 – 6.9 show the measured angular displacement from the encoders on the X and Y axis of the CARR mobile mechanism during the experiments. The measurements from each participant have been overlaid to show the general trends in motion accuracy for each controller and axis. Due to the large number of participants, the associated line colours for each participant and the setpoint are shown in Figure 6.5.

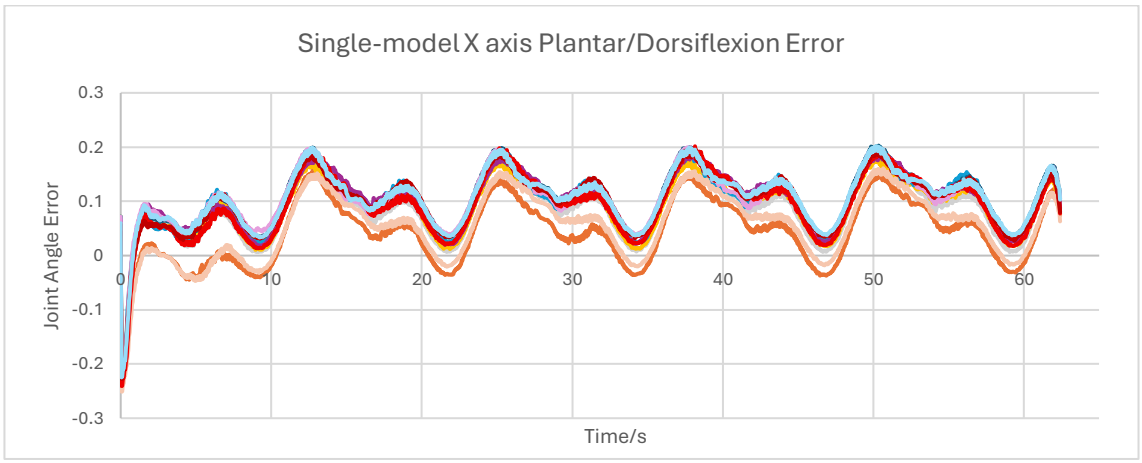


Figure 6.5: Associated line colours for each participant in the displacement measurement graphs



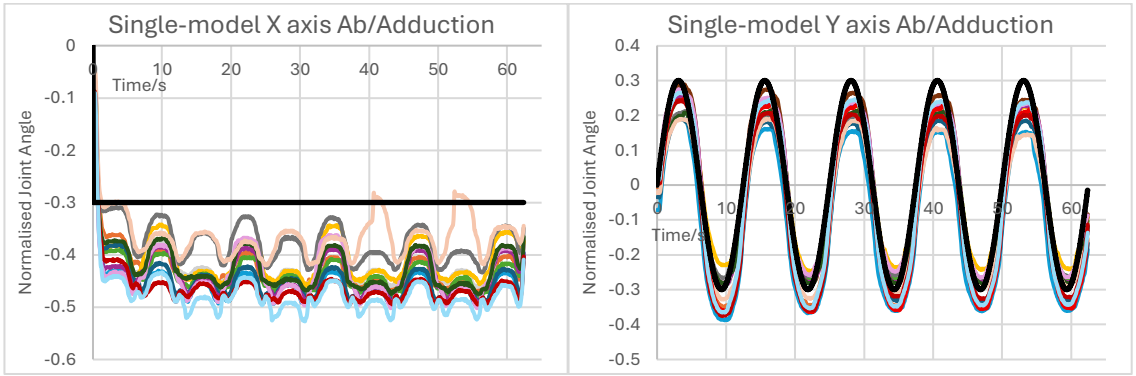
(a)

(b)



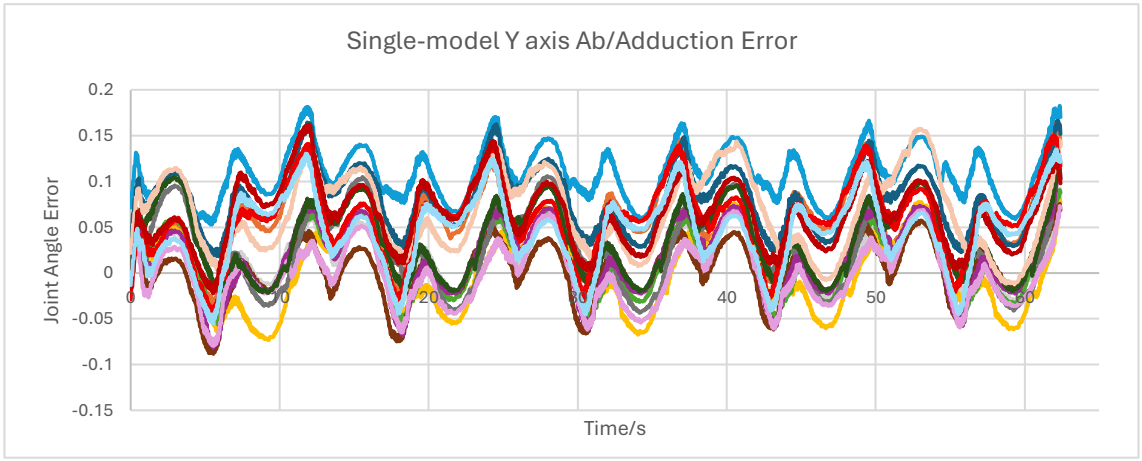
(c)

Figure 6.6: Displacement measurement during the plantar/dorsiflexion motion under single-model MPC. (a) shows the motion of the X axis, (b) shows the motion of the Y axis, and (c) shows the error in the X axis motion. Technical problems with the encoders caused participants 5, 7, 8 and 11's X-axis measurements and participant 8's Y-axis measurement to be omitted.



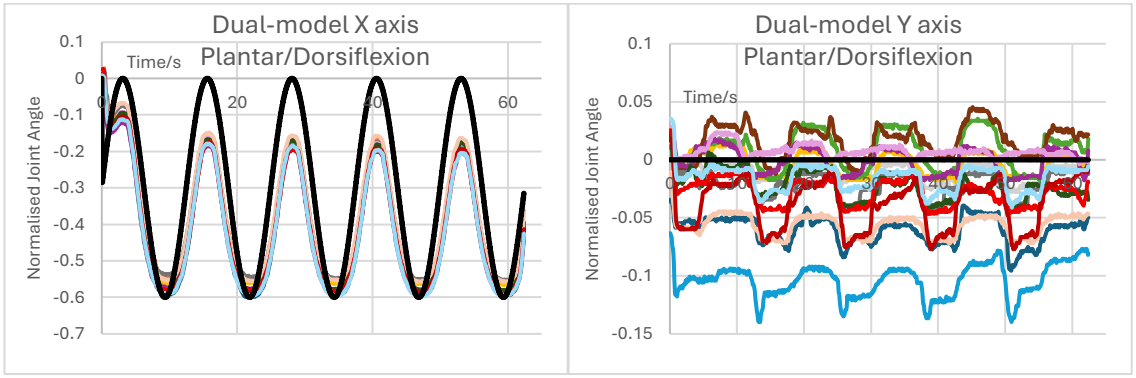
(a)

(b)



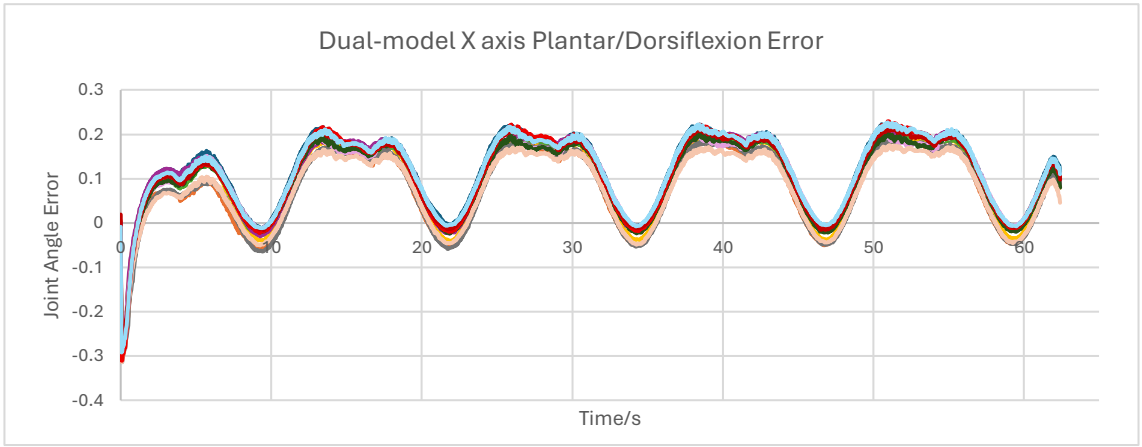
(c)

Figure 6.7: Displacement measurement during the ab/adduction motion under single-model MPC. (a) shows the motion of the X axis, (b) shows the motion of the Y axis, and (c) shows the error in the Y axis motion. Technical problems with the encoders caused participants 7, and 13's X-axis measurements to be omitted.



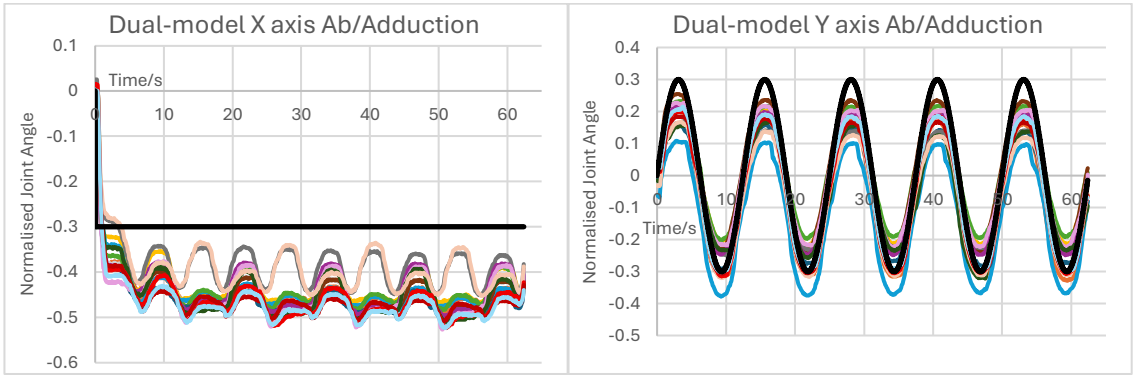
(a)

(b)



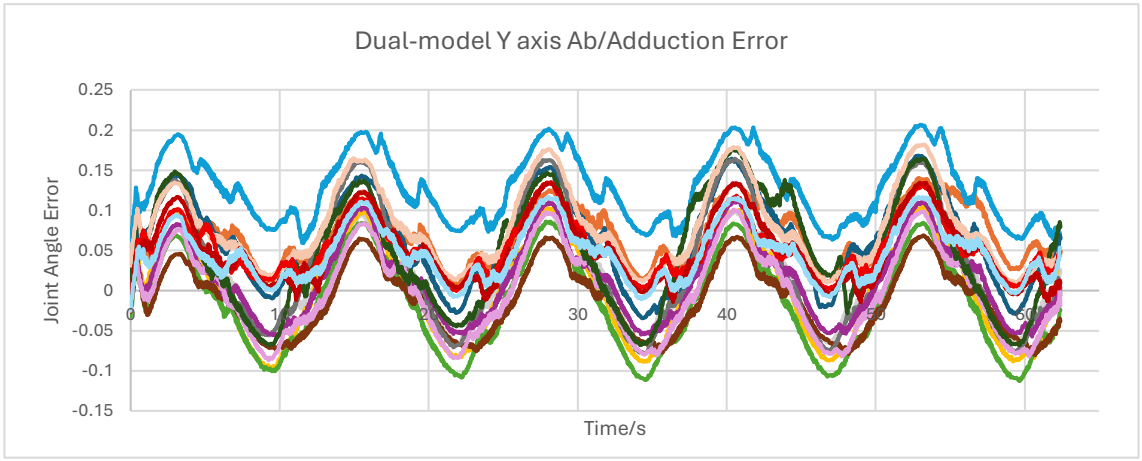
(c)

Figure 6.8: Displacement measurement during the plantar/dorsiflexion motion under dual-model MPC. (a) shows the motion of the X axis, (b) shows the motion of the Y axis, and (c) shows the error in the X axis motion. Technical problems with the encoders caused participants 2, 4, and 7's X-axis measurements and participant 1's Y-axis measurement to be omitted.



(a)

(b)



(c)

Figure 6.9: Displacement measurement during the ab/adduction motion under dual-model MPC. (a) shows the motion of the X axis, (b) shows the motion of the Y axis, and (c) shows the error in the Y axis motion.

6.4.2 Discussion

In comparison with the non-participant experiments conducted previously, the main difference in motion tracking performance of the controllers is a consistently applied offset. This is to be expected with the addition of a participant as the primary disturbance force applied will be the weight of their foot on the CARR, pulling the motion downwards as is most noticeable in the X axis motion where the measured displacement is consistently lower than the

setpoint. Notably this is much more pronounced in the dual-model MPC, with a consistently greater peak error value coinciding with the peaks of displacement. User applied disturbance is much more consistent between participants in the X axis than in the Y axis, with a notably larger spread of measurements in the Y axis during ab/adduction motion for both controllers. This is likely due to participants firstly having been given the option of using their left or right foot for the experiments, generally pushing ab/adduction motion towards the inner of whichever foot they chose, and secondly to differing stiffness in each participant's ankle, causing lesser/greater disturbance in this dimension. In general, while the X axis was in motion during plantar/dorsiflexion motion, the single-model MPC showed lower error values than dual-model, but also a wider spread of values between participants suggesting the dual-model controller is more consistent but less accurate in motion tracking. In the case of ab/adduction motion and the Y axis, the larger spread of values between participants make generalised assessments of the controllers more difficult. The single-model controller showed generally lower error values than dual-model, but the difference is small with both reaching a maximum error value of around 0.18 except in the case of participant 4 whose maximum error reached over 0.2 under dual-model control. It is noted that this participant showed among the largest error values for the Y axis in all experiments, suggesting some particular ab/adduction offset in their joint. Where the axes are expected to remain static a similar phenomenon is present where the X axis values are much more consistent between participants as well as being consistently below the setpoint value, and the Y axis values have a large spread between participants. The X axis under ab/adduction motion also shows more consistent motion under dual-model control than single-model, but unlike when in motion the dual-model controller also has lower average error and

smoother motion. There is little notable difference between the performance of each controller for the Y axis under plantar/dorsiflexion motion. General displacement motion is very similar, and most participants fluctuate about the setpoint value, but participants 4 and 14 showed a consistent offset downwards reaching absolute error values of almost 0.15.

6.5 Questionnaire Results

6.5.1 Participant Responses

The participant questionnaire included 10 questions to be answered in the format of 0-10, with 0 being the least/worst and 10 being the most/best. There was also a section for participants to record any additional notes they had on the experience. The questionnaire is shown in Figure 6.10. One participant did not complete the second series of motions guided by the dual-model MPC, so they did not complete the final 4 questions of the questionnaire. Figures 6.11 – 6.13 show the participant's answers to each question.

School of Electronic and Electrical Engineering

UNIVERSITY OF LEEDS

Ankle Rehabilitation Robot Participant Experiment Questionnaire

Please rate the following 1-10, with 1 being the least/worst and 10 being the most/best

How comfortable did you feel while the robot was stationary?	
How steady did the setup (your sitting position and the robot) feel while the robot was stationary?	
How comfortable did you feel while the robot was in motion during the first series of motions?	
How steady did the setup (your sitting position and the robot) feel during the first series of motions?	
How much effort did you need to apply during the first series of motions?	
How fatigued did you feel after the first series of motions?	
How comfortable did you feel while the robot was in motion during the second series of motions?	
How steady did the setup (your sitting position and the robot) feel during the second series of motions?	
How much effort did you need to apply during the second series of motions?	
How fatigued did you feel after the second series of motions?	

Please write your age here:	

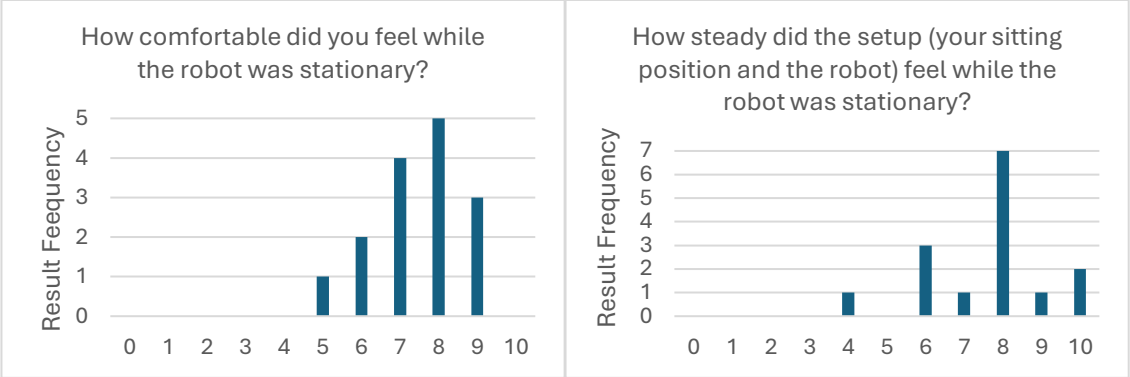
Please write details of any physical impairments you may have here (write None if you have none)

If you have any additional notes about the experience with the ankle rehabilitation robot, please give them here.

Project title	*Document type*	*Version #*	*Date*
Ankle Rehabilitation Robot Participant Experiments	Questionnaire	1	03/10/2025

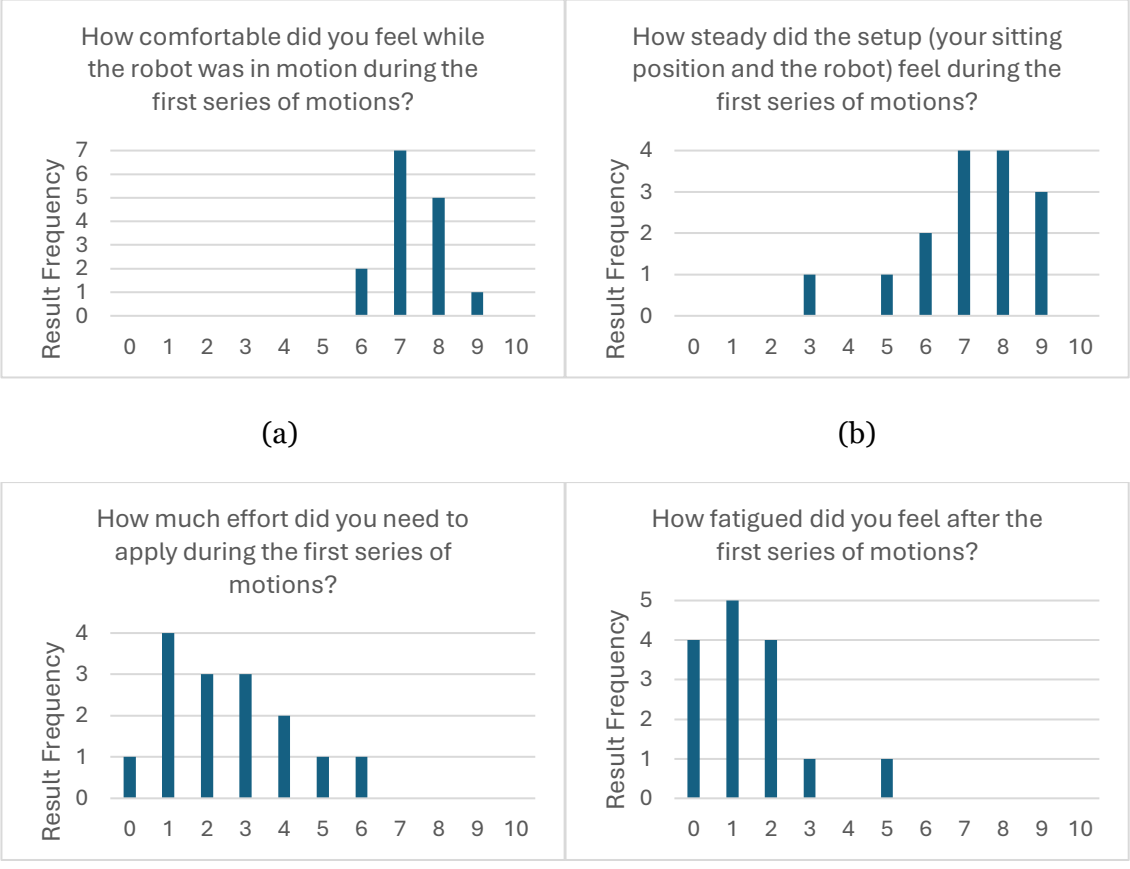
Page 1 of 1

Figure 6.10: Questionnaire used to gather participant responses during experiments.



(a) (b)

Figure 6.11: Participant responses on questionnaire questions concerning the CARR while stationary.



(a) (b)

(c) (d)

Figure 6.12: Participant responses to questionnaire questions concerning the CARR motion under singe-model MPC.

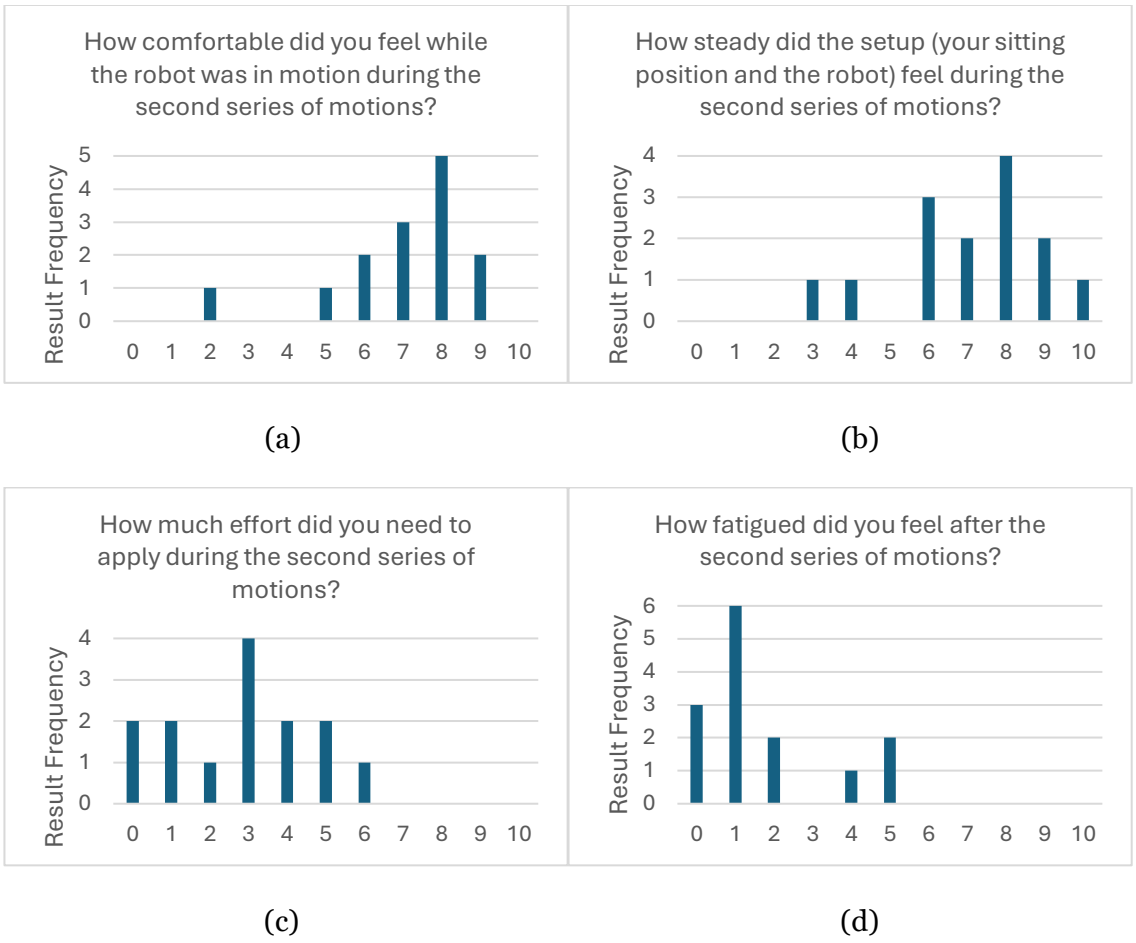


Figure 6.13: Participant responses to questionnaire questions concerning the CARR motion under dual-model MPC.

6.5.2 Discussion

Based on the participants' responses to the questionnaire, the CARR is reasonably comfortable to sit in while stationery with the majority of responses being 7-9, however no one gave a 10 and one participant gave a 5 suggesting there are some improvements to be made. Comments were made by both taller and shorter participants that their height/leg length made the sitting position less comfortable. Some adjustable mechanism may help alleviate this issue. Responses for stability while stationary were also majority 8, however the spread was larger with more participants rating both 6 and 10 suggesting that while the

comfort was generally good the stability of the system was more varied between participants.

During the first series of motions under single-model MPC the responses for both comfort and stability lowered slightly, generally by 1 point, compared to stationery. Several participants commented that the initial inflation of the PAMs before motion started pushed their leg out of position, so they needed to adjust. This could be easily remedied by slowly inflating the PAMs initially rather than immediately. Many also commented that during plantar/dorsiflexion motion their heel was pinched between the footplate and calf rest, another issue that would be fixed by an adjustable footplate/calf rest. During the second series of motions under dual-model MPC the responses for comfort were very similar to those while stationary except for one participant who responded with a 2, commenting that the heel pinch between the footplate and calf rest was particularly bad during this motion, a comment shared by other participants as well. Participant responses for stability were also similar to those while stationary, although again a small number rated this very low. Interestingly, some participants commented that the second series of motion was the more comfortable of the two, while others commented that the motion was more erratic or that they needed to apply more force to keep up with the footplate. Further, more specific studies would need to be conducted to confirm specific personal preferences and characteristics that might cause one MPC to be more comfortable to some people than others. In general, however, based on the results found in this study, the main limitations for comfort and stability in the system is the mechanical design of the CARR and could be mitigated with a redesign of the footplate and calf rest positioning, as well as a smaller and more manageable frame.

In terms of effort applied and ankle fatigue, participant responses suggest that the second series of motion under dual-model MPC required more applied effort to maintain position and keep up with the footplate than during the first series of motion under single-model MPC. Both motions resulted in responses wholly between 0 and 6, with the majority rating 1 for the first series and 3 for the second. Ratings for fatigue after the motion was finished were very similar between each series, with the majority of participants rating 1 with a small number rating up to 5. On an individual basis however, while most participants rated both motions the same in terms of fatigue, those that rated them differently mostly rated the second series higher by one or two points, with only one rating it lower. The measure of applied effort and fatigue is important to determine whether the system is fit for purpose as in a real clinical rehabilitation environment the exercises would generally last a long time, up to an hour, and a user's ability to stay engaged and not get too tired greatly increases the efficacy of the treatment. Therefore, based on these results, the single-model MPC may be better suited for a real rehabilitation environment.

6.6 Chapter Conclusion

The experiments conducted in this study used the CARR controlled by the two novel developed MPC systems, single-model MPC and dual-model MPC, in online tests with 15 healthy participants. During each experiment, the displacement measurement on the X and Y axis of the CARR were measured and the participant was given a questionnaire with a series of questions about the experience, specifically how comfortable and stable they felt using the CARR and how much effort they felt they needed to apply during the motion. The experiments were split into 2 sections, actuated by single-model MPC and dual-model MPC

respectively, with each section including a plantar/dorsiflexion motion in which the X axis was in motion, and an ab/adduction motion in which the Y axis was in motion. As the primary measure for clinical trials of rehabilitation robots in general is improvement to a participant's ankle RoM and strength, they generally take place over an extended period, ranging from two weeks to three months. However, as the intended measures from these experiments were firstly motion tracking accuracy under external disturbance and participant comfort and usability of the system, a single session was performed per participant.

Based on the axis displacement measurements taken during these experiments, the MPC is impacted by the force disturbance of a user's foot pushing down on the footplate as the X axis has a consistent downward offset. The Y axis also experiences an offset unique to each user due to ankle and sitting position, and different ankle stiffnesses. In the X axis, the single-model MPC showed lower error but also more variance between participants than dual-model. Y axis motion was generally similar between the two.

The participants' responses to the questionnaire give some insight into the comfort and usability of the CARR, as well as some good comparison metrics for the two controllers. The main affecting factors for comfort were that some taller and shorter participants had trouble sitting with their foot firmly in the footplate, and during plantar/dorsiflexion motion the close positioning of the footplate and calf rest caused some participants' heels to be pinched between them. Both these issues could be alleviated with a mechanical redesign, shrinking the frame to allow for more comfortable sitting positions, adding an adjustable mechanism to allow for more customisability, and moving the calf rest such that it sits a comfortable distance from the footplate. One other common comment on comfort was that the initial inflation prior to motion was sudden, but this is easily

fixed by changing the control to slowly increase pressure rather than doing it instantaneously. In comparison between the two controllers, single-model MPC was slightly less stable and comfortable than while the CARR was stationary, but opinion was divided on dual-model MPC in terms of comfort, with some participants finding it more comfortable and some finding it less. Responses to how much effort participants needed to apply during motion and how tired their ankle felt afterwards showed a small but clear difference between the two controllers. Responses were very similar, but the single-model MPC was found to require less effort and leave participants less fatigued afterwards than dual-model MPC.

Results show that both MPC systems have merit in usage with the CARR with a user, with single-model MPC requiring less applied effort during motion and leaving users less fatigued afterwards, but dual-model MPC being more comfortable for some users. Further experiments which are more specific to the comfort and usability of the controllers with a wider participant group and more specific user feedback would be required to determine exactly what might make one controller more comfortable for certain users than the other. Measurement results show that single-model MPC is more accurate to the setpoint, but dual-model is more consistent between participants. Both controllers show merit and have some good responses from participants, suggesting they are suitable for further research to improve their relative shortcomings. The most common complaint from participants was results of the mechanical design of the CARR, so a redesign would be necessary to allow the device to be used in more long-term or clinical experiments.

The contributions of this chapter are online experimental results for motion tracking performance of the developed MPC systems, and user responses as to

their experience using the CARR for guided ankle motion. The data gathered as part of these experiments is essential to validating the proper functioning of the MPCs, as the ability of the controllers to mitigate the disturbance and loading of a user's foot on the footplate is important to maintaining accurate motion during rehabilitative exercises. As rehabilitation robots are always intended for use with a human user, recording participants' comments and experience of using the CARR gives valuable insights into the successes of the system, and how it can be improved.

CHAPTER 7

CONCLUSION AND FUTURE WORK

This chapter concludes the thesis with a summary of the outcomes of research performed as part of this project. After a systematic review of the literature concerning intelligent control of rehabilitation robots, several intelligent control strategies were developed for use with a PAM, and a PSO-based modelling method was developed to generate dynamic models of the PAM system for use with model-based controllers. The developed MPC strategy was deemed to be the most suitable for further research. The PSO modelling method and associated MPC were adjusted and used in comparative experiments with the CARR, further validating their functionality, and then used in online experiments with human participants. This chapter will also examine any shortcomings of the work done in this thesis, identifying potential future avenues for research.

7.1 Outcomes and Contributions

The primary aim of the work presented in this thesis was to develop, implement, and experimentally verify an intelligent control system for effective and compliant control of an ankle rehabilitation robot. To achieve this aim, three research objectives were initially defined to guide the work, and a systematic review of the literature concerning the subject field of intelligent control strategies used in rehabilitation robotics was conducted. Based on the findings of the review, certain trends in recent research were found as well as gaps and opportunities to further the literature through this work. These findings included:

- Intelligent control of rehabilitation robots can effectively improve their motion or force tracking accuracy, robustness to disturbance, and customisability over non-intelligent controllers
- Commonly used algorithms in the field include PID as both a benchmark comparison and as a basis for improved intelligent algorithms, learning controllers including neural network deep learning, fuzzy logic, and adaptive control
- Active participation of patients with the rehabilitation exercises can improve the rehabilitation outcome, and this can be achieved using intelligent control algorithms
- While many articles develop novel controllers, few experimentally validate them in comparison to other controllers, and most deem them fit for purpose based on internally determined metrics

- Few rehabilitation robotics systems are used in trials with impaired participants, an important metric for determining their suitability for a clinical environment

The methods and focus of the work presented in this thesis were based on the research objectives and findings from the literature review. The outcomes and contributions of this work are summarised in Table 7.1, and each specific contribution is discussed in more detail in the following sections.

Table 7.1: Outcomes and Contributions Summary

Contribution	Outcome	Chapter
Piecewise PSO-based modelling method for PAM	Model accuracy experimental results prove the PSO-modelling method is suitably accurate for online use, and has much lower complexity than other methods	3
MPC algorithm for PAM motion control	Developed PSO method allows for rapid dynamic model generation of complex systems and allows model-based predictive controllers to function well	4
Experimental comparison results of intelligent controllers for PAM motion	MPC outperforms optimised PID and ILC in motion tracking experiments, but cannot respond to disturbance	
MPC algorithm for CARR motion control	Two separate implementations of MPC using different model setups are created to accommodate for potential dynamic complexities of the CARR	5
Experimental comparison results for CARR control methods	Both MPC implementations outperform PID and ILC, with relative benefits and shortcomings	
User study results for MPC-controlled CARR	Trials performed with human participants using the CARR controlled by both MPC implementations, with measurement results and user feedback	6

7.1.1 PSO-based Modelling Method

The first technical contribution of this work is the PSO-based modelling method for dynamic modelling of PAMs, and the piecewise approach to this method. This optimisation-based modelling approach uses a phenomenological model of a PAM approximated to a mass-spring-damper system. The differential equations

of this approximation therefore have three unknown parameters, associated with spring constant, damping constant, and mass. Optimal solutions for these parameters are generated using a PSO algorithm with a three-dimensional search space, with a fitness function using the RMSE of a solution compared to a measured output sequence from a real PAM. Using this method, dynamics models of PAMs are generated quickly and with good computational efficiency. In addition, to better account for the nonlinearities present in the dynamics of fluid dynamic-based actuators, the piecewise method was also implemented in which different models were generated for different stages of PAM motion. Differentiating the inflating and deflating states accounts for hysteresis in the rubber air bladder and sleeve of the actuator and dividing the stroke length into sections based on input pressure accounts for differing properties and input-output relationships based on the changing rate of air flow. The goal of developing this modelling method was to be able to create mathematical models of the complex dynamics of nonlinear actuators without compromising on generation time and efficiency.

In comparison with other modelling methods for pneumatic actuators present in the literature, other mathematical models [108, 109] show similar model accuracy but do not account for overshooting at maximum stroke length or the hysteresis present in the rubber construction of the actuator. Another phenomenological model approximation presented in [112] used a much smaller stroke length for validation experiments so accurate error comparison is difficult, however the method required measurement of the PAM's physical properties prior to model generation, greatly increasing generation time. Neural network modelling methods are popular in recent work [113, 114, 115, 116] and give excellent model accuracy, however generation time and complexity are typically

significantly larger than the PSO method and requires large data sets which must be either externally sourced, potentially not reflecting the specific properties of the actuator in question, or generated beforehand, again increasing generation time. The main benefits of the PSO modelling method and associated piecewise method are flexibility, as the method can be applied to any nonlinear system with unknown dynamic parameters or unusual output response, and simplicity as the models take a short time to generate and use a low number of parameters.

7.1.2 MPC Algorithm for PAM Motion Control

The second contribution is the MPC strategy developed for PAM motion control. Using the PSO modelling method, dynamic models of the PAM are applied to predictive control which effectively mitigates time variance in the motion tracking of the actuator resulting in improved performance.

With pneumatic actuators becoming more prevalent in rehabilitation robot design [124], but simple traditional control strategies struggle to account for the nonlinear dynamics and other complexities inherent to their design. Therefore, intelligent control strategies are necessary for improved motion control which is essential to the proper functioning of any robot designed to be worn or directly interacted with by a human user. Many examples of pneumatic actuator-driven rehabilitation robots exist [42, 67, 104, 125, 126, 127, 128] with many different control strategies used for motion control including sliding mode control [42, 126, 127] using intelligent algorithms such as fuzzy logic [42] and neural network parameter estimation [127], as well as adaptive controllers [67]. MPC strategies are also used in rehabilitation robotics for better human-robot interaction [91]. The ability of MPC to predict future system states makes it an excellent candidate for use with the time-variant and nonlinear dynamics of PAMs. In comparative

experiments with other intelligent controllers, ILC and PSO-PID, MPC showed lower error values, greatly improved response time, and limited or no chattering when compared to traditional control. While learning control is unable to respond well to changing setpoints and is only suitable for continuously repeating patterns, the predictive algorithm effectively eliminates this issue.

7.1.3 Experimental Comparison Data for Intelligent Control of Pneumatic Artificial Muscle

To properly validate the developed MPC strategy, a series of comparative experiments were performed using MPC, ILC, PSO-PID and PID controllers. The results of these experiments constitute the third contribution of this work. A total of 25 motion tracking experiments were performed with 4 controllers, testing motion tracking on different sections of the PAM stroke length, higher and lower frequency response, unusual setpoint patterns, response to changing setpoints and to external disturbance and loading.

There are few examples of comparative experiments between controller types in the literature aside from those validating a novel control strategy in comparison with a more simple or traditional controller. Of the articles examined in the systematic literature review performed as part of this thesis, only 23 of the 70 included present comparative experiment data. The most common of these [36, 37, 43, 44 47, 54, 58, 68, 69, 70, 71, 76, 77, 78] compare a developed controller with PD/PID as a benchmark and invariably find that the developed controller has the best performance. The majority of other comparisons are performed to validate an improved version of a controller over an earlier or simpler version [40, 48, 53, 58, 61, 67, 68, 70, 80, 88]. While experimental validation is a necessary step in the development of a novel controller, comparison with other

strategies which may also be suitable for the intended application is also necessary to prove the developed controller has benefits over a previously developed one. As such, as well as MPC for PAM control, ILC and optimised PID were also developed for comparison, and PID was used as a benchmark to compare improvements of each intelligent algorithm over traditional control. As expected, results proved that intelligent control outperforms PID with lower error values and worse response time, but the main contributions are the comparison between different intelligent control strategies which are often used in rehabilitation robotics scenarios based on their individual benefits.

7.1.4 MPC Algorithms for CARR Motion Control

The fourth contribution of this work is the implementation of two MPC strategies for motion control of the CARR, using the PSO modelling method to generate dynamic models of the PAMs driving the robot. Four separate MPCs are used to control the CARR, one for each actuator. Two model setups are proposed and developed: single-model, in which all four PAMs are assumed to have the same dynamic properties as each other and are therefore modelled using the same set of parameters, and dual-model, in which the lower and upper pairs of PAMs are assumed to have differing properties based on connection angle to the frame and footplate as well as with level ground causing gravity to act at a different angle, so two sets of model parameters are generated.

MPC is commonly used in the field of rehabilitation robotics [142], in walking-based patient following systems [146, 147] as well as in powered orthoses and exoskeletons [148, 149]. The predictive algorithm allows for accurate motion and impedance control of complex, time-varying systems and can even allow for intention detection in some systems. The main difficulty in using MPC for control

is that a system dynamic model is required, and the accuracy of the controller is directly tied to the accuracy of the model. There are many different modelling techniques used in literature [151, 152, 153, 154, 155, 156, 157, 158] using different algorithms to model rehabilitation robots for improved control. With the inherent trade-off between model complexity and accuracy, both must be considered when developing a new modelling technique. The PSO modelling method developed and validated as part of the first contribution of this work showed initial promise in model accuracy while keeping generation time and complexity low for a single PAM actuator. However, the implementation of this method to a much more complex system like the CARR with multiple actuators connected in parallel and multiple axes of motion introduces more complexity to the system. Through the two model setups, single- and dual-model, two different MPCs were created and experimentally tested alongside ILC and PID as comparison benchmarks with results showing better motion tracking and stability than traditional control, and outperformed learning control when motion was more complex such as when multiple axes were in motion at once. Each model setup showed individual benefits over the other, with single-model performing better for the X axis and while only one axis was in motion at a time, while dual-model performed better for the Y axis and while multiple axes were in motion. While there is evidence that both MPC setups require more development, the initial results are promising and the flexibility in the algorithm and multiple possibilities for improvements make them promising for future work.

7.1.5 User Study for Online Validation of Model Predictive-Controlled CARR

The final contribution of this work is the results from the user study, in which the CARR is controlled using both developed MPC implementations with human participants. Measurement results from the X and Y axes of the CARR are used to determine the performance of the controllers with the addition of external disturbance and loading to the system, and participants' responses are gathered using a questionnaire to check the comfort and usability of the system.

The primary measure of success for most robotic systems is motion or force output tracking response, with an accurate output being associated with a successful trial. However, particularly in rehabilitation robotics, patient comfort and engagement with the exercises is important to the success of a system as well [95]. A successful system will result in improved rehabilitation outcomes, and this is the metric most measured in clinical trials for rehabilitation robots [164, 165, 166, 167, 168] and while the improvement of the participant group is the focus of some studies, others are performed to validate a proposed system [169, 170, 171]. The majority of newly developed rehabilitation robots are not validated in online experiments with participants, which is an essential step to confirming a robotics system is appropriate for use in a clinical setting with impaired human users. Motion tracking results from the user study showed firstly that single-model MPC could closer follow the setpoint resulting in generally more accurate motion than dual-model, but also that there was a larger spread between participants suggesting that dual-model was more consistent between users. Also, the inability of the MPC to respond to disturbances and loading caused consistent offsets in

angular displacement associated with the weight of a participant's foot and the stiffness of their ankle. The responses from the participants in the form of a questionnaire gave results unique to this study concerning the comfort and stability of the CARR, and effort a tiredness associated with guided ankle motion. The main factors affecting comfort were that taller and shorter participants could not sit comfortably in the robot, and that the positioning of the footplate and calf rest caused pinching of the heel in some cases. Comparing the two MPC implementations, opinion was divided as to whether dual-model MPC was more or less comfortable than single-model with some participants rating it significantly higher and some lower. Required effort and associated fatigue were similar between the two controllers but with single-model showing a slight improvement over dual-model. The main takeaway from these results is that differences between participants result in greatly altered experiences with the CARR and the controllers, suggesting adaptive algorithms, personalised exercises, and adjustable mechanisms are the best way to improve the current system.

7.2 Future Work

7.2.1 PSO-based modelling method improvements

The PSO modelling method for PAM dynamic modelling has some downsides. Robustness can be improved by adding additional parameters to the phenomenological model to account for external loading, or alternatively a force measurement can be implemented in control schemes to dynamically adjust parameters accordingly. Simple fine-tuning of the algorithm parameters could improve accuracy and generation time. The piecewise method, while mitigating

many of the complex factors of PAM dynamics, was not used in later parts of this work due to the issues in switching points between different models causing serious accuracy concerns in associated controllers. This issue could be improved on in a few different ways: overlapping models within the piecewise model set would limit the impact of each switching state by blending each state together, or dynamic parameter adjustment during online motion would alleviate the need for switching altogether.

7.2.2 MPC motion tracking accuracy

The primary downside of the MPC developed during this work is the inability to respond to disturbances to the system. The reliance on a system model and predictive algorithm means control signals are calculated prior to actual motion meaning any changes to the system including added loads or disturbance are not accounted for. The addition of robust elements to the controller would help mitigate this, alternatively some adaptive version of MPC with the capability to adjust control signals in real time could be developed. As the motion tracking accuracy outside of disturbance rejection relies heavily on the accuracy of the system model for MPC, any improvements to the dynamic model generation method would necessarily improve motion tracking accuracy.

7.2.3 Further experiments for MPC implementations

Through controller comparison studies and participant involved experiments both the MPC implementations, single-model and dual-model, have been validated and verified to be effective in position control of nonlinear systems. However, some points were left unanswered and results suggested further tests were necessary. The additional actuation of the Z axis of the CARR, which was omitted in this study due to mechanical restrictions, could impact the

effectiveness of the developed controllers. In addition, further development of the controllers would require a new set of validation experiments in comparison with the initial version to confirm any additional functionality improves performance. The results from both the controller comparison study and the user study suggested that the single-model and dual-model setups for MPC have differing traits, with one outperforming the other in certain metrics and on certain axes, and in the case of the user study opinion was divided among the participants as to which was the most comfortable during motion. As such, more research is required to determine what applications each of the single- and dual-model setups are best suited for, whether any new setups are required to mitigate their relative downsides, or whether some adaptive or switching-mode algorithm could be used to best combine the two.

7.2.4 CARR mechanical design

The focus of this work is controller design. However, the eventual aim of the CARR project is to develop a compliant ankle rehabilitation robot that can be used in clinical or home environments to assist healthcare services in providing therapeutic exercises to patients. As part of this, the robot itself must be appropriate for this purpose, and the CARR has several potential improvements to be made. The primary concern in its current configuration is that the Z axis of the CARR cannot be properly controlled, functionally making it a 2 DoF robot with some inherent compliance on the non-actuated axis. A rearrangement of the PAMs to increase the angle they meet the footplate would allow for better control of the Z axis, however using four linear actuators for three rotational DoF will necessarily result in some under-actuation. The addition of additional actuators,

either more PAMs positioned perpendicular to the existing set, or a rotational actuator positioned underneath the footplate, would mitigate this issue.

As discovered during the user study, user comfort is also an issue with the CARR. Some simple adjustments can be made to fix some of the mentioned issues; an adjustable mechanism on the calf brace or on the connection points of the PAMs to the frame would help taller/shorter users sit more comfortably, and moving the calf rest further from the footplate would prevent the issue of heels being pinched between them. The size of the frame is another issue which is more difficult to address, as some users found it difficult to sit comfortably with one foot connected to the robot and the other resting on the ground. Using smaller linkages for the frame of the CARR would limit the force output capability and potentially make the system less stable, so a full redesign taking these issues into account would be necessary.

7.3 Summary

This chapter summarises the primary contributions and outcomes of the work presented in this thesis. The focus of the research was to design, implement, and experimentally validate an intelligent control strategy for use with a compliant ankle rehabilitation robot to allow for improved motion tracking accuracy and improve the performance of the robot, with the eventual goal of providing assistive rehabilitative care to patients in a clinical or home environment, reducing the workload on healthcare services and making the care more accessible. The main contributions of the research are as follows: 1) Development of a PAM dynamic modelling method based on PSO algorithm for rapid, low-cost modelling of complex systems; 2) Development of a MPC strategy for accurate motion control of PAMs; 3) Experimental comparison data for multiple

intelligent motion control strategies for PAMs; 4) Two MPC implementations for motion control of the CARR; 5) Experimental comparison data for multiple controllers on the CARR, and 6) User study results from human participant experiments with the CARR including motion tracking results from the MPCs and user feedback responses. Overall, this work has successfully developed, implemented, and experimentally verified in multiple comparative and participant trials an intelligent controller for motion tracking control of the CARR. Both the controller and the CARR have multiple avenues for future research, eventually resulting in a device suitable for clinical use.

BIBLIOGRAPHY

[1] World Stroke Organisation. (2022). Global Stroke Fact Sheet 2022. [Fact sheet]. Available: https://www.world-stroke.org/assets/downloads/WSO_Global_Stroke_Fact_Sheet.pdf

[2] Amanda Clery, Ajay Bhalla, Anthony G. Rudd, Charles D. A. Wolfe, Yanzhong Wang, "Trends in prevalence of acute stroke impairments: A population-based cohort study using the South London Stroke Register," PLOS Medicine, 17(10): e1003366, October 2020, doi: 10.1371/journal.pmed.1003366.

[3] Dobkin, B.H. Clinical practice. Rehabilitation after Stroke. *N. Engl. J. Med.* **2005**, *352*, 1677–1684. https://doi.org/10.1056/NEJMcp043511.

[4] U.S Department of Health and Human Services, National Institutes of Health. (April 2020) Post Stroke Rehabilitation Fact Sheet. [Fact sheet]. Available: https://www.stroke.nih.gov/documents/Post-Stroke_Rehabilitation_english_brochure_508C.pdf

[5] Birch, Nick & Graham, Jon & Priestley, Tom. "RAPPER II—Robot-Assisted PhysiotheraPy Exercises WITH REX-powered walking aid in patients with spinal cord injury." The Spine Journal. April 2016. S70. 10.1016/j.spinee.2016.01.169.

[6] Díaz, Iñaki & Gil, Jorge Juan & Sánchez, Emilio. "Lower-Limb Robotic Rehabilitation: Literature Review and Challenges." Journal of Robotics. 2011. 10.1155/2011/759764.

[7] Qassim HM, Wan Hasan WZ. "A Review on Upper Limb Rehabilitation Robots." Applied Sciences. 2020. doi: 10.3390/app10196976

[8] Chiaradia, Domenico & Xiloyannis, Michele & Solazzi, Massimiliano & Masia, Lorenzo & Frisoli, Antonio. "Comparison of a Soft Exosuit and a Rigid Exoskeleton in an Assistive Task." 2018.

[9] Summit Medical & Scientific. 2023. University Hospitals Dorset: Pioneering the NHS rehab robotics revolution [Article]. Available: https://summitmedsci.co.uk/2023/02/14/university-hospitals-dorset-pioneering-the-nhs-rehab-revolution-with-robotics/

[10] International Federation of Robotics. 2021. Robots help patients recover faster from stroke [Article]. Available: https://ifr.org/ifr-press-releases/news/robots-help-patients-recover-faster-from-stroke

[11] Shahid Hussain, Sheng Q. Xie, Prashant K. Jamwal, "Control of a robotic orthosis for gait rehabilitation," Robotics and Autonomous Systems, September 2013, doi: 10.1016/j.robot.2013.01.007.

[12] Shahid Hussain, Prashant K Jamwal, Mergen H Ghayesh, "State-of-the-art robotic devices for ankle rehabilitation: Mechanism and control review," Institute of Mechanical Engineers, Part H: Journal of Engineering in Medicine, October 2017, doi: 10.1177/0954411917737584.

[13] H. I. Krebs et al. "Robot-Aided Neurorehabilitation: A Robot for Wrist Rehabilitation," IEEE Transactions on Neural Systems and Rehabilitation Engineering, vol. 15, no. 3, pp. 327-335, September 2007, doi: 10.1109/TNSRE.2007.903899.

[14] Haoyong Yu, Sunan Huang, Gong Chen, Nitish Thakor, "Control design of a novel compliant actuator for rehabilitation robots," Mechatronics, Volume 23, Issue 8, Pages 1072-1083, December 2013, doi: 10.1016/j.mechatronics.2013.08.004.

[15] Iñaki Díaz, Jorge Juan Gil, Emilio Sánchez, "Lower-Limb Robotic Rehabilitation: Literature Review and Challenges," Journal of Robotics, vol. 2011, Article ID 759764, 11 pages, November 2011, doi: 10.1155/2011/759764.

[16] Giacomo Zuccon, Basilio Lenzo, Matteo Bottin, Giulio Rosati. "Rehabilitation robotics after stroke: a bibliometric literature review," Expert Review of Medical Devices, Volume 19, Pages 405-421, July 2022, doi: 10.1080/17434440.2022.2096438.

[17] Zhang, M., Davies, T.C., Xie, S. “Effectiveness of robot-assisted therapy on ankle rehabilitation – a systematic review,” J NeuroEngineering Rehabil 10, 30, March 2013, doi: 10.1186/1743-0003-10-30.

[18] Simonetti D, Zollo L, Milighetti S, Miccinilli S, Bravi M, Ranieri F, Magrone G, Guglielmelli E, Di Lazzaro V, Sterzi S, “Literature Review on the Effects of tDCS Coupled with Robotic Therapy in Post Stroke Upper Limb Rehabilitation,” Front. Hum. Neurosci, 11:268, May 2017, doi: 10.3389/fnhum.2017.00268.

[19] A. S. Niyetkaliyev, S. Hussain, M. H. Ghayesh and G. Alici, "Review on Design and Control Aspects of Robotic Shoulder Rehabilitation Orthoses," IEEE Transactions on Human-Machine Systems, vol. 47, no. 6, pp. 1134-1145, Dec. 2017, doi: 10.1109/THMS.2017.2700634.

[20] Marchal-Crespo, L., Reinkensmeyer, D.J., “Review of control strategies for robotic movement training after neurologic injury,” J NeuroEngineering Rehabil, 6, 20, June 2009, doi: 10.1186/1743-0003-6-20.

[21] Kwakkel G, Kollen BJ, Krebs HI, “Effects of Robot-Assisted Therapy on Upper Limb Recovery After Stroke: A Systematic Review,” Neurorehabilitation and Neural Repair, 2008;22(2):111-121, September 2007, doi: 10.1177/1545968307305457.

[22] Longdom. (2022). Advances in automobile engineering. Control Systems Journals Articles. Available: https://www.longdom.org/scholarly/control-system-journals-articles-ppts-list-1248.html

[23] Legg, S., Hutter, M. “Universal Intelligence: A Definition of Machine Intelligence,” Minds & Machines, 17, 391–444, November 2007, doi: 10.1007/s11023-007-9079-x.

[24] Antsaklis, P.J., Rahnama, A. “Control and Machine Intelligence for System Autonomy,” J Intell Robot Syst, 91, 23–34 ,April 2018, doi: 10.1007/s10846-018-0832-6.

[25] A. Belkadi, H. Oulhadj, Y. Touati, Safdar A. Khan, B. Daachi, “On the robust PID adaptive controller for exoskeletons: A particle swarm optimization based approach,” Applied Soft Computing, Volume 60, Pages 87-100, ISSN 1568-4946, November 2017, doi: 10.1016/j.asoc.2017.06.012.

[26] Taha Z, Abdul Majeed APP, Zainal Abidin AF, Hashem Ali MA, Khairuddin IM, Deboucha A, Wong Paul Tze MY, “A hybrid active force control of a lower limb exoskeleton for gait rehabilitation,” Biomed Tech (Berl), 63(4):491-500, July 2018, doi: 10.1515/bmt-2016-0039.

[27] M. Kamran Joyo, Yarooq Raza, S. Faiz Ahmed, M. M. Billah, Kushsairy Kadir, Kanendra Naidu, Athar Ali, Zukhairi Mohd Yusof, “Optimized Proportional-Integral-Derivative Controller for Upper Limb Rehabilitation Robot,” Electronics 2019, 8(8), 826, Special Issue Cognitive Robotics & Control, July 2019, doi: 10.3390/electronics8080826.

[28] M. K. Joyo, Y. Raza, K. Kadir, K. Naidu, S. F. Ahmed, S. Khan, “Firefly Optimised PID Control for Upper Extremity Rehabilitation Robot,” in 2019 IEEE International Conference on Smart Instrumentation, Measurement and Application (ICSIMA), pp. 1-5, August 2019, doi: 10.1109/ICSIMA47653.2019.9057342.

[29] X. Wu, D. Li, Y. Qian, Y. Guan, Y. Chen, “An ASA Based Feedforward Control of Skeleton Post-Stroke Rehabilitation Robot System,” in 2018 37th Chinese Control Conference (CCC), pp. 5647-5652, July 2018, doi: 10.23919/ChiCC.2018.8484182.

[30] Wahab Amini Azar, Peiman Shah Nazar, “An optimized and chaotic intelligent system for a 3DOF rehabilitation robot for lower limbs based on neural network and genetic algorithm,” Biomedical Signal Processing and Control, Volume 69, 102864, ISSN 1746-8094, August 2021, doi: 10.1016/j.bspc.2021.102864.

[31] J. Chen, Y. Li, J. Zeng, “Active interactive genetic control for lower limb rehabilitation robots with uncertainties,” in 2021 40th Chinese Control

Conference (CCC), pp. 491-496, July 2021, doi: 10.23919/CCC52363.2021.9549638.

[32] Buongiorno D, Barsotti M, Barone F, Bevilacqua V, Frisoli A, "A Linear Approach to Optimize an EMG-Driven Neuromusculoskeletal Model for Movement Intention Detection in Myo-Control: A Case Study on Shoulder and Elbow Joints," Front Neurorobot, 12:74, November 2018, doi: 10.3389/fnbot.2018.00074.

[33] M. Babaiasl, S. N. Goldar, M. H. Barhaghtalab, V. Meigoli, "Sliding mode control of an exoskeleton robot for use in upper-limb rehabilitation," in 2015 3rd RSI International Conference on Robotics and Mechatronics (ICROM), pp. 694-701, October 2015, doi: 10.1109/ICRoM.2015.7367867.

[34] Hashemi A, McPhee J, "Assistive Sliding Mode Control of a Rehabilitation Robot with Automatic Weight Adjustment," in Annu Int Conf IEEE Eng Med Biol Soc., 2021:4891-4896, November 2021, doi: 10.1109/EMBC46164.2021.9631110.

[35] C. Wang, L. Peng, L. Luo, Z. -G. Hou, W. Wang, "Genetic Algorithm Based Dynamics Modeling and Control of a Parallel Rehabilitation Robot," in 2018 IEEE Congress on Evolutionary Computation (CEC), pp. 1-6, July 2018, doi: 10.1109/CEC.2018.8477768.

[36] Z. Shen, J. Zhou, J. Gao and R. Song, "Fuzzy Logic Based PID Control of a 3 DOF Lower Limb Rehabilitation Robot," in 2018 IEEE 8th Annual International Conference on CYBER Technology in Automation, Control, and Intelligent Systems (CYBER), pp. 818-821, July 2018, doi: 10.1109/CYBER.2018.8688089.

[37] S. Zhang, C. Wang, Y. Hu, D. Liu, T. Zhang, X. Wu, "Rehabilitation with lower limb exoskeleton robot joint load adaptive server control," in 2016 IEEE International Conference on Information and Automation (ICIA), pp. 13-18, August 2016, doi: 10.1109/ICInfA.2016.7831790.

[38] Peng Suo, Xueqiang Zhu, Shu Wang, Mei Li, Ting Yu, Chunning Song, Haodi Ning, Yi Xin, "A Training Method for a Sensor-Based Exercise Rehabilitation

Robot," Journal of Sensors, Special Issue Image Analysis of Vision Sensors 2022, Volume 2022, Article 4336664, August 2022, doi: 10.1155/2022/4336664.

[39] X. Yuan, T. Zhou, J. Ji, Y. Liu, W. Wang and F. Yue, "Design of adaptive compliance control algorithm for upper limb exoskeleton rehabilitation robot," in 2021 China Automation Congress (CAC), pp. 2737-2743, October 2021, doi: 10.1109/CAC53003.2021.9727655.

[40] Q. Wu, D. Xu, B. Chen and H. Wu, "Integral Fuzzy Sliding Mode Impedance Control of an Upper Extremity Rehabilitation Robot Using Time Delay Estimation," IEEE Access, vol. 7, pp. 156513-156525, October 2019, doi: 10.1109/ACCESS.2019.2949197.

[41] Y. -L. Wang, K. -Y. Wang, X. Li, Z. -J. Mo and K. -C. Wang, "Control Strategy and Experimental Research of Cable-Driven Lower Limb Rehabilitation Robot," IEEE Access, vol. 9, pp. 79182-79195, May 2021, doi: 10.1109/ACCESS.2021.3083810.

[42] Li IH, Lin YS, Lee LW, Lin WT, "Design, Manufacturing, and Control of a Pneumatic-Driven Passive Robotic Gait Training System for Muscle-Weakness in a Lower Limb," Sensors (Basel), 21(20):6709, October 2021, doi: 10.3390/s21206709.

[43] Q. Wu, X. Wang, F. Du, Q. Zhu, "Fuzzy sliding mode control of an upper limb exoskeleton for robot-assisted rehabilitation," in 2015 IEEE International Symposium on Medical Measurements and Applications (MeMeA) Proceedings, pp. 451-456, May 2015, doi: 10.1109/MeMeA.2015.7145246.

[44] J. Wang, Y. Li, A. An, H. Zhang, "Sliding Mode Control of Upper Limb Rehabilitation Robot Based on Fuzzy Compensation," in 2019 Chinese Automation Congress (CAC), pp. 2338-2343, November 2019, doi: 10.1109/CAC48633.2019.8997503.

[45] Q. Wu, X. Wang, B. Chen, H. Wu, “Design and Fuzzy Sliding Mode Admittance Control of a Soft Wearable Exoskeleton for Elbow Rehabilitation,” IEEE Access, vol. 6, pp. 60249-60263, October 2018, doi: 10.1109/ACCESS.2018.2875550.

[46] Cheng, Gaoxin; Xu, Linsen; Xu, Jiajun; Liu, Jinfu; Shi, Jia; et al., “Robotic mirror therapy system for lower limb rehabilitation,” The Industrial Robot; Bedford Vol. 48, Iss. 2, July 2021, doi: 10.1108/IR-06-2020-0112.

[47] Y. Wang, Z. Liu, L. Zhu, X. Li, H. Wang, “An Impedance Control Method of Lower Limb Exoskeleton Rehabilitation Robot Based on Predicted Forward Dynamics,” in 2020 IEEE 19th International Conference on Trust, Security and Privacy in Computing and Communications (TrustCom), pp. 1515-1518, January 2021, doi: 10.1109/TrustCom50675.2020.00206.

[48] T. Goyal, S. Hussain, E. Martinez-Marroquin, N. A. T. Brown, P. K. Jamwal, “Stiffness-Observer-Based Adaptive Control of an Intrinsically Compliant Parallel Wrist Rehabilitation Robot,” IEEE Transactions on Human-Machine Systems, October 2022, doi: 10.1109/THMS.2022.3211164.

[49] Huang, YC., Hu, H., Chen, CH. et al., “Assistive Robot Design for Lower Limbs Rehabilitation Using Fuzzy Control,” Int. J. Fuzzy Syst., 23, 2384–2395, November 2021, doi: 10.1007/s40815-021-01152-4.

[50] Z. Sun, F. Li, Y. Lian, S. Liu, K. Liu, “An adaptive iterative learning control approach for lower limb rehabilitation robot in noisy environments,” in 2019 IEEE 9th Annual International Conference on CYBER Technology in Automation, Control, and Intelligent Systems (CYBER), pp. 905-910, August 2019, doi: 10.1109/CYBER46603.2019.9066748.

[51] X. Huang, F. Naghdy, H. Du, G. Naghdy, C. Todd, “Reinforcement learning neural network (RLNN) based adaptive control of fine hand motion rehabilitation robot,” in 2015 IEEE Conference on Control Applications (CCA), pp. 941-946, September 2015, doi: 10.1109/CCA.2015.7320733.

[52] Q. Wu, B. Chen, H. Wu, “Adaptive Admittance Control of an Upper Extremity Rehabilitation Robot With Neural-Network-Based Disturbance Observer,” IEEE Access, vol. 7, pp. 123807-123819, August 2019, doi: 10.1109/ACCESS.2019.2938566.

[53] P. Zhang, J. Zhang, Z. Zhang, “Design of RBFNN-Based Adaptive Sliding Mode Control Strategy for Active Rehabilitation Robot,” IEEE Access, vol. 8, pp. 155538-155547, August 2020, doi: 10.1109/ACCESS.2020.3018737.

[54] J. Li, Y. Zhou, M. Dong, X. Rong, “Isokinetic muscle strength training strategy of an ankle rehabilitation robot based on adaptive gain and cascade PID control,” IEEE Transactions on Cognitive and Developmental Systems, January 2022, doi: 10.1109/TCDS.2022.3145998.

[55] M. Zhang et al., “Adaptive Patient-Cooperative Control of a Compliant Ankle Rehabilitation Robot (CARR) With Enhanced Training Safety,” IEEE Transactions on Industrial Electronics, vol. 65, no. 2, pp. 1398-1407, February 2018, doi: 10.1109/TIE.2017.2733425.

[56] Rastegar M, Kobravi HR, “A Hybrid-FES Based Control System for Knee Joint Movement Control,” Basic Clin Neurosci. 12(4):441-452, August 2021, doi: 10.32598/bcn.2021.173.3.

[57] Asín-Prieto G, Martínez-Expósito A, Barroso FO, Urendes EJ, Gonzalez-Vargas J, Alnajjar FS, González-Alted C, Shimoda S, Pons JL, Moreno JC, “Haptic Adaptive Feedback to Promote Motor Learning With a Robotic Ankle Exoskeleton Integrated With a Video Game,” Front Bioeng Biotechnol. 8:113, February 2020, doi: 10.3389/fbioe.2020.00113.

[58] W. Qian, L. Ai, Z. Zhou, J. Liao, X. Xiao, Z. Guo, “Adaptive impedance control of a 6-DOF cable-driven compliant upper limb rehabilitation robot,” in 2021 27th International Conference on Mechatronics and Machine Vision in Practice (M2VIP), pp. 534-539, November 2021, doi: 10.1109/M2VIP49856.2021.9665097.

[59] Wang Y, Zhang W, Shi D, Geng Y, “Design and Control of an Adaptive Knee Joint Exoskeleton Mechanism with Buffering Function,” Sensors (Basel), 21(24):8390, December 2021, doi: 10.3390/s21248390.

[60] Maggioni S, Reinert N, Lünenburger L, Melendez-Calderon A, “An Adaptive and Hybrid End-Point/Joint Impedance Controller for Lower Limb Exoskeletons,” Front Robot AI., 5:104, October 2018, doi: 10.3389/frobt.2018.00104.

[61] Wilian M. dos Santos, Adriano A.G. Siqueira, “Optimal impedance via model predictive control for robot-aided rehabilitation,” Control Engineering Practice, Volume 93, 104177, ISSN 0967-0661, December 2019, doi: 10.1016/j.conengprac.2019.104177.

[62] Rajasekaran V, López-Larraz E, Trincado-Alonso F, Aranda J, Montesano L, Del-Ama AJ, Pons JL, “Volition-adaptive control for gait training using wearable exoskeleton: preliminary tests with incomplete spinal cord injury individuals,” J Neuroeng Rehabil. 15(1):4, January 2018, doi: 10.1186/s12984-017-0345-8.

[63] Liu Q, Liu A, Meng W, Ai Q, Xie SQ, “Hierarchical Compliance Control of a Soft Ankle Rehabilitation Robot Actuated by Pneumatic Muscles,” Front Neurorobot., 11:64, December 2017, doi: 10.3389/fnbot.2017.00064.

[64] M. Zhang, A. McDaid, A. J. Veale, Y. Peng, S. Q. Xie, “Adaptive Trajectory Tracking Control of a Parallel Ankle Rehabilitation Robot With Joint-Space Force Distribution,” IEEE Access, vol. 7, pp. 85812-85820, June 2019, doi: 10.1109/ACCESS.2019.2925182.

[65] Bardi E, Dalla Gasperina S, Pedrocchi A, Ambrosini E, “Adaptive Cooperative Control for Hybrid FES-Robotic Upper Limb Devices: a Simulation Study,” in Annu Int Conf IEEE Eng Med Biol Soc., 2021:6398-6401, November 2021, doi: 10.1109/EMBC46164.2021.9630331.

[66] Nunes PF, Ostan I, Siqueira AAG, “Evaluation of Motor Primitive-Based Adaptive Control for Lower Limb Exoskeletons,” Front Robot AI., 7:575217, December 2020, doi: 10.3389/frobt.2020.575217.

[67] Y. Li, Q. Liu, W. Meng, Y. Xie, Q. Ai, S. Q. Xie, “MISO Model Free Adaptive Control of Single Joint Rehabilitation Robot Driven by Pneumatic Artificial Muscles,” in 2020 IEEE/ASME International Conference on Advanced Intelligent Mechatronics (AIM), pp. 1700-1705, July 2020, doi: 10.1109/AIM43001.2020.9158805.

[68] G. Ding, W. Huo, J. Huang, Y. Amirat, S. Mohammed, “Robust and Safe Control of a Knee Joint Orthosis,” in 2018 IEEE International Conference on Intelligence and Safety for Robotics (ISR), pp. 343-348, August 2018, doi: 10.1109/IISR.2018.8535984.

[69] A. M. M. Ali, I. Ishtiaq, E. H. Aboadla, K. A. Kadir, S. R. C. Ahmad, “Comparative Analysis of Conventional PID and Adaptive Control For Upper Limb Rehabilitation Robot,” in 2021 IEEE 7th International Conference on Smart Instrumentation, Measurement and Applications (ICSIMA), pp. 1-4, August 2021, doi: 10.1109/ICSIMA50015.2021.9525934.

[70] J. Liu, Y. Zhang, J. Wang, W. Chen, “Adaptive sliding mode control for a lower-limb exoskeleton rehabilitation robot,” in 2018 13th IEEE Conference on Industrial Electronics and Applications (ICIEA), pp. 1481-1486, June 2018, doi: 10.1109/ICIEA.2018.8397943.

[71] Shen, Z., Zhuang, Y., Zhou, J. et al., “Design and Test of Admittance Control with Inner Adaptive Robust Position Control for a Lower Limb Rehabilitation Robot,” Int. J. Control Autom. Syst., 18, 134–142, August 2019, doi: 10.1007/s12555-018-0477-z.

[72] Fitzsimons K, Kalinowska A, Dewald JP, Murphey TD. “Task-based hybrid shared control for training through forceful interaction,” The International Journal of Robotics Research, 2020;39(9):1138-1154, June 2020, doi:10.1177/0278364920933654.

[73] A. U. Pehlivan, D. P. Losey and M. K. O'Malley, "Minimal Assist-as-Needed Controller for Upper Limb Robotic Rehabilitation," IEEE Transactions on

Robotics, vol. 32, no. 1, pp. 113-124, February 2016, doi: 10.1109/TRO.2015.2503726.

[74] W. Meng, S. Q. Xie, Q. Liu, C. Z. Lu, Q. Ai, “Robust Iterative Feedback Tuning Control of a Compliant Rehabilitation Robot for Repetitive Ankle Training,” IEEE/ASME Transactions on Mechatronics, vol. 22, no. 1, pp. 173-184, February 2017, doi: 10.1109/TMECH.2016.2618771.

[75] Xiang Li, Yun-Hui Liu, Haoyong Yu, “Iterative learning impedance control for rehabilitation robots driven by series elastic actuators,” Automatica, Volume 90, Pages 1-7, ISSN 0005-1098, April 2018, doi: 10.1016/j.automatica.2017.12.031.

[76] L. Cheng, M. Chen, Z. Li, “Design and Control of a Wearable Hand Rehabilitation Robot,” IEEE Access, vol. 6, pp. 74039-74050, December 2018, doi: 10.1109/ACCESS.2018.2884451.

[77] Q. Miao et al., “Performance-based iterative learning control for task-oriented rehabilitation: a pilot study in robot-assisted bilateral training,” IEEE Transactions on Cognitive and Developmental Systems, April 2021, doi: 10.1109/TCDS.2021.3072096.

[78] X. Zhu, J. Wang, X. Wang, “Nonlinear iterative learning control of 5 DOF upper-limb rehabilitation robot,” in 2015 IEEE International Conference on Robotics and Biomimetics (ROBIO), pp. 793-798, December 2015, doi: 10.1109/ROBIO.2015.7418866.

[79] Tu X, Han H, Huang J, Li J, Su C, Jiang X, He J, “Upper Limb Rehabilitation Robot Powered by PAMs Cooperates with FES Arrays to Realize Reach-to-Grasp Trainings,” J Healthc Eng., 2017:1282934, doi: 10.1155/2017/1282934.

[80] M. Ketelhut, S. Husmann, J. Haas, D. Abel, “Iterative Learning Control of Gravity Compensation for Upper-Arm Robot-Assisted Rehabilitation,” in 2020 European Control Conference (ECC), pp. 2-9, May 2020, doi: 10.23919/ECC51009.2020.9143805.

[81] Miao, M.d., Gao, X.s., Zhao, J. et al., “Rehabilitation robot following motion control algorithm based on human behavior intention,” Appl Intell, July 2022, doi: 10.1007/s10489-022-03823-7.

[82] Y. WANG, A. ZHU, H. WU, P. ZHU, X. ZHANG, G. CAO, “Control of Lower Limb Rehabilitation Exoskeleton Robot Based on CPG Neural Network,” in 2019 16th International Conference on Ubiquitous Robots (UR), pp. 678-682, June 2019, doi: 10.1109/URAI.2019.8768691.

[83] Wang, W., Zhang, J., Kong, D., Su, S., Yuan, X., & Zhao, C, “Research on control method of upper limb exoskeleton based on mixed perception model,” Robotica, 40(10), 3669-3685, April 2022, doi:10.1017/S0263574722000480.

[84] Li K, Li Z, Zeng H, Wei N, “Control of Newly-Designed Wearable Robotic Hand Exoskeleton Based on Surface Electromyographic Signals,” Front Neurorobot., 15:711047, September 2021, doi: 10.3389/fnbot.2021.711047.

[85] Chen X, Zeng Y, Yin Y, “Improving the Transparency of an Exoskeleton Knee Joint Based on the Understanding of Motor Intent Using Energy Kernel Method of EMG,” IEEE Trans Neural Syst Rehabil Eng., 25(6):577-588, June 2017, doi: 10.1109/TNSRE.2016.2582321.

[86] Ali Foroutannia, Mohammad-R Akbarzadeh-T, Alireza Akbarzadeh, “A deep learning strategy for EMG-based joint position prediction in hip exoskeleton assistive robots,” Biomedical Signal Processing and Control, Volume 75, 103557, ISSN 1746-8094, May 2022, doi: 10.1016/j.bspc.2022.103557.

[87] Z. -Q. Ling, G. -Z. Cao, Y. -P. Zhang, H. -R. Cheng, B. -B. He, S. -B. Cao, “Real-time Knee Joint Angle Estimation Based on Surface Electromyograph and Back Propagation Neural Network,” in 2021 18th International Conference on Ubiquitous Robots (UR), pp. 256-263, July 2021, doi: 10.1109/UR52253.2021.9494639.

[88] Xiu-Feng ZHANG, Xia LI, Ji-Tao DAI, Guo-Xin PAN, Ning ZHANG, Hui-Qun FU, Jian-Guang XU, Zhi-Chao ZHONG, Tao LIU, Yoshio INOUE, “The design of

a hemiplegic upper limb rehabilitation training system based on surface EMG signals," Journal of Advanced Mechanical Design, Systems, and Manufacturing, Volume 12, Issue 1, Pages JAMDSM0031, 2018, doi: 10.1299/jamdsm.2018jamdsm0031.

[89] George JA, Gunnell AJ, Archangeli D, Hunt G, Ishmael M, Foreman KB, Lenzi T, "Robust Torque Predictions From Electromyography Across Multiple Levels of Active Exoskeleton Assistance Despite Non-linear Reorganization of Locomotor Output," Front Neurorobot, 15:700823, November 2021, doi: 10.3389/fnbot.2021.700823.

[90] Zhang et al., "iLeg—A Lower Limb Rehabilitation Robot: A Proof of Concept," IEEE Transactions on Human-Machine Systems, vol. 46, no. 5, pp. 761-768, Oct. 2016, doi: 10.1109/THMS.2016.2562510.

[91] B. Ghannadi, N. Mehrabi, R. S. Razavian, J. McPhee, "Nonlinear model predictive control of an upper extremity rehabilitation robot using a two-dimensional human-robot interaction model," in 2017 IEEE/RSJ International Conference on Intelligent Robots and Systems (IROS), pp. 502-507, September 2017, doi: 10.1109/IROS.2017.8202200.

[92] Liu Y, Li X, Zhu A, Zheng Z, Zhu H, "Design and evaluation of a surface electromyography-controlled lightweight upper arm exoskeleton rehabilitation robot," International Journal of Advanced Robotic Systems, 18(3), May 2021, doi:10.1177/17298814211003461.

[93] T. Goyal, S. Hussain, E. Martinez-Marroquin, N. A. T. Brown, P. K. Jamwal, "Impedance Control of a Wrist Rehabilitation Robot Based on Autodidact Stiffness Learning," IEEE Transactions on Medical Robotics and Bionics, vol. 4, no. 3, pp. 796-806, August 2022, doi: 10.1109/TMRB.2022.3194528.

[94] W. Nicholas Price II. "Risks and remedies for artificial intelligence in health care," Brookings, November 2019.

[95] A.A., French, J.A., Pehlivan, A.U. et al., “Current Trends in Robot-Assisted Upper-Limb Stroke Rehabilitation: Promoting Patient Engagement in Therapy,” Curr Phys Med Rehabil Rep 2, 184–195, June 2014, doi: 10.1007/s40141-014-0056-z.

[96] S. Wang, H. Su, M. Huang, Y. Chen, Y. Zheng and R. Yang, "A Motor Imagery-based Lower Limb Rehabilitation Robot System," in 2023 IEEE International Biomedical Instrumentation and Technology Conference (IBITeC),November 2023, doi: 10.1109/IBITeC59006.2023.10390931.

[97] M. Cheng, W. Zhu and Q. Ren, "Bio-inspired Control of a Rehabilitation Robot Actuated by Pneumatic Artificial Muscles," in 2023 WRC Symposium on Advanced Robotics and Automation (WRC SARA), August 2023, doi: 10.1109/WRCSARA60131.2023.10261853.

[98] G. Li, S. Ye, J. Meng, G. Zuo, J. Zhang and C. Shi, "A Compliance Control Strategy for an Upper-Limb Rehabilitation Robot with a Quick and Real-Time Human-Robot Interactive Force Estimation," in 2023 International Symposium on Intelligent Robotics and Systems (ISoIRS), May 2023, doi: 10.1109/ISoIRS59890.2023.00019.

[99] Kalita, B.; Leonessa, A.; Dwivedy, S.K. A Review on the Development of Pneumatic Artificial Muscle Actuators: Force Model and Application. Actuators 2022, 11, 288. https://doi.org/10.3390/act11100288.

[100] Reva, E.J.; Jonathon, W.S. Chapter Two—Actuator Technologies. In Handbook of Biomechatronics; Academic Press: Cambridge, MA, USA, 2019; pp. 31–59. https://doi.org/10.1016/B978-0-12-812539-7.00002-7.

[101] Lizehn, W.; Peng, G.; Yao, W.; Biggar, S.; Hu, C.; Yin, X.; Fan, Y. 10—Soft robotics for hand rehabilitation. In Intelligent Bio-mechatronics in Neurorehabilitation; Academic Press: Cambridge, MA, USA, 2020; pp. 167–176. https://doi.org/10.1016/B978-0-12-814942-3.00010-6.

[102] Kelasidi, E.; Andrikopoulos, G.; Nikolakopoulos, G.; Manesis, S. A survey on pneumatic muscle actuators modeling. In Proceedings of the 2011 IEEE International Symposium on Industrial Electronics, Gdansk, Poland, 27–30 June 2011; pp. 1263–1269. https://doi.org/10.1109/ISIE.2011.5984340.

[103] Reynolds, D.B.; Repperger, D.W.; Phillips, C.A.; Bandry, G. Modeling the Dynamic Characteristics of Pneumatic Muscle. Ann. Biomed. Eng. 2003, 31, 310–317. https://doi.org/10.1114/1.1554921.

[104] Shameek, G.; Akash, G.; Akshay, P.; Dwivedy, S.K. Control of pneumatic artificial muscle system through experimental modelling. Mechatronics 2012, 22, 1135–1147. https://doi.org/10.1016/j.mechatronics.2012.09.010.

[105] Antonelli, M.G.; Zobel, P.B.; Durante, F.; Raparelli, T. Numerical modelling and experimental validation of a McKibben pneumatic muscle actuator. J. Intell. Mater. Syst. Struct. 2017, 28, 2737–2748. https://doi.org/10.1177/1045389X17698245.

[106] Al-Ibadi, A.; Nefti-Meziani, S.; Davis, S. Valuable experimental model of contraction pneumatic muscle actuator. In Proceedings of the 2016 21st International Conference on Methods and Models in Automation and Robotics (MMAR), Miedzyzdroje, Poland, 29 August–1 September 2016; pp. 744–749. https://doi.org/10.1109/MMAR.2016.7575229.

[107] Al-Ibadi, A.; Nefti-Meziani, S.; Davis, S. Novel models for the extension pneumatic muscle actuator performances. In Proceedings of the 2017 23rd International Conference on Automation and Computing (ICAC), Huddersfield, UK, 7–8 September 2017; pp. 1–6. https://doi.org/10.23919/IConAC.2017.8081973.

[108] Andrikopoulos, G.; Nikolakopoulos, G.; Manesis, S. Pneumatic artificial muscles: A switching Model Predictive Control approach. Control Eng. Pract. 2013, 21, 1653–1664. https://doi.org/10.1016/j.conengprac.2013.09.003.

[109] Kotkas, L.; Zhurkin, N.; Donskoy, A.; Zharkovskij, A. Design and Mathematical Modeling of a Pneumatic Artificial Muscle-Actuated System for Industrial Manipulators. Machines 2022, 10, 885. https://doi.org/10.3390/machines10100885.

[110] Sarosi, J.; Biro, I.; Nemeth, J.; Cveticanin, L. Dynamic modeling of a pneumatic muscle actuator with two-direction motion. Mech. Mach. Theory 2015, 85, 25–34. https://doi.org/10.1016/j.mechmachtheory.2014.11.006.

[111] Cao, J.; Xie, S.Q.; Zhang, M.; Das, R. A New Dynamic Modelling Algorithm for Pneumatic Muscle Actuators. In Intelligent Robotics and Applications. ICIRA 2014. Lecture Notes in Computer Science; 2014; Volume 8918. Springer, Cham. https://doi.org/10.1007/978-3-319-13963-0_44.

[112] Serres, J.L.; Reynolds, D.B.; Phillips, C.A.; Gerschutz, M.J.; Repperger, D.W. Characterisation of a phenomenological model for commercial pneumatic muscle actuators. Comput. Methods Biomech. Biomed. Eng. 2009, 12, 423–430. https://doi.org/10.1080/10255840802654327.

[113] Jamwal, P.K.; Xie, S.Q. Artificial Neural Network based dynamic modelling of indigenous pneumatic muscle actuators. In Proceedings of the 2012 IEEE/ASME 8th IEEE/ASME International Conference on Mechatronic and Embedded Systems and Applications, Suzhou, China, 8–10 July 2012; pp. 190–195. https://doi.org/10.1109/MESA.2012.6275560.

[114] Chavoshian, M.; Taghizadeh, M. Recurrent neuro-fuzzy model of pneumatic artificial muscle position. J. Mech. Sci. Technol. 2020, 34, 499–508. https://doi.org/10.1007/s12206-019-1154-8.

[115] Ahn, K.K.; Anh, H.P.H. A new approach for modelling and identification of the pneumatic artificial muscle manipulator based on recurrent neural networks. Proc. Inst. Mech. Eng. Part I J. Syst. Control. Eng. 2007, 221, 1101–1121. https://doi.org/10.1243/09596518JSCE432.

[116] Ahn, K.K.; Anh, H.P.H. Comparative study of modeling and identification of the pneumatic artificial muscle (PAM) manipulator using recurrent neural networks. J. Mech. Sci. Technol. 2008, 22, 1287–1298. https://doi.org/10.1007/s12206-008-0416-7.

[117] Mat Dzahir, M.A.; Yamamoto, S.-i. Dynamic Modeling of McKibben Muscle Using Empirical Model and Particle Swarm Optimization Method. Appl. Sci. 2019, 9, 2538. https://doi.org/10.3390/app9122538.

[118] Dzahir, M.A.M.; Yamamoto, S.-i. Inverse Modeling of Nonlinear Artificial Muscle Using Polynomial Parameterization and Particle Swarm Optimization. Adv. Mater. Sci. Eng. 2020, 8189157 . https://doi.org/10.1155/2020/8189157.

[119] Du, W.; Li, B. Multi-strategy ensemble particle swarm optimization for dynamic optimization. Inf. Sci. 2008, 178, 3096–3109. https://doi.org/10.1016/j.ins.2008.01.020.

[120] Huang, J.; Qian, J.; Liu, L.; Wang, Y.; Xiong, C.; Ri, S. Echo state network based predictive control with particle swarm optimization for pneumatic muscle actuator. J. Frankl. Inst. 2016, 353, 2761–2782. https://doi.org/10.1016/j.jfranklin.2016.05.004.

[121] Masia, L.; Xiloyannis, M.; Khanh, D.B.; Wilson, A.C.; Contu, S.; Yongtae, K.G. Chapter 4—Actuation for robot-aided rehabilitation: Design and control strategies. In *Rehabilitation Robotics*; Academic Press: Cambridge, MA, USA, 2018. https://doi.org/10.1016/B978-0-12-811995-2.00003-5.

[122] Pan, M.; Yuan, C.; Liang, X.; Dong, T.; Liu, T.; Zhang, J.; Zou, J.; Yang, H.; Bowen, C. Soft Actuators and Robotic Devices for Rehabilitation and Assistance. *Adv. Intell. Syst.* **2022**, *4*, 2100140. https://doi.org/10.1002/aisy.202100140.

[123] Vallery, H.; Veneman, J.; van Asseldonk, E.; Ekkelenkamp, R.; Buss, M.; van Der Kooij, H. Compliant actuation of rehabilitation robots. *IEEE Robot. Autom. Mag.* **2008**, *15*, 60–69. https://doi.org/10.1109/MRA.2008.927689.

[124] Dzahir, M.A.M.; Yamamoto, S.-I. Recent Trends in Lower-Limb Robotic Rehabilitation Orthosis: Control Scheme and Strategy for Pneumatic Muscle Actuated Gait Trainers. *Robotics* **2014**, *3*, 120–148. https://doi.org/10.3390/robotics3020120.

[125] Wang, D.; Wang, Y.; Zi, B.; Cao, Z.; Ding, H. Development of an active and passive finger rehabilitation robot using pneumatic muscle and magnetorheological damper. *Mech. Mach. Theory* **2020**, *147*, 103762. https://doi.org/10.1016/j.mechmachtheory.2019.103762.

[126] Choi, H.S.; Lee, C.H.; Baek, Y.S. Design and Validation of a Two-Degree-of-Freedom Powered Ankle-Foot Orthosis with Two Pneumatic Artificial Muscles. *Mechatronics* **2020**, *72*, 102469. https://doi.org/10.1016/j.mechatronics.2020.102469.

[127] Guo, X.; Liu, Q.; Zuo, J.; Meng, W.; Ai, Q.; Zhou, Z.; Xu, W. A Novel Pneumatic Artificial Muscle-driven Robot for Multi-joint Progressive Rehabilitation. In Proceedings of the 2018 Joint IEEE 8th International Conference on Development and Learning and Epigenetic Robotics (ICDL-EpiRob), Tokyo, Japan, 17–20 September 2018. https://doi.org/10.1109/DEVLRN.2018.8761014.

[128] Shao, F.; Meng, W.; Ai, Q.; Xie, S.Q. Neural Network Adaptive Control of Hand Rehabilitation Robot Driven by Flexible Pneumatic Muscles. In Proceedings of the 2021 7th International Conference on Mechatronics and Robotics Engineering (ICMRE), Budapest, Hungary, 3–5 February 2021. https://doi.org/10.1109/ICMRE51691.2021.9384827.

[129] Schindele, D.; Aschemann, H. Nonlinear model predictive control of a fast parallel robot actuated by pneumatic muscles. *IFAC Proc. Vol.* **2007**, *40*, 591–596. https://doi.org/10.3182/20070822-3-ZA-2920.00097.

[130] Bone, G.M.; Xue, M.; Flett, J. Position control of hybrid pneumatic–electric actuators using discrete-valued model-predictive control. *Mechatronics* **2015**, *25*, 1–10. https://doi.org/10.1016/j.mechatronics.2014.10.009.

[131] Qi, H.; Bone, G.M.; Zhang, Y. Position Control of Pneumatic Actuators Using Three-Mode Discrete-Valued Model Predictive Control. *Actuators* **2019**, *8*, 56. https://doi.org/10.3390/act8030056.

[132] Cao, Y.; Huang, J. Neural-network-based nonlinear model predictive tracking control of a pneumatic muscle actuator-driven exoskeleton. *IEEE/CAA J. Autom. Sin.* **2020**, *7*, 1478–1488. https://doi.org/10.1109/JAS.2020.1003351.

[133] Chu, W.-L.; Lin, C.-J.; Chen, Y.-Y. Redundant Robot with Pneumatic Artificial Muscles for Rehabilitation Works Using Iterative Learning Control. *Appl. Sci.* **2022**, *12*, 8419. https://doi.org/10.3390/app12178419.

[134] Rwafa, J.; Ghayoor, F. Implementation of Iterative Learning Control on a Pneumatic Actuator. *Actuators* **2022**, *11*, 240. https://doi.org/10.3390/act11080240.

[135] Chavoshian, M.; Taghizadeh, M.; Mazare, M. Hybrid Dynamic Neural Network and PID Control of Pneumatic Artificial Muscle Using the PSO Algorithm. *Int. J. Autom. Comput.* **2020**, *17*, 428–438. https://doi.org/10.1007/s11633-019-1196-5.

[136] Humaidi, A.J.; Ibraheem, I.K.; Azar, A.T.; Sadiq, M.E. A New Adaptive Synergetic Control Design for Single Link Robot Arm Actuated by Pneumatic Muscles. *Entropy* **2020**, *22*, 723. https://doi.org/10.3390/e22070723.

[137] Mayetin, U.; Kucuk, S. A low cost 3-DOF force sensing unit design for wrist rehabilitation robots. *Mechatronics* **2021**, *78*, 102623. https://doi.org/10.1016/j.mechatronics.2021.102623.

[138] Mayetin, U.; Kucuk, S. Design and Experimental Evaluation of a Low Cost, Portable, 3-DOF Wrist Rehabilitation Robot with High Physical Human–Robot

Interaction. *J. Intell. Robot. Syst.* **2022**, *106*, 65. https://doi.org/10.1007/s10846-022-01762-6.

[139] Toz, M.; Küçük, S. Development of derivation of inverse Jacobian matrices for 195 6-DOF GSP mechanisms. *Turk. J. Electr. Eng. Comput. Sci.* **2016**, *24*, 4142–4153. https://doi.org/10.3906/elk-1501-110.

[140] Zhang Y, Liu X, Qiao X, Fan Y. "Characteristics and Emerging Trends in Research on Rehabilitation Robots from 2001 to 2020: Bibliometric Study." Journal of Medical Internet Research. May 2023 May. doi: 10.2196/42901

[141] Neuro Rehab Times (Dec 2024). Rehabilitation robotics market may see big move. [Article]. Available at: https://nrtimes.co.uk/rehabilitation-robotics-market-may-see-big-move/

[142] Mashud G, Hasan S, Alam N. "Advances in Control Techniques for Rehabilitation Exoskeleton Robots: A Systematic Review." Actuators. 2025. doi:10.3390/act14030108

[143] Dzahir MAM, Yamamoto S-i. "Recent Trends in Lower-Limb Robotic Rehabilitation Orthosis: Control Scheme and Strategy for Pneumatic Muscle Actuated Gait Trainers." Robotics. 2014. doi: 10.3390/robotics3020120

[144] Li IH, Lin YS, Lee LW, Lin WT. "Design, Manufacturing, and Control of a Pneumatic-Driven Passive Robotic Gait Training System for Muscle-Weakness in a Lower Limb." Sensors (Basel). Oct 2021. doi: 10.3390/s21206709

[145] Junpeng Wu, Jinwu Gao, Rong Song, Rihui Li, Yaning Li, Lelun Jiang. "The design and control of a 3DOF lower limb rehabilitation robot." Mechatronics. 2016. doi: 10.1016/j.mechatronics.2015.11.010

[146] S. Yan, J. Tao, J. Huang and A. Xue. "Model Predictive Control for Human Following Rehabilitation Robot." In 2019 IEEE International Conference on Advanced Robotics and its Social Impacts (ARSO), Beijing, China. 2019. doi: 10.1109/ARSO46408.2019.8948803

[147] Z. Liu, X. Qiu and Y. Xing. "A Following Control Method for Lower Limb Rehabilitation Robots Using MPC and Fiducial Marker System." in 2025 IEEE International Conference on Industrial Technology (ICIT), Wuhan, China. 2025. doi: 10.1109/ICIT63637.2025.10965322

[148] Wilian M. dos Santos, Adriano A.G. Siqueira. “Optimal impedance via model predictive control for robot-aided rehabilitation.” Control Engineering Practice. 2019. doi: 10.1016/j.conengprac.2019.104177

[149] H. Hmida, S. Hafsi and F. Bouani. "An efficient MPC controller for the rehabilitation of an actuated knee joint orthosis." in 2021 18th International Multi-Conference on Systems, Signals & Devices (SSD), Monastir, Tunisia. 2021. doi: 10.1109/SSD52085.2021.9429299

[150] A. Ali, S. F. Ahmed, M. K. Joyo and K. Kushsairy. "MPC-PID comparison for controlling therapeutic upper limb rehabilitation robot under perturbed conditions." in 2017 IEEE 3rd International Conference on Engineering Technologies and Social Sciences (ICETSS), Bangkok, Thailand. 2017. doi: 10.1109/ICETSS.2017.8324166

[151] L. Peng, Z. -G. Hou and W. Wang. "Dynamic modeling and control of a parallel upper-limb rehabilitation robot." in 2015 IEEE International Conference on Rehabilitation Robotics (ICORR), Singapore. 2015. doi: 10.1109/ICORR.2015.7281254

[152] Metcalf AG, Gallagher JF, Jackson AE, Levesley MC. “Multi-Domain Dynamic Modelling of a Low-Cost Upper Limb Rehabilitation Robot.” Robotics. 2021. doi: 10.3390/robotics10040134

[153] P.K. Jamwal, S.Q. Xie, Y.H. Tsoi, K.C. Aw. “Forward kinematics modelling of a parallel ankle rehabilitation robot using modified fuzzy inference.” Mechanism and Machine Theory. 2010. doi: 10.1016/j.mechmachtheory.2010.06.017

[154] Batista J, Souza D, dos Reis L, Barbosa A, Araújo R. “Dynamic Model and Inverse Kinematic Identification of a 3-DOF Manipulator Using RLSPSO.” Sensors. 2020. doi: 10.3390/s20020416

[155] O.N. Almasi. M.H. Khooban, H. Behzad. “Non-Linear MIMO Identification of a Phantom Omni using LS-SVR with a Hybrid Model Selection.” IET Science, Measurement, and Technology. Aug 2018. doi: 10.1049/iet-smt.2017.0193

[156] H. P. H. Anh and N. H. Phuc. "Inverse Neural MIMO NARX Model Identification of Nonlinear System Optimized with PSO." in 2010 Fifth IEEE International Symposium on Electronic Design, Test & Applications, Ho Chi Minh City, Vietnam. 2010. doi: 10.1109/DELTA.2010.61

[157] Jin Lei Wang, Yafeng Li, Aimin An. “Dynamic parameter identification of upper-limb rehabilitation robot system based on variable parameter particle swarm optimisation.” IET Cyber Systems and Robotics. Sep 2020. doi: 10.1049/iet-csr.2020.0023

[158] Long Y, Du Z-J, Wang W-D, Zhao G-Y, Xu G-Q, He L, Mao X-W, Dong W. “PSO-SVM-Based Online Locomotion Mode Identification for Rehabilitation Robotic Exoskeletons.” Sensors. 2016. doi: 10.3390/s16091408

[159] G. Zhu et al. "Robot-assisted ankle rehabilitation for the treatment of drop foot: A case study." in 2016 12th IEEE/ASME International Conference on Mechatronic and Embedded Systems and Applications (MESA), Auckland, New Zealand. 2016. doi: 10.1109/MESA.2016.7587130

[160] M. Zhang et al. "Adaptive Patient-Cooperative Control of a Compliant Ankle Rehabilitation Robot (CARR) With Enhanced Training Safety." IEEE Transactions on Industrial Electronics. Feb 2018. doi: 10.1109/TIE.2017.2733425

[161] Liu Quan, Liu Aiming, Meng Wei, Ai Qingsong, Xie Sheng Q. “Hierarchical Compliance Control of a Soft Ankle Rehabilitation Robot Actuated by Pneumatic Muscles.” Frontiers in Neurorobotics. 2017. doi: 10.3389/fnbot.2017.00064

[162] Mingming Zhang, Jinghui Cao, Guoli Zhu, Qing Miao, Xiangfeng Zeng, Sheng Q. Xie. “Reconfigurable workspace and torque capacity of a compliant ankle rehabilitation robot (CARR).” Robotics and Autonomous Systems. 2017. doi: 10.1016/j.robot.2017.06.006

[163] TDF Health & Fitness. Nov 2023. Ankle Injuries. [Article]. Available at: https://tfdgym.co.uk/blog/ankle-injuries/

[164] Zhai X, Wu Q, Li X, Xu Q, Zhang Y, Fan S, Zhang L-Q and Pan Y. “Effects of Robot-Aided Rehabilitation on the Ankle Joint Properties and Balance Function in Stroke Survivors: A Randomized Controlled Trial.” Frontiers in Neurology. 2021. doi: 10.3389/fneur.2021.719305

[165] Forrester LW, Roy A, Krywonis A, Kehs G, Krebs HI, Macko RF. “Modular Ankle Robotics Training in Early Subacute Stroke: A Randomized Controlled Pilot Study: A Randomized Controlled Pilot Study.” Neurorehabilitation and Neural Repair. 2014. doi: 10.1177/1545968314521004

[166] Kai Chen, Yi-Ning Wu, Yupeng Ren, Lin Liu, Deborah Gaebler-Spira, Kelly Tankard, Julia Lee, Weiqun Song, Maobin Wang, Li-Qun Zhang. “Home-Based Versus Laboratory-Based Robotic Ankle Training for Children With Cerebral Palsy: A Pilot Randomized Comparative Trial.” Archives of Physical Medicine and Rehabilitation. 2016. doi: 10.1016/j.apmr.2016.01.029.

[167] Forrester, L.W., Roy, A., Hafer-Macko, C. et al. “Task-specific ankle robotics gait training after stroke: a randomized pilot study.” Journal of NeuroEngineering and Rehabilitation. 2016. doi: 10.1186/s12984-016-0158-1

[168] Zhang Q, Wang Y, Zhou M, et al. “Ankle rehabilitation robot training for stroke patients with foot drop: Optimizing intensity and frequency.” NeuroRehabilitation. 2023. doi: 10.3233/NRE-230173

[169] J. A. Saglia, N. G. Tsagarakis, J. S. Dai and D. G. Caldwell, "Control Strategies for Patient-Assisted Training Using the Ankle Rehabilitation Robot (ARBOT),"

IEEE/ASME Transactions on Mechatronics. Dec. 2013. doi: 10.1109/TMECH.2012.2214228

[170] Zhou Z, Sun Y, Wang N, Gao F, Wei K and Wang Q. “Robot-Assisted Rehabilitation of Ankle Plantar Flexors Spasticity: A 3-Month Study with Proprioceptive Neuromuscular Facilitation.” Frontiers in Neurorobotics. 2016. doi: 10.3389/fnbot.2016.00016

[171] Yunju Lee, Kai Chen, Yupeng Ren, Jongsang Son, Bruce A. Cohen, James A. Sliwa, Li-Qun Zhang. “Robot-guided ankle sensorimotor rehabilitation of patients with multiple sclerosis.” Multiple Sclerosis and Related Disorders. 2017. doi: 10.1016/j.msard.2016.12.006

APPENDIX A

ETHICAL APPROVAL FOR RESEARCH PROJECTS INVOLVING HUMAN PARTICIPANTS

UNIVERSITY OF LEEDS

10 December 2025

Dear Dexter,

Research ethics project I.D. reference: EPS FREC 3587

Research project title: Ankle Rehabilitation Robot Participant Experiments

I am pleased to inform you that the above research ethics application has been reviewed by the Research Ethics Committee for Engineering and Physical Sciences which has issued a favourable ethical opinion based on the application submitted. **Please retain this email in your project file as it is evidence of the Committee's approval.**

Matters you should note:

- Ethics approval does not infer you have the right of access to any member of staff or student or documents and the premises of the University of Leeds. Nor does it imply any right of access to the premises of any other organisation, including clinical areas. The Committee takes no responsibility for you gaining access to staff, students and/or premises prior to, during or following your research activities.
- It is your responsibility to comply with all relevant Health and Safety, Data Protection and other legal and professional requirements and guidelines.
- You are expected to keep a record of all your approved documentation, as well as documents such as sample consent forms, risk assessments and other documents relating to the research project. This should be kept in your project file.
- Audits are undertaken on approved ethics applications. Your project could be chosen for such an audit. You should therefore ensure your project files are kept up to date and readily available for audit purposes. You will be given a two week notice period if your project is selected.
- Please always include the above research ethics application reference in any correspondence with the Research Ethics team.

If you need to make **amendments** to the original submitted research project, you are expected to seek approval from the Committee before taking any further action. Changes could include (but are not limited to) the project end date, project design or recruitment methodology, or study documentation. Please go to https://secretariat.leeds.ac.uk/research-ethics/how-to-apply-for-research-ethics-amendment/ or contact the Research Ethics team for further information at Research Ethics.

I hope your research project goes well.

Yours sincerely,

Ms Rachel Prinn, Research Ethics, Governance & Compliance Directorate,, University of Leeds

On behalf of Dr Raymond Holt, Chair, EPS FREC

APPENDIX B

LIST OF MATERIALS

Feasibility Study

Functionality	Component	Specification	Quantity
Actuation	PAM	FESTO DMSP-20-400N	1
	Proportional Pressure Regulator	FESTO VPPM-6L-L-1-G18-0L6H	1
Sensing	Linear Displacement Encoder	FESTO MLO-POT-300-TLF 300lb	1
	Singe-Axis Load Cell	FUTEK LCM300	1
		FUTEK IAA100 amplifier	1
Control	Real-Time Controller	NI roboRIO	1

CARR

Functionality	Component	Specification	Quantity
Actuation	PAM	FESTO DMSP-20-400N	4
	Proportional Pressure Regulator	FESTO VPPM-6L-L-1-G18-0L6H	4
Sensing	Rotary Encoder	AS5048A	3
	Single-Axis Load Cell	FUTEK LCM 300 250Ib	4
		FUTEK CSG110 amplifier	4
	Six-Axis Load Cell	ATI Omega85	1
		ATI 9105-DAQ	1
Control	Real-Time Controller	NI Compact RIO-9022	1
	Signal I/O	Digital I/O NI-9401	1
		Analog Input NI-9205	1
		Analog Output NI-9263	1
		Synchronization NI USB-6210	1